SEAFLOOR IRON MOBILIZATION ACROSS THE DEEP-WATER REDOX GRADIENTS OF THE BLACK SEA AND THE SEA OF MARMARA

A THESIS SUBMITTED TO
THE GRADUATE SCHOOL OF NATURAL AND APPLIED SCIENCES
OF
MIDDLE EAST TECHNICAL UNIVERSITY

BY

NIMET ALIMLI

IN PARTIAL FULFILLMENT OF THE REQUIREMENTS
FOR
THE DEGREE OF MASTER OF SCIENCE
IN
OCEANOGRAPHY

AUGUST 2022

Approval of the thesis:

SEAFLOOR IRON MOBILIZATION ACROSS THE DEEP-WATER REDOX GRADIENTS OF THE BLACK SEA AND THE SEA OF MARMARA

submitted by **NIMET ALIMLI** in partial fulfillment of the requirements for the degree of **Master of Science** i**n Oceanography, Institute of Marine Sciences, Middle East Technical University** by,

Prof. Dr. Barış Salihoğlu
Director, **Institute of Marine Sciences, METU** _____

Assoc. Dr. Bettina Fach-Salihoğlu
Head of the Department, **Oceanography, METU** _____

Assoc. Prof. Dr. Mustafa Yücel
Supervisor, **Oceanography, METU** _____

Examining Committee Members:

Prof. Dr. Nuray Çağlar
Institute of Marine Sciences and Management, **Istanbul University** _____

Assoc. Prof. Dr. Mustafa Yücel
Supervisor, **Oceanography, METU** _____

Assoc. Prof. Dr. Mustafa Koçak
Oceanography, METU _____

Date: 29.08.2022

I hereby declare that all information in this document has been obtained and presented in accordance with academic rules and ethical conduct. I also declare that, as required by these rules and conduct, I have fully cited and referenced all material and results that are not original to this work.

Name Last name : Nimet Alımlı

Signature :

ABSTRACT

SEAFLOOR IRON MOBILIZATION ACROSS THE DEEP-WATER REDOX GRADIENTS OF THE BLACK SEA AND THE SEA OF MARMARA

Alımlı, Nimet
Master of Science, Oceanography
Supervisor: Assoc. Prof. Dr. Mustafa Yücel

August 2022, 121 pages

Iron is one of the key elements in the ocean which has wide interconnections with other essential elements (i.e., C, N, P, O, Mn, S) and fundamental mechanisms (i.e., photosynthesis, respiration, chemosynthesis). The critical role of iron, since the beginning of life until the modern oceans, was increasing with biogeochemical evolution creating new niches for iron. Despite iron is ubiquitous on land, its trace level presence in the ocean creates difficulties for iron studies. Hence, the complex cycle of iron still has many gaps and filling the gaps is crucial to understand the past, present and the future of oceans and moreover Earth. In this thesis work, benthic dissolved iron patterns in the Black Sea and for the first time in the Sea of Marmara was studied in the comparison of recent redox changes and well-established redox environments. High amounts of dissolved iron were measured, and high benthic fluxes estimated for the Sea of Marmara showing that, in terms of iron source, it is comparable to other oxygen minimum zones. The potential connection between the organic complexation and porewater size fractions is examined with comparison of more established iron fraction species. The results from seawater and porewater size fractionations indicated that the nature of the seawater and porewater species are different at least to the extent of different influences by sample handling. In summary, the iron patterns in the Sea of Marmara indicates the recent hypoxia have already cause iron to be mobilized at the seafloor and the sedimentary colloidal and

soluble phases needs a more detailed attention to understand the effective scale of benthic iron species.

Keywords: Iron Biogeochemistry, The Sea of Marmara, The Black Sea, Marine Iron Cycle, Size Pools of Iron

ÖZ

KARADENİZ VE MARMARA DENİZİ'NİN DERİN SU REDOX ORTAMLARINDA BENTİK DEMİR MOBİLİZASYONU

Alımlı, Nimet
Yüksek Lisans, Oşinografi
Tez Yöneticisi: Doç. Dr. Mustafa Yücel

Ağustos 2022, 121 sayfa

Demir, diğer temel elementler (C, N, P, O, Mn, S) ve temel mekanizmalar (fotosentez, solunum, kemosentez) ile sıkı bağlantıları olan okyanustaki kilit elementlerden biridir. Yaşamın başlangıcından modern okyanuslara kadar demirin kritik rolü, demir için yeni nişler yaratan biyojeokimyasal evrimle artış gösterdi. Demirin karada bol miktarda bulunmasına rağmen, okyanusta eser düzeylerde bulunması demir çalışmalarının başlıca zorluklarındandır. Bu nedenle, demirin bu grift döngüsünde hala birçok boşluk vardır ve bu boşlukları doldurmak, okyanusların ve dahası Dünya'nın geçmişini, bugününü ve geleceğini anlamak için çok önemlidir. Bu tez çalışmasında, Karadeniz'de ve ilk kez Marmara Denizi'nde bentik çözünmüş demir paternleri, değişen ve kararlı redoks ortamlarının karşılaştırılmıştır. Marmara Denizi'nde demir kaynağı açısından diğer oksijen minimum bölgeleriyle karşılaştırılabilir miktarlarda çözünmüş demir ölçülmüştür ve yüksek bentik girdileri hesaplanmıştır. Organik kompleksleşme ve gözenek suyu boyutu fraksiyonları arasındaki muhtemel bağlantı, nispeten daha iyi bilinen demir fraksiyon türlerinin karşılaştırılmasıyla incelenmiştir. Deniz ve gözenek suyunda demir boyutu fraksiyonlarından elde edilen sonuçlar, deniz suyu ve gözenek suyu demir türlerinin doğasının, en azından örneklemeden farklı derecelerde etkilenecek farklılıklarda olduğunu göstermiştir. Özetle, Marmara Denizi'ndeki sediman demir paternleri, son hipoksinin deniz tabanında demirin mobilize olmasına neden olduğunu; sediman

kolloidal ve çözünür faz sonuçları ise, bentik demir türlerinin etkisini anlamak için daha ayrıntılı çalışmalar gerektiğini göstermektedir.

Anahtar Kelimeler: Demir Biyojeokimyası, Marmara Denizi, Karadeniz, Demir Döngüsü, Demir Boyut Fraksiyonları

ACKNOWLEDGMENTS

I am deeply thankful for my supervisor, Assoc. Prof. Dr. Mustafa Yücel, for the perspective he gave me studying a multidisciplinary field and for the guidance, advice, criticism, and encouragement he provided throughout my master's education.

I would like to thank my thesis committee members Prof. Dr. Nuray Çağlar and Assist. Prof. Dr. Mustafa Koçak.

I am grateful to Dr. Hasan Örek, Shipmaster Burhan Tekin, scientific cruise participants, crew of R/V Bilim-2 and METU-IMS technical personnel for their kind assistance which was so crucial during this study.

I would like to thank to my colleagues Serhat Sevgen, İsmail Akçay, Mertcan Esti, Esra Ermiş, Gamze Tanık for their support during this study.

I am grateful to my family, Gülçin Çetin, Merve Kurt, Begüm Tohumcu, Fatmanur Oğul, Emel Kocaman, Buse Uysaler, Betül Bitir Soylu, for their mental support.

This study has been supported by DEKOSIM (Centre for Marine Ecosystem and Climate Research, Project Code BAP-08-11-DPT.2012K120880) Project, the Scientific and Technological Research Council of Turkey (TUBİTAK-2247, 119C027) ERC Supporting Program DEEPREDOX Project, the Scientific and Technological Research Council of Turkey (TUBİTAK-1001, 118Y424), MARMOD Project and TUBA-GEBIP Program of the Turkish Academy of Sciences.

TABLE OF CONTENTS

LIST OF TABLES

TABLES

LIST OF FIGURES

FIGURES

CHAPTER 1

INTRODUCTION

Iron has unique complex relations with other element that are significant for marine biogeochemistry such as C, N, P, O, S, Mn. Its availability, retention in marine cycle and durability is controlled by different biologically and chemically mediated reactions (Kappler et al., 2021). Iron's distribution over the global oceans are heterogenous and global oceans production is under limitation of iron availability. Heterogeneity is a consequence of different dispersion mechanisms acting on different major iron sources which are atmospheric dust input, hydrothermal vent fluid input and coastal sediment recycling (Tagliabue et al., 2017). Coastal sediment iron recycling and the affective scale of released iron, its retention in marine iron cycle are the missing parts of the shelf iron release mechanism. The highest iron effluxes are known to be sourced from the low oxygen but not highly reducing conditioned seafloors. The "narrow redox window" conditions are generally met by the oxygen minimum zones and hypoxic areas (Scholz et al., 2014b). Hypoxic areas are the hotspots to understand the mechanisms dominating benthic iron release. Examining the iron species having different characteristics in terms of chemical, physical and biological reactivities is required to understand the faith of the released iron (P. W. Boyd & Ellwood, 2010a; Tagliabue et al., 2017). Considering the scarce levels and of iron in seawater and impact of sample handling, only with fast on-board detection methods, sub-species for iron can be studied.

1.1 Aim of the Study

The Black Sea is the biggest euxinic basin and is known to be anoxic for thousands of years. The iron release from the Black Sea shelf is a component of "iron-shuttle" mechanism which transports iron from the shelf towards the deeper basin laterally. Additionally, the Black Sea has different well-established redox zones at the seafloor corresponding to favored condition for benthic iron release. The Sea of Marmara having recent deoxygenation is under our focus to examine the current redox state and its potential to source iron from the sea floor.

Briefly, the Black Sea is an ideal location to study iron biogeochemistry and to build on earlier studies and the Sea of Marmara is an optimum area to apply same approaches to assess the redox states of these two similar but unique areas. With this approach, with this thesis work, studying the benthic iron mobilization patterns over the redox gradients of the Sea of Marmara and the Black Sea was aimed.

1.2 Significance of Iron

Life in the oceans is supported by a multitude of elements including nitrogen, phosphorus, and silicon - the major and minor limiting nutrients in the oceans. Trace metals, including iron, gained its importance in oceanography quite late compared to these nutrient elements due to the detection challenges in seawater. Hence, the essentiality of iron in primary production processes was overseen until 1990s so-called Iron Age in Oceanography (Coale et al., 1999). On the other hand, only after the advancements in technology, first iron profiles as dissolved and particulate iron in seawater was reported in 1982 (Gordon et al., 1982), different iron fractions and pools could be studied and the importance of iron in marine systems could be revealed (von der Heyden & Roychoudhury, 2015). The nutrient-like profile of the iron in the water column hinted that the iron is strongly controlled by the biological uptake and remineralization. Scavenging of iron in the column decrease the amount of the available iron and the balance between biological uptake, remineralization and

scavenging creates a hybrid type of distribution (Lohan & Tagliabue, 2018). The intact relation between iron and C, O, P, N, S, Mn is revealed with more findings about the characteristic features of iron cycle (Raiswell & Canfield, 2012).

Idea of iron acting as a limiting factor on primary production appeared firstly in the studies of high nutrient low chlorophyll areas (the Southern Ocean, the eastern equatorial Pacific, the subarctic Pacific) which was not understood well at the time. Iron was claimed to be limiting factor in HNLCs along with temperature and light (Gran, 1931) supported with the observations of incubation experiments. After about a half century, the iron enrichment exhibited that the iron might be limiting nutrient for marine production in HNLC regions (J. H. Martin & Fitzwater, 1988). Followed by in-situ iron-fertilization studies, iron was approved to be a limiting nutrient (Philip W. Boyd et al., 2000; de Baar et al., 2005). Besides being a limiting nutrient, iron had critical role during glacial times by inducing higher biological pump activity (J. H. Martin & Michael Gordon, 1988). On top of understanding the importance of iron for marine production, impact of iron cycle on net primary production and higher trophic levels under future climate change scenarios took attention and started to be included in model studies for open ocean projections (Tagliabue et al., 2020). Within a wider point of view now, marine iron cycle has effect on production, phytoplankton ecosystems (larger cells -diatom- favored) and even on evolution of higher trophic levels.

Iron's relation with the primary production is because of the co-factor nature of the iron that takes role in photosynthesis. Among other important biological processes, iron is also a co-factor for nitrogen fixing enzymes which couples the nitrogen and iron cycle (Raiswell & Canfield, 2012). On the one hand, iron can increase primary production activity via direct fertilization and via inducing more fixed nitrogen by stimulating nitrogen fixation (Mark Moore et al., 2009; J. K. Moore et al., 2001). On the other hand, iron may decrease primary production by scavenging phosphorus in the water column via adsorption. Adsorbed phosphorus onto iron oxyhydroxide particles transports the phosphorus to sediment and release it back upon reduction of

iron (Raiswell & Canfield, 2012). Furthermore, iron is an electron acceptor that can be involve in reductive iron respiration of organic matter under anoxic conditions.

Iron reductive respiration (Bethke et al., 2011):

$CH_3COO^- + 8FeOOH(s) + 15\ H^+ \rightarrow 8\ Fe^{+2} + 2HCO_3^- + 12\ H_2O$

Iron respiration is strongly linked to manganese and sulfur cycles as well which are other anaerobic electron acceptors; overall iron and it's linkage with the other electron acceptors has impacts on marine carbon storage (Donald E. Canfield et al., 1993). Some of the major reactions occurring between other redox sensitive species are given below (Kappler et al., 2021):

$Fe^{+2} + O_2 + 4H^+ \rightarrow Fe^{+3} + 2H_2O$ Iron oxidation by oxygen

$4Fe^{+2} + 2NO_2^- + 5H_2O \rightarrow 4FeOOH + N_2O + 6H^+$ Iron oxidation by nitrite

$2Fe^{+2} + MnO_2 + 2H_2O \rightarrow Mn^{+2} + 2FeOOH + 2H^+$ Iron oxidation by manganese

$2FeOOH + 3H_2S \rightarrow 2FeS + S^0 + 4H_2O$ Iron reduction by hydrogen sulfide

On top of the modern ocean biogeochemical cycle, iron was also a crucial element in the Earth's evolution. One of the core hypothesis for the emergence of life is the hydrothermal vents are a potential site for hosting the first forms of life (W. Martin et al., 2008; Russell & Hall, 2006). Remaining of an ancient iron metabolizing bacteria found in hydrothermal vent precipitates dated back to 3.7-4.2Ga suggests that iron and hydrothermal vent areas were key members of life in the ocean since the beginning (Dodd et al., 2017). Recent studies aiming to understand metabolic evolution with respect to metal availabilities in ancient oceans by combining genetic studies with biogeochemistry clarifies that key co-factor metals and their redox dynamics was and still important to understand the essence of life (Garcia et al., 2020; E. K. Moore et al., 2017). Fe, Mn, Mo, W, Cu, Ni, Co, Zn and V can be counted as the key co-factor metals throughout the history (Broderick, 2015). Among these cofactors, iron is one of the most common co-factors for most of the fundamental redox processes such as sulfate/sulfur reduction, methanogenesis/methane oxidation,

nitrification/denitrification, oxygenic/anoxygenic photosynthesis. Therefore, iron is also utilized by microbial life to be incorporated in the enzymes on top of having a role as electron acceptor/donor in fundamental redox processes. These redox biogeochemical processes caused significant changes in the Earth's history. For instance, emergence of oxygenic photosynthesis, required incorporation of Fe and other metals which in return expanded the oxidative redox potential range for biology and consequently shifted the redox state of Earth (E. K. Moore et al., 2017). Shortly, the biogeochemical redox regulation exerted by the redox species and life can be untangled by only understanding the linked cycles of each. Iron as one of the most important key co-factor and electron acceptor hosted and shaped the evolution of Earth, oceans, and life.

1.3 The General Characteristics of the Black Sea

1.3.1 Hydrography, Water Masses and Circulation in the Black Sea

The Black Sea is a semi-enclosed system and fed with only Mediterranean seawater from the Marmara, via the Bosphorus while receiving large amount of riverine inputs. The water mass budget of the Black Sea is dependent on riverine input, precipitation, evaporation and, deep inflow and surface outflow via the Bosphorus. The freshwater inputs exceed the loss by evaporation and the remaining compound of the water budget is out flowed through the Bosphorus. The fresh water inputs shows seasonal and interannual variability (Özsoy & Ünlüata, 1997; Ünlülata et al., 1990). Dramatic difference in salinity of the water sources of the Black Sea creates a two-layered (surface water salinities < 18 ppt; deeper water salinities = 22 ppt) sea with limited mixing in between due to permanent halocline (Oguz et al., 1992). The density stratification is determined by salinity, except for near surface which temperature effect is more pronounced, pycnocline and halocline coincides at the depths of 100-200m. The extent of mixing is controlled by these coincident clines and consequently builds oxycline and chemocline at the same density layers. The

seasonality in the upper water column is observed as a seasonal thermocline in the first 30 m and followed by the Cold Intermediate Layer along the profile with core temperatures of 6°C and the upper and lower CIL boundaries are described as 8°C isothermal layer (J. W. Murray et al., 1991). Deeper water parts below the halocline does not exhibit seasonal variabilities (Oguz et al., 1991). The surface waters are physically controlled by the circulations given in Figure 1. The general circulation has the characteristics of being mainly cyclonic, time dependent and having basin wide spatial structures. One of the major seasonal/interannual components is Rim Current flowing along the margin of the Black Sea. The interior of the Rim Current is controlled by the multi-centered cyclonic cells and in between the Rim Current and coast, by a series of anti-cyclonic eddies (Oguz et al., 1993).

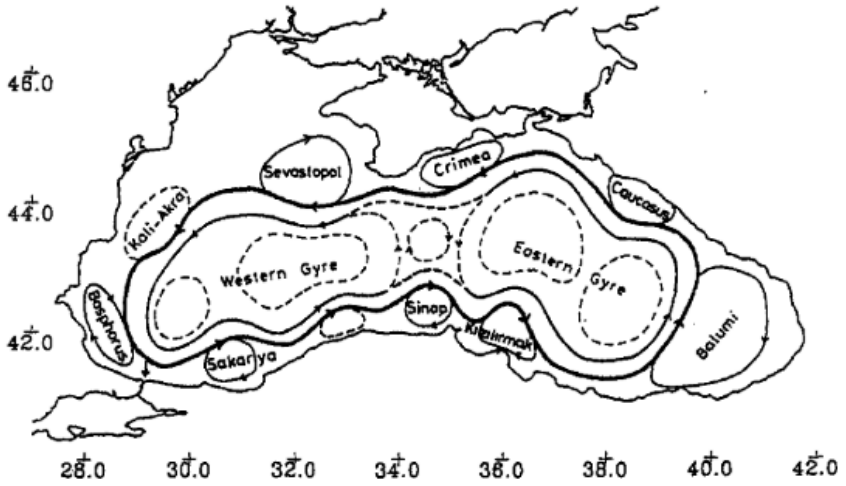

Figure 1: General circulation in the upper layer of the Black Sea. (Oguz et al., 1993)

1.3.2 Redox Layers in the Black Sea

Riverine inputs stimulate primary production on the surface and consumes oxygen in the bottom layer as a consequence of exportation of the produced organic matter. The strong stratification limits the O_2 ventilation to bottom layer and dissolved hydrogen sulfide accretion occurs up to 400 μM levels in the deepest parts (Codispoti et al., 1991; Tugrul et al., 1992). In between the two distinct layers, a unique

transitional “sub-oxic” layer exists with <10uM dissolved oxygen and <0.3uM dissolved hydrogen sulfide (James W. Murray et al., 1999; James W. Murray & Yakushev, 2006; Yemenicioglu et al., 2006a). As a result, Black Sea is an euxinic area hosting various anoxic respiration pathways below oxycline and exhibits large redox layers up to hydrogen sulfide production at the bottom, see Figure 2.

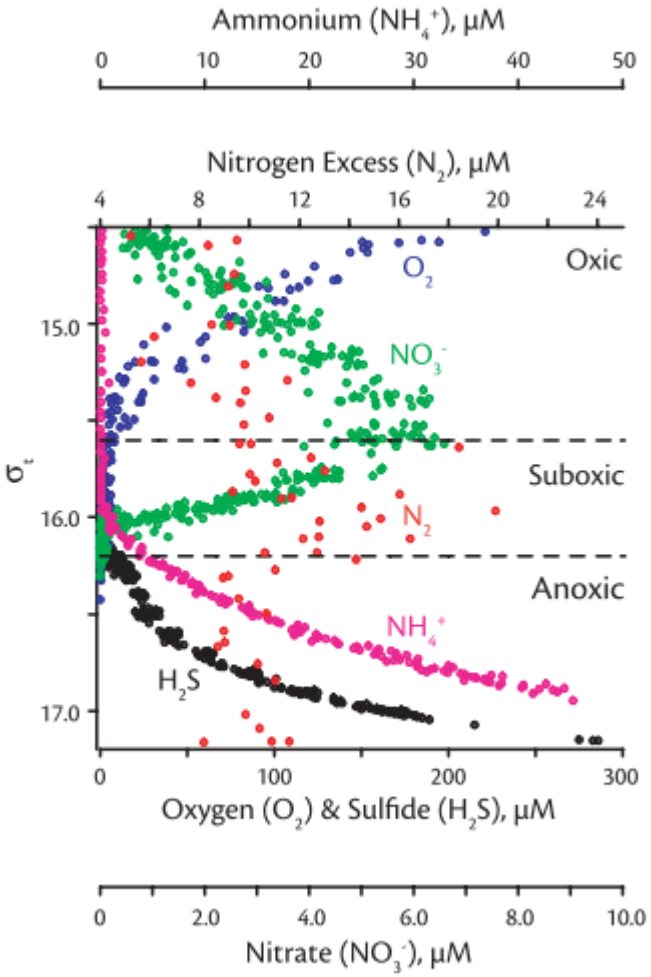

Figure 2: Redox biogeochemical structure of the Black Sea water column (Konovalov et al., 2005).

Black Sea is the largest area in the world being euxinic and special for being euxinic for over thousands of years (Deuser, 1974; Glazer et al., 2006; Piper, 2016; Piper & Calvert, 2011; Wilkin et al., 1997). Because of the natural characteristic features, the Black Sea has become an interest in oceanography since 1980s (Codispoti et al.,

1991) and now it is a well-established area to study iron in different redox conditions in seawater and sediment. For instance, because the sub oxic layer enables iron dissolution in seawater, the analysis of dissolved and particulate iron in the seawater is less challenging compared to open ocean studies (Lewis & Landing, 1991b). The dissolved iron levels in sub oxic seawater are significantly higher than oxic seawater average levels, the former being around 300nM (dFe<0.4um) (Haraldsson & Westerlund, 1988; Lewis & Landing, 1991a; Yemenicioglu et al., 2006b). Moreover, the sedimentary iron studies have shown that except for sulfidic sea floors, the anoxic areas in the Black Sea is a hotspot for reductive dissolution of Fe (Kraal et al., 2019; Scholz et al., 2014a). The transport of the dissolved iron from the shelves of the Black Sea to sulfidic basin is a well-known process, known as "shuttling" (Donald E. Canfield et al., 1996; W. K. Lenstra et al., 2019). Porewater sediment biogeochemistry in terms of iron has started to be studied since 2001 with increasing number of studies (Konovalov et al., 2007; Jeroen W.M. Wijsman et al., 2001). The relatively higher dissolved iron levels in the sediment porewaters (dFe~100uM) of suboxic sea floor implicated that the sediment porewaters are a source for water column iron (dFe~200-300nM) (Konovalov et al., 2007). The transport of this iron from shelf acts on the sulfur cycle in the anoxic basin and creates an interconnection between the different redox areas of the basin and the depositional layers within the sediment (Yücel, Konovalov, et al., 2010). The interplay between the carbon and coupled Mn-Fe-P-S cycles in the Black Sea was studied extensively (Kraal et al., 2019; Yücel, Luther, et al., 2010).

1.4 Boundaries and Thresholds of Redox Layers

Redox thresholds and related terminology have various definitions which weakens a consistent classification. For this reason, in this thesis work, the following thresholds are taken as the limits of redox conditions, see Figure 3.

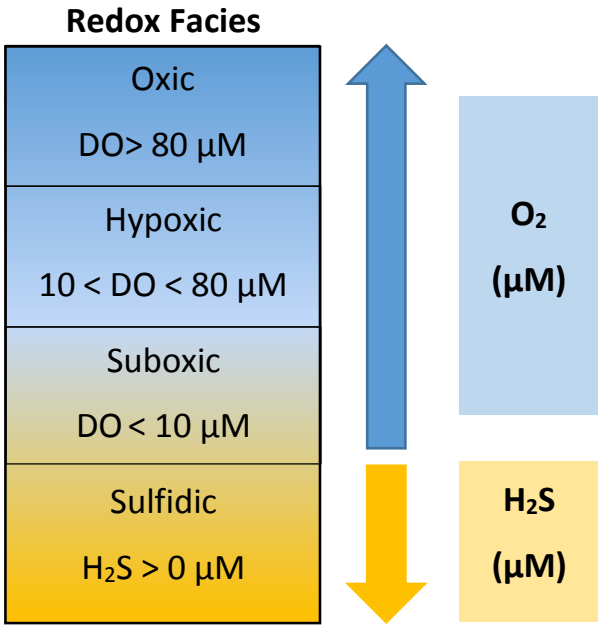

Figure 3: Referred redox thresholds in this thesis work. The structure of the scheme is sourced by Algeo & Li (2020).

The redox conditions referring to "suboxic" is defined as the DO <10 µM as defined by James W. Murray and coworkers (1999). For the hypoxia threshold, DO < 2 ml/l threshold used in the literature is taken which corresponds to ~89 µM (Diaz & Rosenberg, 2008; Yakushev & Newton, 2013). The presence of dissolved hydrogen sulfide is described as sulfidic and the oxygen levels higher than 89 µM are classified as oxic conditions at the sea floor.

1.5 Vertical Distribution and Cycling of Elements (O, N, P, C, S, Mn, Fe)

The vertical distribution of carbon, oxygen, phosphorus, nitrogen, sulfur, manganese, and iron is controlled by the abiotic and biotic reactions occurring along the water column and continues in the sediment porewaters. The zonation is determined mainly by the thermodynamics of the metabolic pathways of organic matter degradation reactions, see Figure 4 (Jorgensen, 2006).

Pathway and stoichiometry of reaction	ΔG^0 (kJ mol^{-1})
Oxic respiration:	
$[CH_2O] + O_2 \rightarrow CO_2 + H_2O$	-479
Denitrification:	
$5[CH_2O] + 4NO_3^- \rightarrow 2N_2 + 4HCO_3^- + CO_2 + 3H_2O$	-453
Mn(IV) reduction:	
$[CH_2O] + 3CO_2 + H_2O + 2MnO_2 \rightarrow 2Mn^{2+} + 4HCO_3^-$	-349
Fe(III) reduction:	
$[CH_2O] + 7CO_2 + 4Fe(OH)_3 \rightarrow 4Fe^{2+} + 8HCO_3^- + 3H_2O$	-114
Sulfate reduction:	
$2[CH_2O] + SO_4^{2-} \rightarrow H_2S + 2HCO_3^-$	-77
$4H_2 + SO_4^{2-} + H^+ \rightarrow HS^- + 4H_2O$	-152
$CH_3COO^- + SO_4^{2-} + 2H^+ \rightarrow 2CO_2 + HS^- + 2H_2O$	-41
Methane production:	
$4H_2 + HCO_3^- + H^+ \rightarrow CH_4 + 3H_2O$	-136
$CH_3COO^- + H^+ \rightarrow CH_4 + CO_2$	-28
Acetogenesis:	
$4H_2 + 2CO_3^- + H^+ \rightarrow CH_3COO^- + 4H_2O$	-105
Fermentation:	
$CH_3CH_2OH + H_2O \rightarrow CH_3COO^- + 2H_2 + H^+$	10
$CH_3CH_2COO^- + 3H_2O \rightarrow CH_3COO^- + HCO_3^- + 3H_2 + H^+$	77

Figure 4: Thermodynamically ordered metabolic pathways of organic matter degradation (Jorgensen, 2006).

Zonation accompanies redox stratification along a decreasing redox potential gradient. The redox interactions at the interfaces determines the cycling and the distribution of key redox species along the column (Kappler et al., 2021).

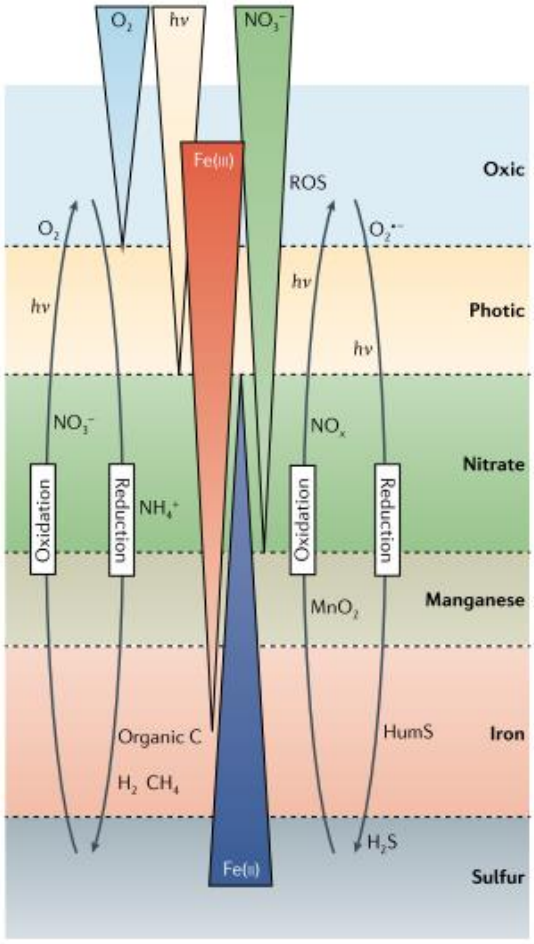

Figure 5: A scheme of redox stratified environments (Kappler et al., 2021)

The Black Sea water column characteristics shows strong redox stratification and zonation is observable along the water column down to sulfate reduction at the bottom. In the Sea of Marmara, upon deoxygenation, the following redox zones starts to appear, for instance Izmıt Bay exhibited sulfidic characteristics indicating high levels of sulfate reduction at the bottom waters, see section 2.2.

1.6 The General Characteristics of the Sea of Marmara

The Sea of Marmara is located in between the Black Sea and the Mediterranean Sea by the Bosphorus and the Dardanelles straits, respectively. The bottom layer is fed by the denser, warmer and more saline Mediterranean waters (salinity = 38ppt) while

the surface layer is fed by the Black Sea nutrient rich, less saline and buoyant waters (salinity = 18ppt). These interconnected marine system is called Turkish Straits System (Beşiktepe et al., 1994; Ünlülata et al., 1990). The resulting halocline forms a dominates density stratification and forms a permanent pycnocline which prevents mixing between layers. The turbulent entrainment cause exchange between the two layers and the upper layer salinity varies along the surface from Dardanelles towards to the Bosphorus. The strongest impact is created at the onset of the jet inflow from the Black Sea. The surface circulation is dominated by anticyclonic gyre which is driven by the sea-surface level differences between the Black Sea and the Aegean Sea. The jet inflow from the Black Sea creates additional impact on the surface circulation depending on the winter wind stress and seasonal variations. The entrance of Mediterranean waters from the Dardanelles dominates the sub-halocline circulation. Both layers of the circulations vary with seasonality. The Mediterranean intrusions are most pronounced at the western part of the basin thus, the minimum salinity and oxygen zones placed at the eastern basin (Beşiktepe et al., 1994).

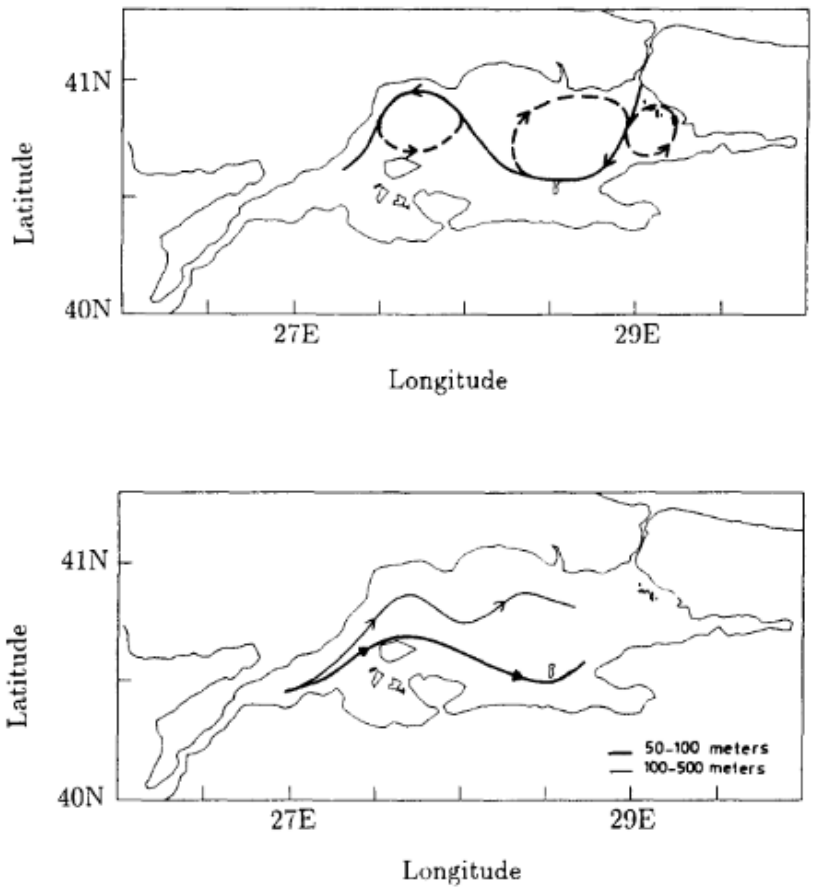

Figure 6: Circulation patterns in the Sea of Marmara: (top) surface circulation; (below) circulation below the halocline (Beşiktepe et al., 1994).

The sea of Marmara was reported be experiencing the anthropogenic stress from the surrounding urban areas since the 1970s (Ediger et al., 2016) and the dissolved oxygen levels below the euphotic zone was reported to be declining drastically to form "oxycline" since 2000s (Yilmaz, 2002). Similar to Black Sea's permanent pycnocline structure inhibits oxygen ventilation to deeper layers, the two-layered system in the sea of Marmara restricts the oxygen ventilation from the surface. Despite the bottom layer is fed by oxygen rich Mediterranean waters, the oxygen input cannot compensate the oxygen consumption by the organic matter degradation (Beşiktepe et al., 1994; Tuğrul et al., 2002). In this aspect, especially the eastern part of the sea of Marmara, having less exposure to oxygen-rich Mediterranean waters, reported to be experiencing significant decreases in the bottom water oxygen levels to hypoxic limits over the last 20 years (Yucel et al., 2020; 2021;Ediger et al., 2016;

Hélène et al., 2020). The iron in the sediments' solid phase was studied broadly to assess the pollution (A. O. Algan et al., 1999; O. Algan et al., 2004; Balkis & Çağatay, 2001; Ergin et al., 1991; Mülayim et al., 2012; Okay et al., 2008; Topcuoğlu et al., 2004) however porewater dissolved iron studies was missing. Only pore water geochemistry involved study aimed to study sulfate-methane transition zone depth did not report any data. Thus, the sea of Marmara is a potential area for benthic iron release however it is understudied in terms of biogeochemical dynamics and redox mechanisms.

1.7 Overview of Marine Iron Cycle and Sources

Iron is scarce in oceans, being less than 0.2 nmol/kg and 0.07nmol/kg on average at the surface waters. Below depth of 500m, the iron concentration is about 0.76nmol/kg (Johnson et al., 1997), however the distribution of iron is not homogenous. Strong regional variations are associated with the regionality of major iron sources: atmospheric (meridional distribution), hydrothermal fluids (mainly around ridges) and coastal and shallow sediments i.e. atmospheric dust input is predominant in low-latitudes while in higher latitudes continental margin and hydrothermal iron sources are more important (Tagliabue et al., 2014a, 2017).

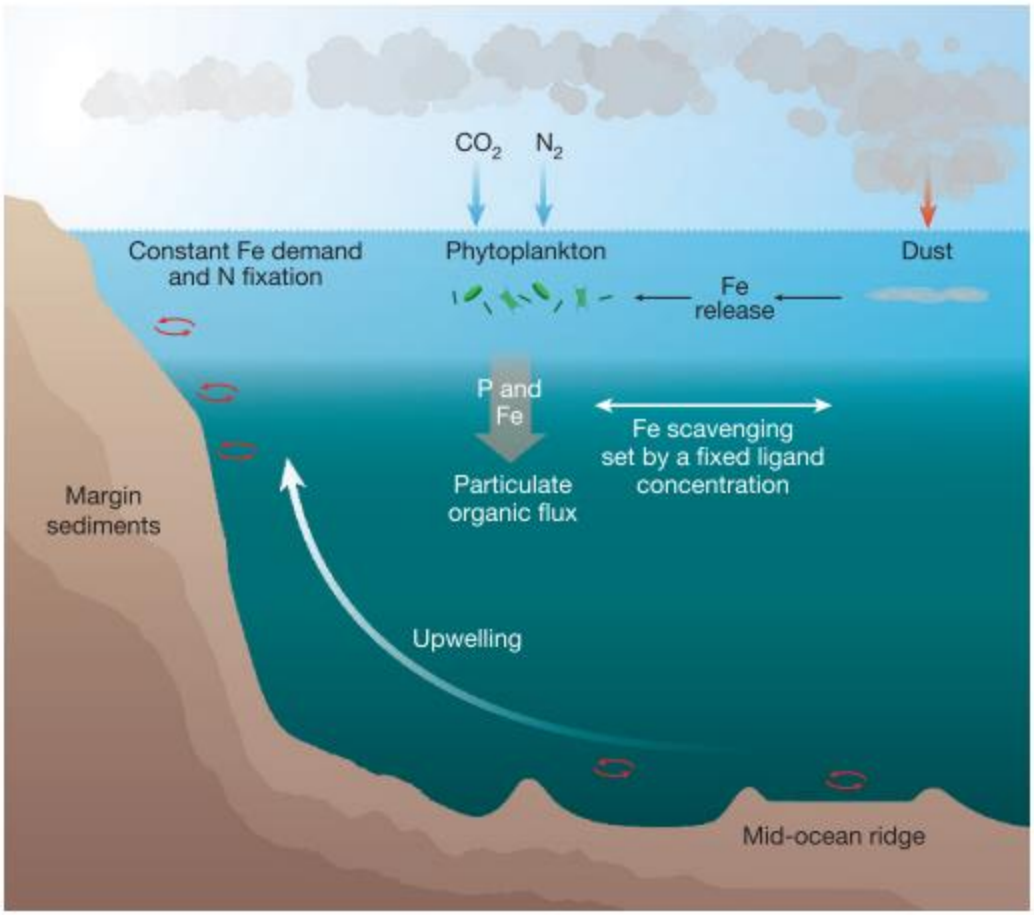

Figure 7: A scheme of marine iron cycle (Tagliabue et al., 2017)

According to result of a model study by Tagliabue (2014b), the integral iron inventory contributions partitioning between sedimentary, hydrothermal and atmospheric dust is 74%, 23% and 2%, respectively. However, for carbon export from the euphotic zone, the partitioning changes between dust and hydrothermal sediment as the contributions of 79–81% from sedimentary, 12–16% from dust input and 3% from hydrothermal vent. The distribution is controlled by the processes of stabilization by ligands and different lifetime of iron species which determines the effective distance scale of the source (Tagliabue et al., 2017). Because iron originated from hydrothermal fluids and coastal sediments is thought to have only local effect and, higher solubility of aeolian iron, predominant iron source was thought to be atmospheric dust on the surface waters and in iron cycle (MOORE et

al., 1984) [Moore et al., 2002; Fung et al., 2000; Archer and Johnson, 2000; Aumont et al., 2003]. However, recent studies, controls and stabilization on different iron pools indicates that these sources have bigger parts in marine iron cycle than it was assumed to be (Elrod et al., 2004). To understand the further transport of iron, fractions of iron was aimed to be understood since the different fractions of iron has different half-life and durability (P. W. Boyd & Ellwood, 2010a). Especially organically complexed iron in the oxidized form can remain in the dissolved pool as colloids in stabilized forms enhancing the durability of the mobilized iron. The colloidal fraction of iron is an important fraction of upper water column iron inventory (von der Heyden & Roychoudhury, 2015). Size fraction studies reveals more on the characteristics of different iron sources. The sFe and cFe in the upper column decouples significantly during the spring time due to seasonality of biological uptake and surface iron supply from atmosphere (von der Heyden & Roychoudhury, 2015). The hydrothermal and benthic sources however are not affected by the seasonality.

Until the beginning of 2000s, hydrothermal input for iron cycle was perceived as a local source because of the acceptance that iron was being oxidized and settled around the vent area thus not being dispersed in ocean. In 2006, the iron source for deep ocean of Pacific was shown to be mostly due to hydrothermal activity originating from the fast spreading East Pacific Rise (Chu et al., 2006). Following this, the observations of unexpectedly high dissolved iron concentrations around the hydrothermal vent areas (Bennett et al., 2008) showed that dissolved iron can be stabilized in the forms of organic complexes or colloids which contradicts the idea of iron being precipitated and sink back to the ground. Detailed iron measurements in major ocean areas (Chever et al., 2010; Klunder et al., 2012; Saito et al., 2013) and further, the correlation between the higher iron anomalies in the water column and ^{3}He which is a tracer for vent fluids near the East Pacific Rise (Fitzsimmons et al., 2014) clarified the hydrothermal vent iron inputs had larger impacts enhanced by the formation of more durable species (Tagliabue et al., 2010). Fitzsimmons et al., (2014) showed that in the abyssal of southeast to southwest transect of Pacific Ocean

had 0.4-0.9 nmol/kg higher dissolved iron than global average levels sourced by hydrothermal vents. Studies focusing on the stabilization of dissolved iron by organic complexation (Bennett et al., 2008; Hawkes et al., 2013; Toner et al., 2009) and colloidal nanoparticles (Findlay et al., 2019; Yücel et al., 2011, 2021) shown that iron inputs from the deep ocean can deliver iron without removal resulting in higher spatial and temporal effectiveness. These studies reassures that the outcomes of similar approaches onto benthic iron sources can enhance the global iron cycle studies.

Benthic release and transport of iron from continental shelf sediments is one of the major iron source in global ocean iron cycle (Lyons & Severmann, 2006; Raiswell & Canfield, 2012). The production of dissolved iron in the sediments porewater is mainly controlled by reductive dissolution of iron coupled to organic matter degradation (Burdige, 1993). Produced dissolved iron can either take place in diagenetic reactions in sediment or can be released to overlying bottom waters (Burdige, 1993; Wytze K. Lenstra et al., 2021; Raiswell & Canfield, 2012). Diagenetic controls such as precipitation by sulfur to form authigenic minerals of Fe-S immobilizes iron and inhibits its release to overlying waters (Berner, 1984). The dissolved iron release to overlying waters is favored by low-oxygen and non-sulfidic conditions (W. B. Homoky et al., 2011; Pakhomova et al., 2007; Scholz et al., 2014b). Under long-term oxygen depletion and anoxia, the oxidized iron deposition onto the surface of the sediment is limited and thus the dissolved iron release is restricted (Slomp et al., 1997; J. W.M. Wijsman et al., 2001). Although the mobilized dissolved iron can be transported to overlying waters, it can be re-oxidized and remain in the suspension or settle down to sediment surface leading to a cycle at the sediment surface called “refluxing” (Adelson et al., 2001). Bio-irrigation increases the flux from porewaters to overlying waters (W. K. Lenstra et al., 2019). Thus, iron mobilization patterns under changing redox conditions are important to identify so that the scale of sedimentary iron sources can be understood better.

Upon already known characteristics of different iron sources, their impact scale, durability to different mechanisms and conditions remains to be unrecognized.

Within sedimentary iron release, how and to what scale the various and shifting redox conditions affecting the form and the amount of iron is yet to be answered.

1.8 Objectives

This thesis is structured around these central questions and aiming to resolve the following 4 objectives:

1) To identify for the first time the benthic iron flux patterns in the Black Sea and in the Sea of Marmara over various redox conditions,
2) To improve the shipboard and fast detection of dissolved iron species in marine porewaters and seawater,
3) To compare the Sea of Marmara - a newly developing hypoxic sea - with the other hypoxic and iron-rich areas in Earth Oceans
4) To propose controls on the partitioning between colloidal and soluble phases of benthic iron and their role in seafloor iron mobilization under hypoxic areas.

CHAPTER 2

MATERIAL METHOD

2.1 Study Area

2.1.1 December 2020 R/V Bilim-2 Cruise

2.1.1.1 Stations of porewater and size fractions in December 2020 cruise

In December 2020, we visited 9 stations and sampled the water column with CTD operations in order to have bottom water conditions before the sediment sampling (Figure 8). The seawater salinity, temperature, density and dissolved oxygen were measured by in-situ sensors of SEABIRD CTD Probe, and the seawater samples were obtained from the selected depths by the remotely controlled Niskin bottles via the 12- bottle Rosette System of CTD Probe. Stations selected as: 3 in southwestern shelf of the Black Sea as one transects, and 6 in the Sea of Marmara as two transects (Figure 9). Transects were selected to investigate oxic, hypoxic, suboxic and sulfidic conditions of the Sea of Marmara and the Black Sea.

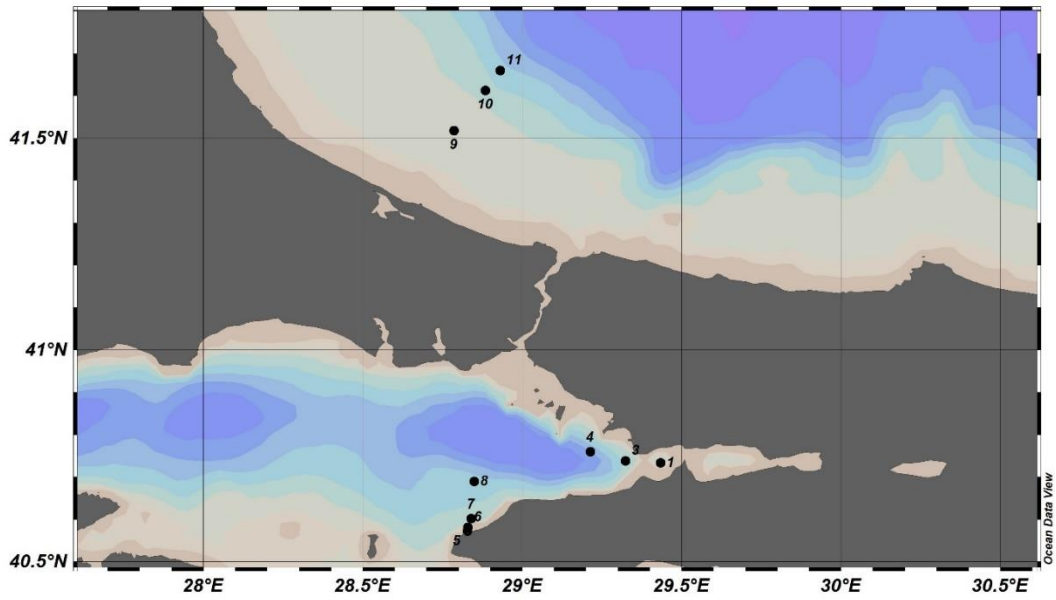

Figure 8: Map of stations visited for water column sampling in December 2020 R/V Bilim-2 Cruise.

After water column studies, we revisited the station areas to sample sediments by deploying the Multi Corer (Oktopus, Kiel). For sediment sampling, we revisited 9 stations given in Figure 9 in red dots (for station 11, we sampled one more sulfidic station to obtain a better-quality sediment core named as 11C). These sediments were sampled for dissolved iron, dissolved hydrogen sulfide, nutrients, and major ions in porewater. Dissolved iron and hydrogen sulfide analysis done on-board so that the stations for size-fractionation analysis. Nutrients and major ions in porewater and solid-state samples were stored for onshore analysis. After porewater dissolved iron results obtained on-board, we revisited 3 stations to sample for size fractionation analysis of dissolved iron pool (green dots in Figure 9).

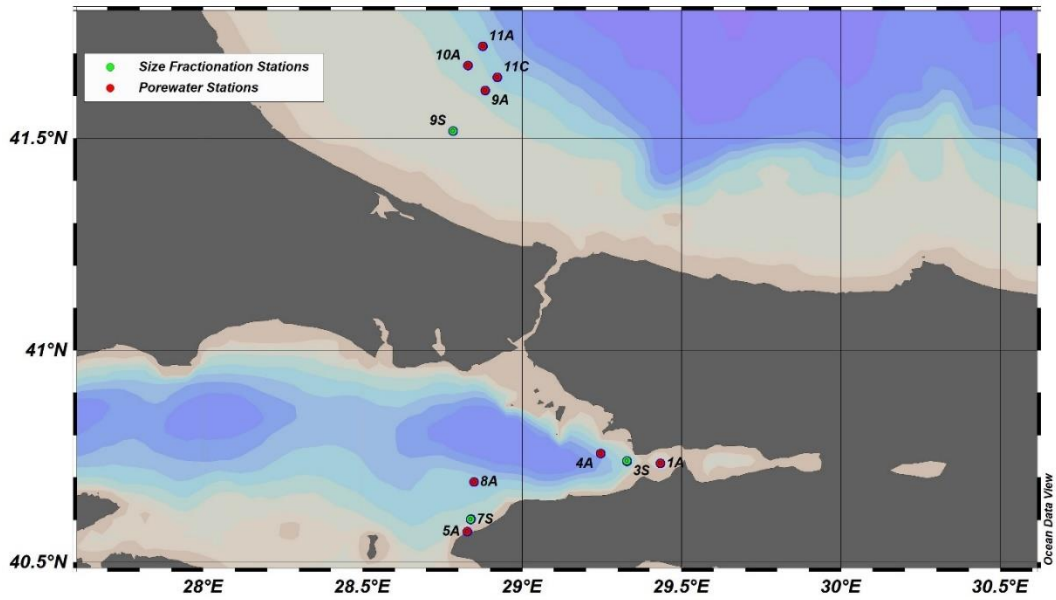

Figure 9. Map of stations visited for porewater sampling in December 2020 R/V Bilim-2 Cruise. Red dots are the stations sampled for nutrient, major ions, dFe and H_2S analysis in porewater and green dots are the stations revisited to sample for only size fractionation of dissolved Fe in porewater.

2.1.1.2 Stations of seawater iron in December 2020 cruise

In December 2020, we visited 6 stations in Black Sea and in the Sea of Marmara to sample seawater for dissolved iron measurements (Figure 10). In the Sea of Marmara stations, we also sampled seawater for particulate iron(<1.0μm) analysis.

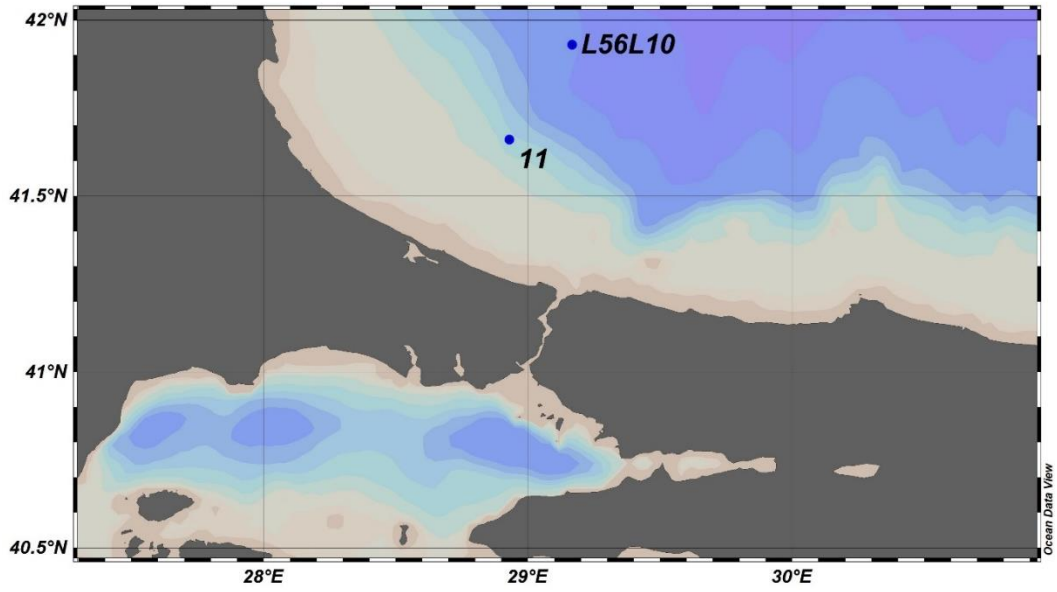

Figure 10: Seawater stations for particulate iron (<1.0µm) analysis in December 2020 R/V Bilim-2 Cruise.

2.1.2 June 2021 R/V Bilim-2 Cruise

2.1.2.1 Stations of porewater and size fractions in June 2021 cruise

In June 2021, we visited 11 stations and sampled the water column with CTD operations, likewise December 2020 cruise (Figure 11). Stations selected as: 3 in southwestern shelf of the Black Sea as one transects, 3 in shelf in east of Bosphorus in the Black Sea as one transects and 5 in the sea of Marmara as 1 transect (Figure 12). The Black Sea transects was selected as 3 main stations in each transect representing oxic, suboxic, hypoxic and sulfidic seafloors. The Sea of Marmara stations studied as 1 transect along the Izmıt Bay which is sulfidic at the bottom to Çınarcık Basin which is suboxic. After water column studies, we revisited the stations to sample sediments by deploying the Multi Corer (Oktopus, Kiel). These sediments are sampled for dissolved iron, dissolved hydrogen sulfide, nutrients, and major ions in porewater. Nutrients and major ions in porewater and solid-state

samples are stored for onshore analysis. Dissolved iron and hydrogen sulfide analysis done on-board. In this cruise, no size fractionation sample in porewater was taken.

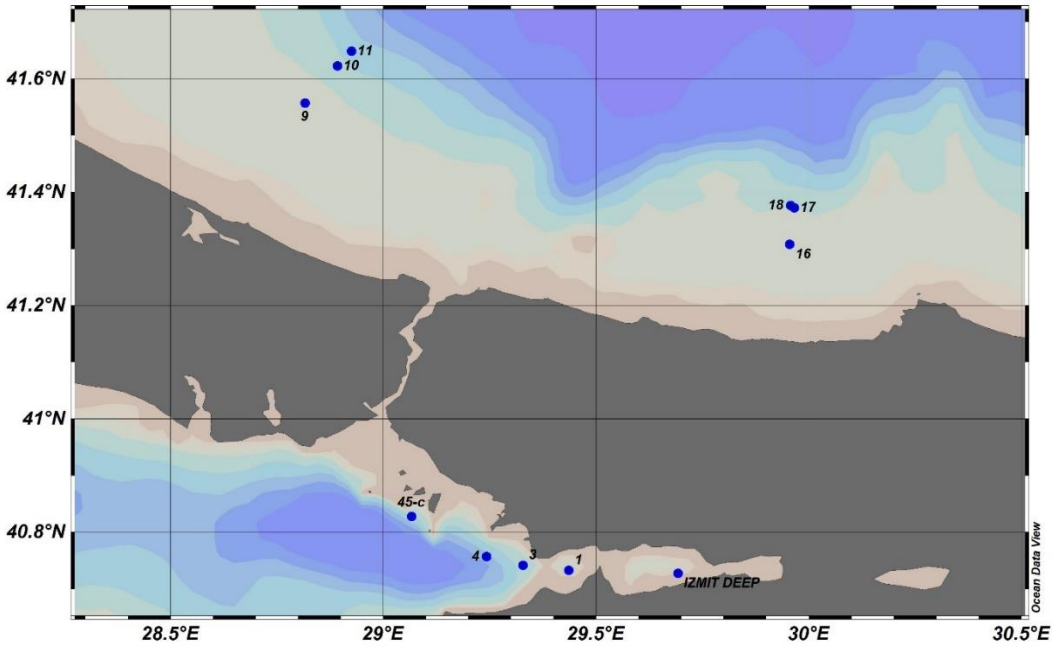

Figure 11: Map of stations visited for water column sampling in June 2021 R/V Bilim-2 Cruise.

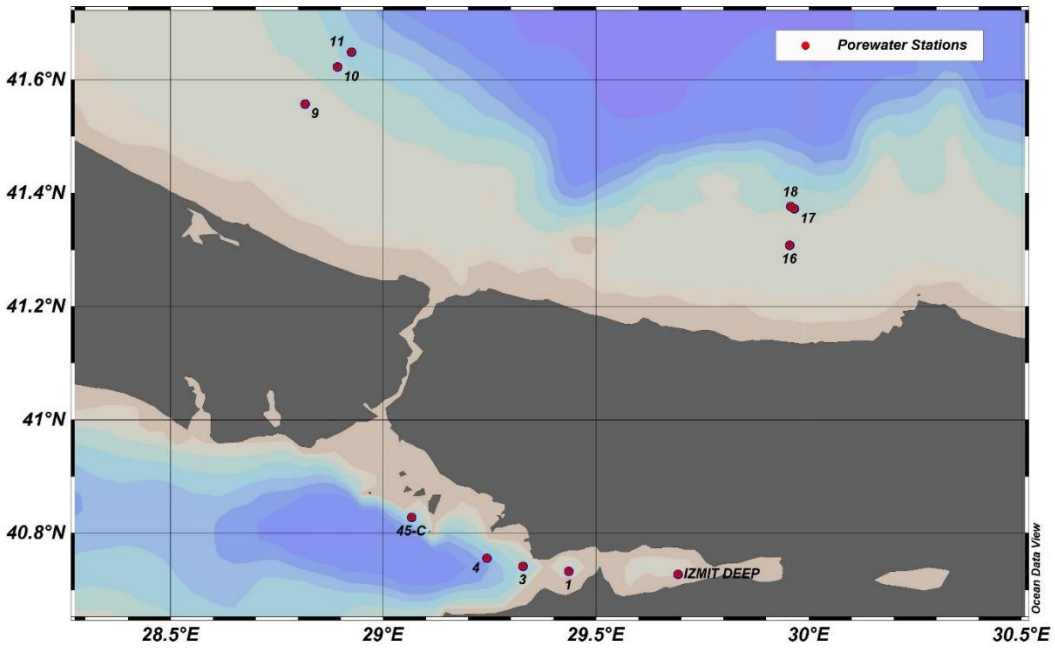

Figure 12: Map of stations visited for porewater sampling in June 2021 R/V Bilim-2 Cruise. Red dots are the stations sampled for nutrient, major ions, dFe and H2S analysis in porewater.

2.1.2.2 Stations of seawater iron in June 2021 cruise

In June 2021, we visited 3 stations to sample iron in seawater (Figure 13). In the Black Sea stations, we also sampled sub-oxic layer in 3 depths for further analysis of size fractionation in seawater.

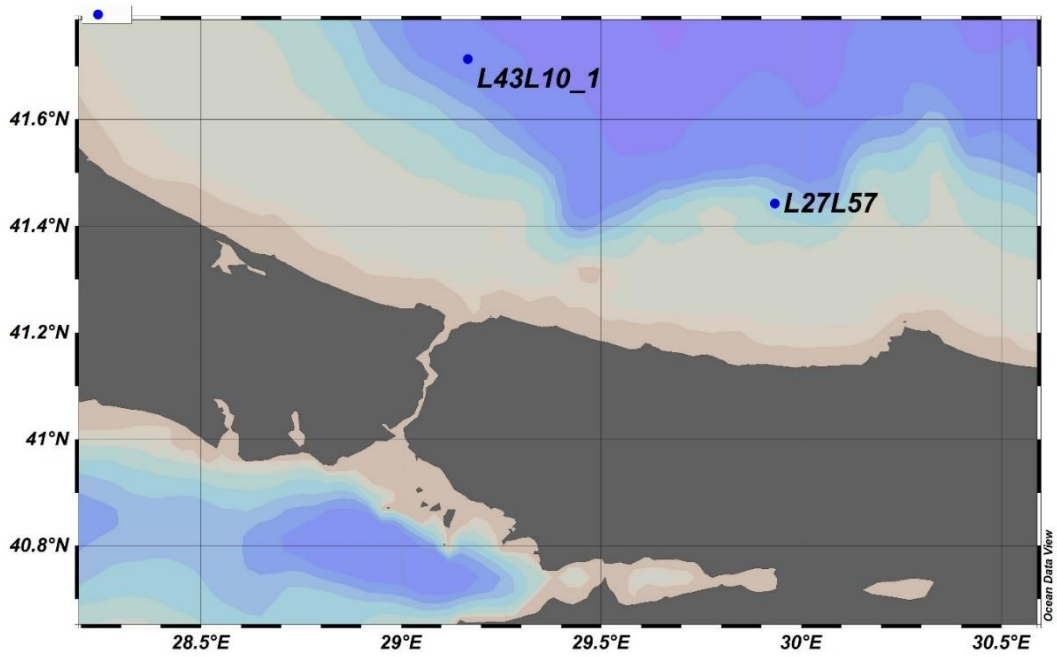

Figure 13: Seawater stations for dissolved iron (<0.45µm) and size fractionation (colloids and soluble phase) analysis in June 2021 R/V Bilim-2 Cruise.

2.2 Bottom Water Biogeochemistry in Stations Sampled for Porewaters and Size Fractions

In each station, CTD operation was conducted to measure oceanographic parameters such as salinity, temperature, and dissolved oxygen as well as to sample seawater in the water column above the target sedimentary area. Samples were obtained for dissolved oxygen, nutrients, and dissolved hydrogen sulfide (only in

sulfidic/expected to be sulfidic stations) and the samples were analyzed on board as quickly as possible after retrieval. Sediment and porewater sampling stations were chosen according to bottom conditions of our research area. In Figure 14, bottom water conditions during December 2020 cruise are shown which were used in the selection of sediment core locations. In line with the objectives of this thesis work, we have chosen 2 hypoxic areas in Marmara: Armutlu and Izmıt Bay. These areas corresponding to the southern and eastern rim of the Çınarcık Basin and both areas have similar DO conditions at the bottom however, in terms of nitrate concentrations, Armutlu Transect differs from Izmit Transect with higher NO_3^- distribution at the bottom. Thus, the two areas represent different redox states in the Marmara Sea. In Black Sea, however, selected stations were chosen to the better-known classification of as oxic, suboxic and sulfidic bottom water conditions, hence yielding in three stations corresponding to these conditions.

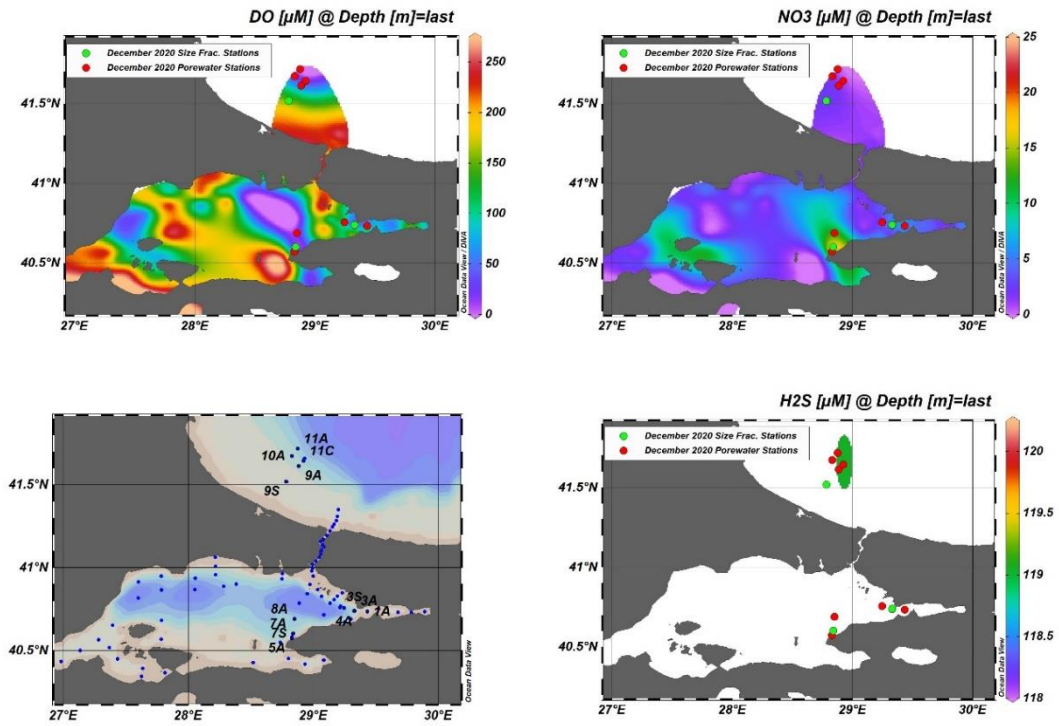

Figure 14: December 2020 R/V Bilim-2 Cruise stations given over bottom water DO, NO_3^- and H_2S concentrations indicating redox conditions.

In each transect, we selected a core with higher dFe in porewaters to further subsample for and analyze the iron size fractionation. To do so, after sampling the whole transect cores and measurements for dFe in porewater, the R/V Bilim-2 spent one extra day in the site to obtain extra cores, to subsample and analyze the size fractionated porewaters.

In Figure 14, bottom water biogeochemical conditions during second cruise of this thesis work - the June 2021 cruise are shown. In June 2021, the porewater sampling stations were revised according to the December 2020 results and June 2021 bottom water conditions. Armutlu transect was excluded this time and a greater focus on Izmit Bay was given with inclusion of the deepest parts of the Izmit Bay (Izmit-Deep station) and Çınarcık-Deep stations.

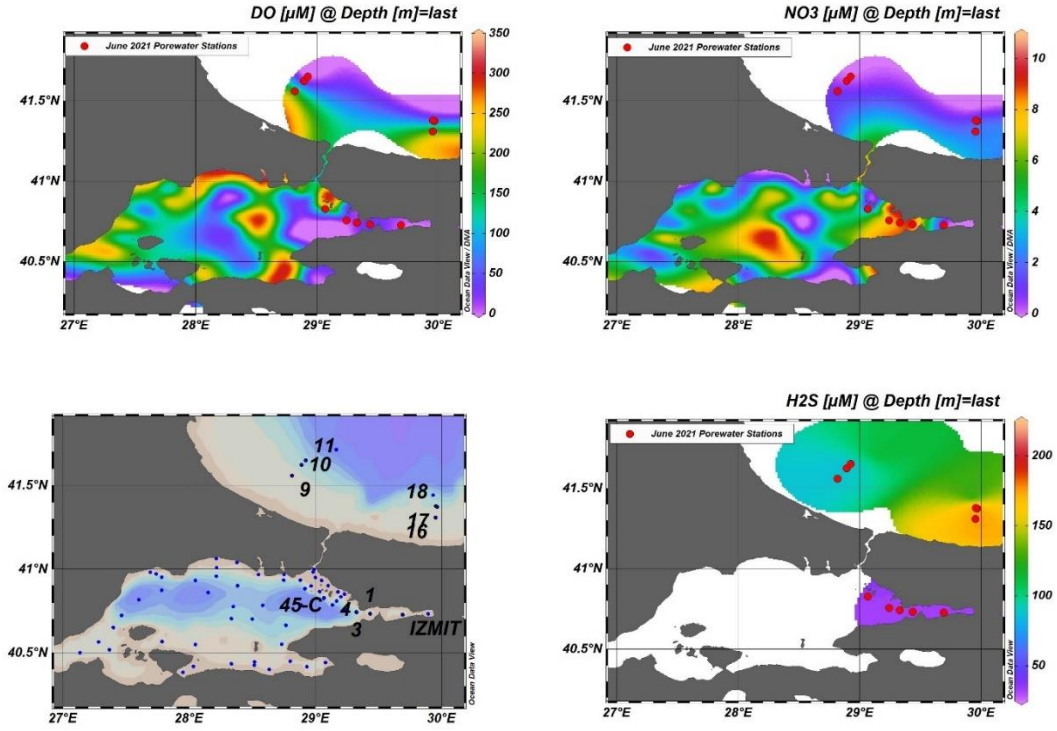

Figure 15: June 2021 R/V Bilim-2 Cruise: stations given over bottom water DO, NO_3^- and H_2S concentrations indicating redox conditions.

2.3 Categorization of the Stations According to Their Bottom Conditions

The bottom redox conditions are categorized according to thresholds given in section 1.4. The categorized stations are given in Table 1.

Table 1: Redox categorization of the stations according to their bottom conditions.

Area	Cruise	Station	Bot. Depth (m)	Bot. DO [µM]	Redox Category
the sea of Marmara	December 2020	1	70	69	hypoxic
		3	286	11	hypoxic
		4	475	14	hypoxic
		5	84	39	hypoxic
		7	243	11	hypoxic
		8	381	17	hypoxic
	June 2021	1	67	49	hypoxic
		3	195	22	hypoxic
		4	649	7	suboxic
		IZMIT DEEP	206	0	sulfidic
		45-C	1214	5	suboxic
the Black Sea	Dec. 2020	9	81	157	oxic
		10	107	57	hypoxic
		11	448	0	sulfidic
	June 2021	9	87	181	oxic
		10	142	8	suboxic
		16	83	195	oxic
		17	120	65	hypoxic

2.4 Sample Handling

2.4.1 Porewater Filtration

Upon arrival of sediment core to the deck of the ship, the interface water was sampled immediately after cores arrived. Interface water was filtered by using Minisart Nylon syringe-tip filters (0.45µm) and divided into subsamples for the analysis of dissolved iron, dissolved hydrogen sulfide, nutrient, and major ions. The rest of the sediments were sliced accordingly to intervals of 1-2-3-4-6-8-10-15-20-25-30-35-40 cm

quickly with care to avoid oxidation and the sliced sediments were filled into 50ml centrifuge tubes. Samples were centrifuged for 6000 rpm for 10 minutes to obtain porewaters. Porewater was filtered by Minisart Nylon syringe-tip filters (0.45µm) and divided into sub-samples likewise the interface water. Nutrient and major ion samples were stored in the -18°C until the preparation for on-shore analysis. Dissolved iron samples were acidified with HCl (Analytical Grade) to adjust the pH to 3. Hydrogen sulfide sub-samples were added on top of tubes pre-filled with zinc acetate and infused with argon gas to avoid oxidation. Dissolved iron was measured with ferrozine spectrophotometric method on-board. Dissolved hydrogen sulfide was measured with methylene blue assay on-board (see below for further details of on-board measurements).

2.4.2 Seawater Sampling for Trace-Level Iron Measurements

The tubes for seawater samplings were prepared by immersing them in detergent and in 10% hydrochloric acid solutions for 1 day in each solution and rinsed with distilled water for 3 times in between the steps. The blank measurements were carried out to check the contamination levels. 5 blank samples were measured, and the average of blanks were 5.93±2.98 nM. The cleaning protocol was adequate for expected Fe levels in the Black Sea (100-300nM). The sampling was done with care and quickly to avoid contamination. To sample particulate iron (<1.0µm), seawater was filtered with Nuclepore Hydrophilic Membrane (pore size of 1.0µm); for colloidal iron (<0.20µm) Nuclepore Hydrophilic Membrane (pore size of 0.2µm), and for soluble iron (<0.02µm) anodisc membrane (pore size of 0.02 µm) was used. Nuclepore membranes were pre-cleaned with 10% hydrochloric acid and dried under laminar-flow hood. Anodisc membranes cannot be cleaned with hydrochloric acid due to inorganic composition, thus a freshly opened package was used. For dissolved iron (<0.45µm), Minisart Nylon syringe-tip filters (pore size of 0.45µm) was used and flushed with hydrochloric acid before filtration. Samples was acidified to adjust the

pH=3 with suprapur hydrochloric acid or suprapur nitric acid for fixation until analysis.

2.4.3 Sequential Filtration for Size Fractionation of Dissolved Iron Pool

Size fraction analysis were done only in selected stations and media. The seawater size fractionation is given in section 2.4.2. For porewater size fractionation, we collected an extra core to dedicate all the porewater for size fractionation analysis. Colloidal iron (<0.20μm) and soluble iron(<0.02μm) fractions were aimed to be analyzed within the dissolved iron (<0.45μm) pool. To do so, upon centrifuging and obtaining the porewaters, all the liquid was firstly filtered with Minisart Nylon syringe-tip filters (0.45μm). Two 15ml centrifuge tube having HCl acid (Suprapur inorganic trace analysis grade) and HNO_3 (Suprapur inorganic trace analysis grade) acid was prepared beforehand in the amounts of fixing the sample to pH=3. 2ml of porewater is added into these tubes before filtration for next step. For 0.20 filtration, Minisart Nylon syringe-tip filters (0.20μm) was used and again sub-sampled the <0.20 fraction twice with HCl and HNO_3, fixed same as 0.45 fraction. For the soluble fraction, we used anodisc membrane (pore size of 0.02 μm) to filter the rest of the solution. The soluble fraction is fixed with HCl only. At the end, 5 sub-samples of 3 different iron size pools were obtained (Figure 16). This protocol was followed from (Yücel et al., 2011, 2021).

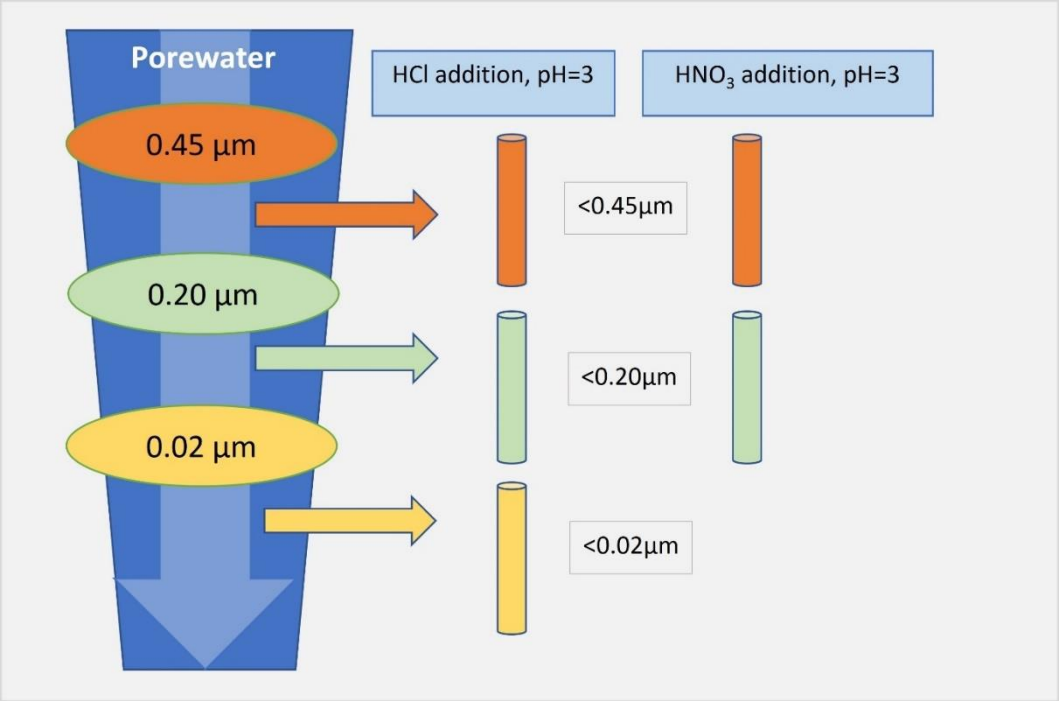

Figure 16: Scheme of size-fraction sub-sampling.

2.5 Measurements On Board

2.5.1 Dissolved Hydrogen Sulfide

Dissolved hydrogen sulfide (H_2S, HS^-, S^{-2}) was measured by spectrophotometric methylene blue method (CLINE, 1969). Measurements for dissolved hydrogen sulfide was made on-board, and some samples were measured on shore due to limited time during the cruise. The pathlength of the quartz cuvette used was 1cm. Calibration standards were prepared as 5-10-20-30-40 µM and every tube and distilled water used during the preparation was infused with argon gas. Samples for H_2S measurements taken with care to avoid contamination of air and was infused with argon gas prior to sampling. The samples were fixed with 0.05 M zinc acetate (reference standard) solution until the analysis. After fixation, samples were treated with the 2M N,N-dimethyl-p-phenylene diamine (coloring reagent) with 0.1 M

Reagent Grade ferric chloride (catalyst) and waited for 10-15 minutes to complete the reaction time until the readings.

2.5.2 Dissolved Iron

For dissolved iron measurement ferrozine spectrophotometric method was used (Stookey, 1970). For nM levels of analysis, the spectrophotometer was coupled with 50cm liquid waveguide capillary cell. For µM levels of analysis, if the levels are known, measurements done with 1cm pathlength quartz cuvettes. Acidified (pH=3) samples were treated with 2.5 M ammonium acetate (pH buffer), and 0.1M hydroxylamine hydrochloride (reducing agent to analyze $Fe^{+2/+3}$) and finally with colored with 0.05M ferrozine reagent. Iron concentrations were determined at 562 nm wavelength in the visible range. The calibration curve is prepared using ferrous ammonium sulfate as standard solution.

Lower detection limits were required for seawater iron and dissolved iron in sulfidic seafloor porewater was expected to be needed. A portable and modular spectroscopy system of Ocean Insight was used for the analysis. 50 cm length liquid waveguide capillary cell is used in conjunction with the spectroscopic method to enhance detection limits (Waterbury et al., 1997). With the liquid waveguide capillary cell, a peristaltic pump is used to inject the sample into cell (Figure 17).

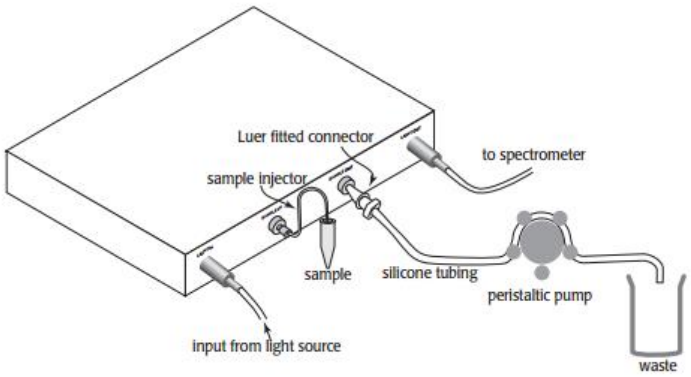

Figure 17: Scheme of spectroscopy setup in conjunction with LWCC (World Precision Instruments, https://www.wpiinc.com/lwcc-3050-liquid-waveguide-capillary-cell-50-cm-pathlength, last visited on August 2022).

Use of liquid waveguide capillary cell was preferred for several reasons: i) enables on-board and fast analysis while decreasing the detection limit by factor of 50, ii) capillary cell volume is 0.125µL and requires very small amount of sample to obtain a reading including the volumes needed for washing the cell. Sub sampling the porewater, which is already limited, decreases the volume to 1-2ml for each sub-sample. 50cm length is decided to be optimal for our analysis considering longer cells would require higher analyte volumes and more effort would be necessary to clean the cell which would compromise on-board fast detection efforts.

Lowering the detection limit at least by the factor of 50 with 50 times longer pathlength cell was expected according to Beer's Law. The optimal range of standards with 1cm cuvette method is 10-50µM. Therefore, with LWCC, 200-1000nM range was optimal; moreover, with the longer reading times for absorption is used to enhance detection limits more notably. Hence, 10-200nM of standards were included for the calibration curve. With the trials, the absorption of 600nM standard was larger than 1 and very noisy due to increased integration time of absorptions. At the end, standards were selected in the range of 10-500nM in the order of 10-20-30-40-50-100-150-200-250-300-400-500nM. The calculated detection limit is 11.5 nM. The calculated molecular absorptivity for ferrozine which is specific to method is 30000 L/mol.cm which is consistent with Stookey (1970)'s empirical data (Figure 18).

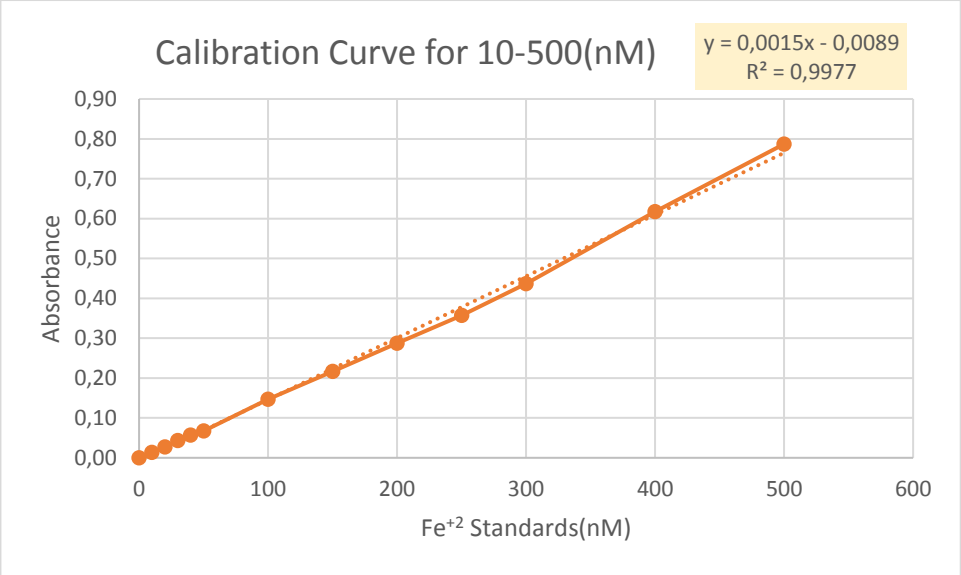

Figure 18. Calibration curve for nano-molar level iron measurements.

2.5.3 Size Fractionation

The sub-samples of size divided dissolved iron pool were measured as in section 2.5.2 . The smaller size groups are being subtracted from the larger one to obtain the only colloids and only soluble fractions. Operationally defined colloidal and soluble fractions are calculated by the subtraction of the fractions. Colloidal fraction is obtained by exclusion of soluble phase (dFe<0.02 µm) from the (dFe<0.20 µm) pool. This protocol was followed from (Yücel et al., 2011, 2021).

Table 2: Table for sub-samples of size-fractionation

Filt, 0.45µm		Filt, 0.20µm		Filt, 0.02µm
sFe + cFe + dFe>0.20µm		cFe + sFe		sFe
dFe(µM) <0.45 HCl	dFe(µM) <0.45 HNO_3	dFe(µM) <0.20 HCl	dFe(µM) <0.20 HNO_3	dFe(µM) <0.02 HCl

2.6 Measurements On Shore

2.6.1 Dissolved Nutrients

Porewater samples prepared by diluting by 1/10 to overcome seawater salt interferences. Porewater dissolved inorganic nutrients NO_3^- + NO_2^-, NO_2^-, NH_4^+ analysis was done according to colorimetric methods (K. Grasshoff, M. Ehrhardt, 1983) using four channel autoanalyzer (Bran+Luebbe Model) in the METU-IMS laboratory. The detection limits are reported as 0.05µM for NO_3^- + NO_2^-, 0.05µM for NO_2^- and 0.04µM for NH_4^+.

2.6.2 Solid TC, TOC and TN

Sediments after porewater extraction were preserved as Ar gas infused and froze in -20°C until analysis. Solid samples were weighed to obtain wet weight. Afterwards freeze-drying the sediment samples, weighed again to get dry weight in order to obtain porosity of sediments. Freeze-dried sediments are then powdered with marble mortar and sieved for homogenization. Dried and homogenized samples were prepared for TC, TOC and TN analysis with the Vario El Cube Elementar Model CHN Analyzer (UNEP/MAP, 2006) with dry oxidation method. To have TOC and TC measurements, duplicates of the samples were prepared; one is treated with HCl to remove inorganic carbon from sediment to give TOC values. Approximately 30 mg of dry sediment powders are put into pre-combusted silver cups. For TOC measurement preparations, 5-10µL of distilled water and 10µL of 20% HCl (vol/vol) was added initially and added more as needed until all the inorganic carbon was removed as CO_2. Treated sediment samples are dried again prior to analysis at 60°C for 24 hours. The silver cups filled with sediments are compacted and placed in the autosampler of CHN Elemental analyzer. TN concentrations were measure for all duplicates and used as control parameter to check any significant difference in treated and non-treated samples.

CHAPTER 3

RESULTS

3.1 The Black Sea

3.1.1 Water column profiles of porewater stations

In this section, as commonly used in the Black Sea oceanographic literature (Tugrul et al., 1992), water column parameters are given as plots of variable of interest versus density (expressed as σ_θ), to be able to compare the biogeochemical shifts better via excluding physical effects. For better interpretation between the stations, the scales kept same.

Area	Cruise	Station	Bot. Depth (m)	Bot. DO [µM]	Redox Category
the Black Sea	Dec. 2020	9	81	157	oxic
		10	107	57	hypoxic
		11	448	0	sulfidic
	June 2021	9	87	181	oxic
		10	142	8	suboxic
		16	83	195	oxic
		17	120	65	hypoxic

3.1.1.1 Oxic Water Column Profiles

Stations has DO > 89 µM are categorized as “oxic” stations. Station 9 and 16 has oxic conditions among the stations in the Black Sea.

Station 9 of the southwestern transect in Black Sea (Figure 19 in December 2020 and Figure 20 in June 2021), exhibited oxic conditions at the bottom with 156 µM DO in Dec. 2020 and 181 µM DO in June 2021. Bottom density layer was 14.98 and 15.28 σ_θ in Dec. 2020 and June 2021, respectively. Dissolved nitrate in the bottom waters was 2.2µM in Dec. 2020 and decreased by half in June 2021 to 0.95µM while dissolved phosphate levels were comparable for each cruise (0.25 and 0.22 µM). Related porewater results are given in section 3.1.2 Figure 28.

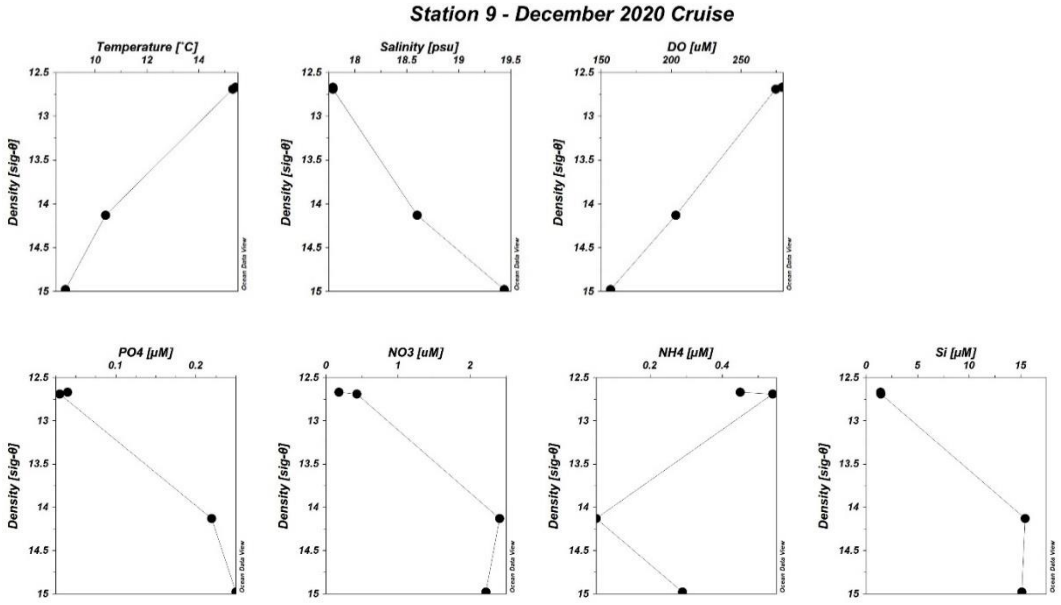

Figure 19: Station 9, December 2020 Black Sea R/V Bilim-2 Cruise: Water column physical and biogeochemical parameters vs. density graphs. Bottom depth: 81 m

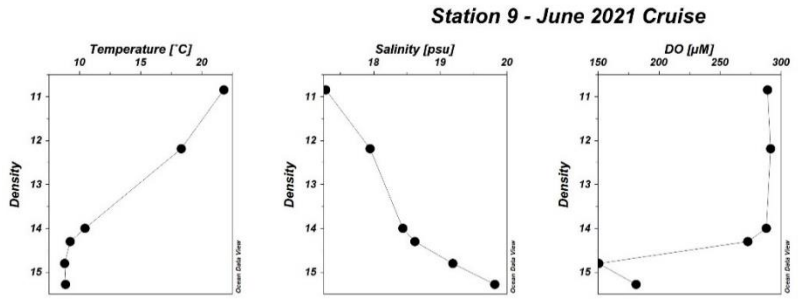

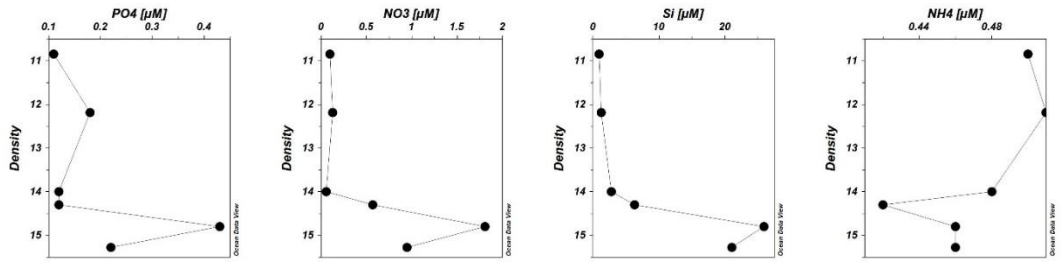

Figure 20: Station 9, June 2021 the Black Sea R/V Bilim-2 Cruise: Water column physical and biogeochemical parameters vs. density graphs. Bottom depth: 87 m

Oxic station (16) of the west of Bosphorus transect in Black Sea (Figure 21) was visited only in June 2021 Cruise. Station bottom waters had dissolved oxygen at level of 195 µM DO. Bottom density layer is at 15.07 σ_θ. Dissolved nitrate was 2.02 µM and dissolved phosphate was 0.31 µM. Compared to other oxic station 9 in southwestern shelf result in June 2021, station 16 has more nitrate and phosphate at the bottom despite the bottom waters were less dense, representing surface features hence nutrient depletion must be expected. Related porewater results are given in section 3.1.2 Figure 29.

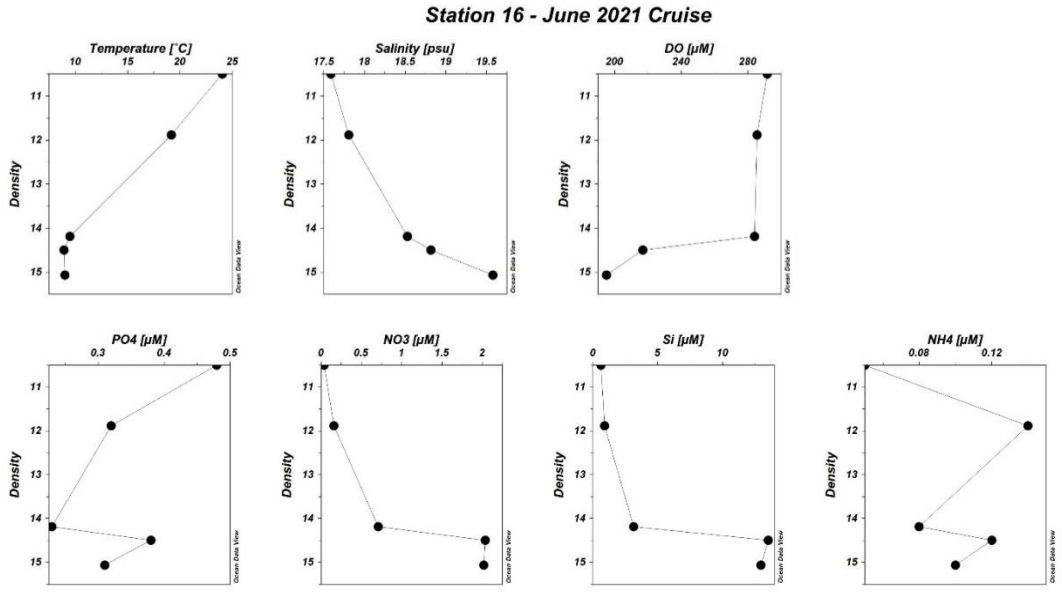

Figure 21: Station 16, June 2021 the Black Sea R/V Bilim-2 Cruise: Water column physical and biogeochemical parameters vs. density graphs. Bottom depth: 83 m

3.1.1.2 Hypoxic Stations Water Column Profiles

Station 10 of the southwestern transect in Black Sea (Figure 22) had hypoxic conditions at the bottom with 57.40 µM DO in December Cruise 2020. Bottom density layer was 15.67 in Dec. 2020. Dissolved nitrate was 3.79 µM in Dec. 2020 Dissolved phosphate levels were 0.64 µM in Dec. 2020. Related porewater results are given in section 3.1.2 Figure 32.

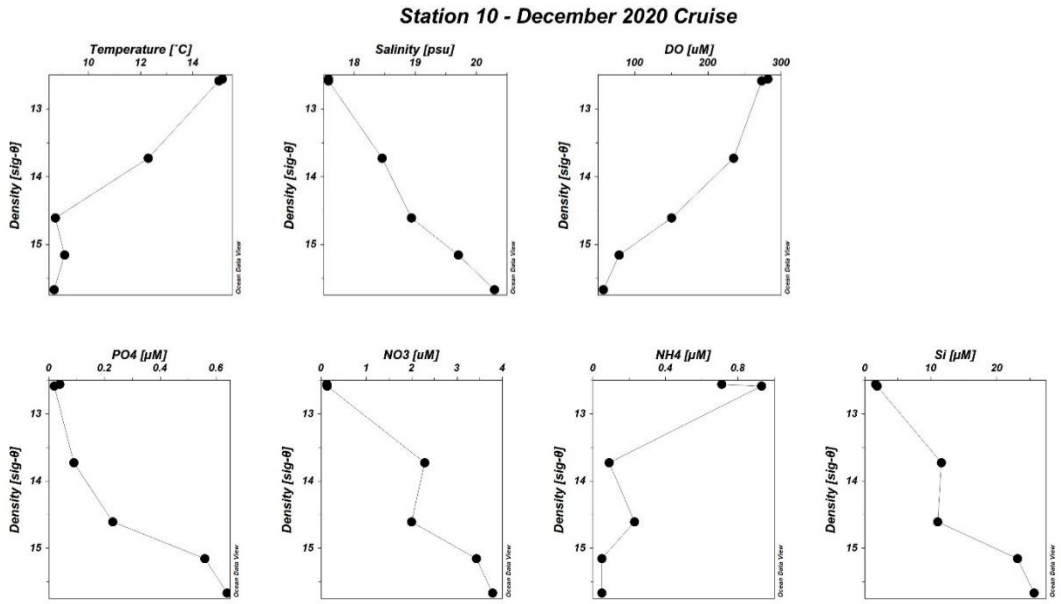

Figure 22: Station 10, December 2020 Black Sea R/V Bilim-2 Cruise: Water column physical and biogeochemical parameters vs. density graphs. Bottom depth: 107 m

Station 17 of the west of Bosphorus transect in Black Sea (Figure 23) was visited only in June 2021 Cruise. Stations bottom waters have oxygen at level of 65 µM DO. Bottom density layer was at 15.97 σ_θ approaching towards the onset of suboxic layer. Dissolved nitrate was 3.36 µM and dissolved phosphate was 1.21 µM. Compared to other hypoxic station 10 in southwestern shelf result in December 2020, despite the bottom density layer had higher σ_θ values, bottom dissolved oxygen was higher than station 10, possibly due to intrusions from Bosphorus (Konovalov et al., 2003). Also, the small increase of DO from 56 µM DO at 15.84 σ_θ to 65 µM DO at 15.97 σ_θ

(bottom) might be indicative of oxygen impact from Bosphorus. Related porewater results are given in section 3.1.2 Figure 31.

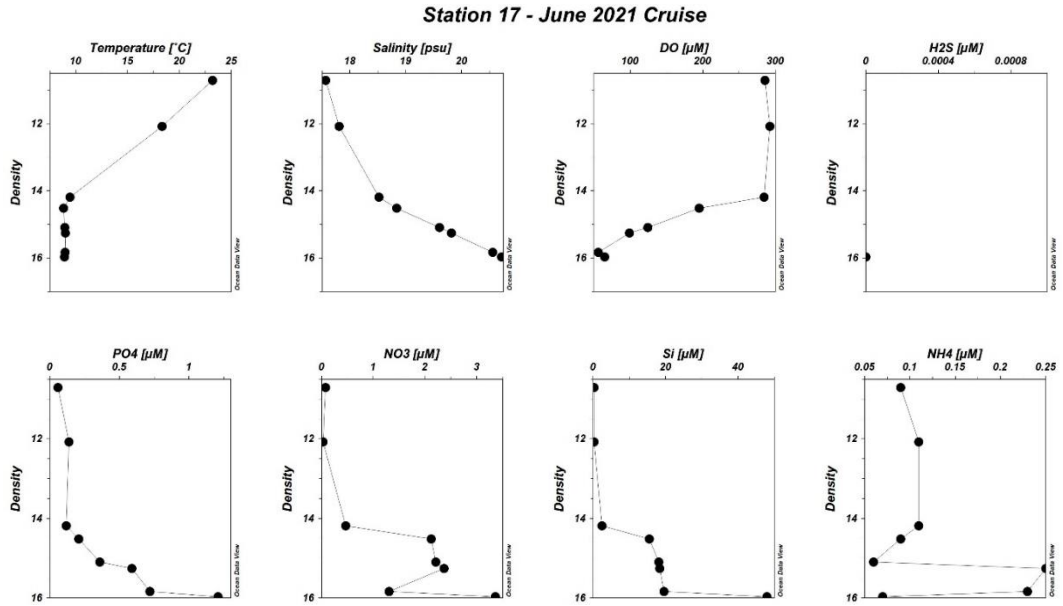

Figure 23: Station 17, June 2021 the Black Sea R/V Bilim-2 Cruise: Water column physical and biogeochemical parameters vs. density graphs. Bottom depth: 120 m

3.1.1.3 Suboxic Stations Water column Profiles

Station 10 of the southwestern transect in Black Sea (Figure 20), had suboxic conditions 8.20 µM DO in June 2021. Bottom density layer was 16.17 σ_θ in June 2021. Dissolved nitrate was 0.10 µM. and dissolved phosphate were 4.67 µM. In June 2021, compared to December 2020, the suboxic onset was observed better at the bottom with lower DO and nitrate. Related porewater results are given in section 3.1.2 Figure 32.

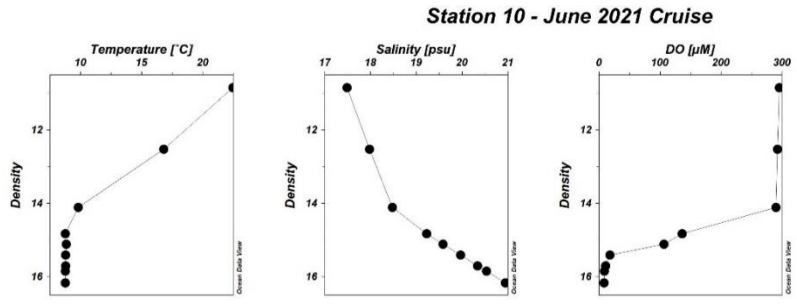

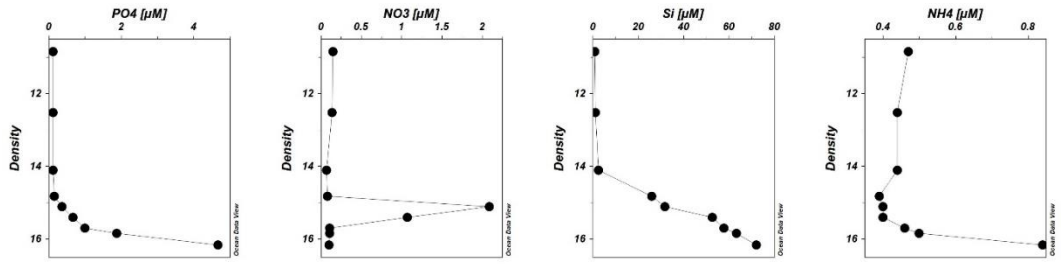

Figure 24: Station 10, June 2021 the Black Sea R/V Bilim-2 Cruise: Water column physical and biogeochemical parameters vs. density graphs. Bottom depth: 142 m

3.1.1.4 Sulfidic Stations Water Column Profiles

Permanently sulfidic station (11) of the southwestern transect in Black Sea (Figure 25 in December 2020 and Figure 26 in June 2021), had high levels of dissolved sulfide at the bottom waters with 119 µM H_2S in Dec. 2020 and 83 µM H_2S in June 2021. Bottom waters were denser compared to the shallower sites of this transect with 16.96 and 16.87 σ_θ in Dec. 2020 and June 2021, respectively. Dissolved nitrate was 0.17 µM in Dec. 2020, which was unexpectedly high and might be reflecting an oxidation of ammonia during sampling and was below detection in June 2021. Dissolved ammonia was 33.65 and 16.85 µM in 2020 and 2021, respectively. Dissolved phosphate levels were 4.63 µM in Dec. 2020 and 5.35 µM in June 2021.

The water column distributions of nutrients, according to Black Sea's redox regulated characteristic distributions (Tugrul et al., 1992), the density layers are higher than expected, in December 2020 cruise. First peak of phosphate maximum and nitrate maximum appears at 14.5 and phosphate minima appears at 15.84; however, the second and bigger peak appears at 16.19 as expected. On the other hand, in June 2021, the phosphate peaks were at 15.41 and 16.2 with minima at 15.84, additionally the nitrate peak was also at 15.41, the nutrient distributions seem consistent with literature. As a result, for both cruises, with high levels of NH_4^+ and H_2S, the bottom water represents strongly reducing conditions. Related porewater results are given in section 3.1.2 Figure 33.

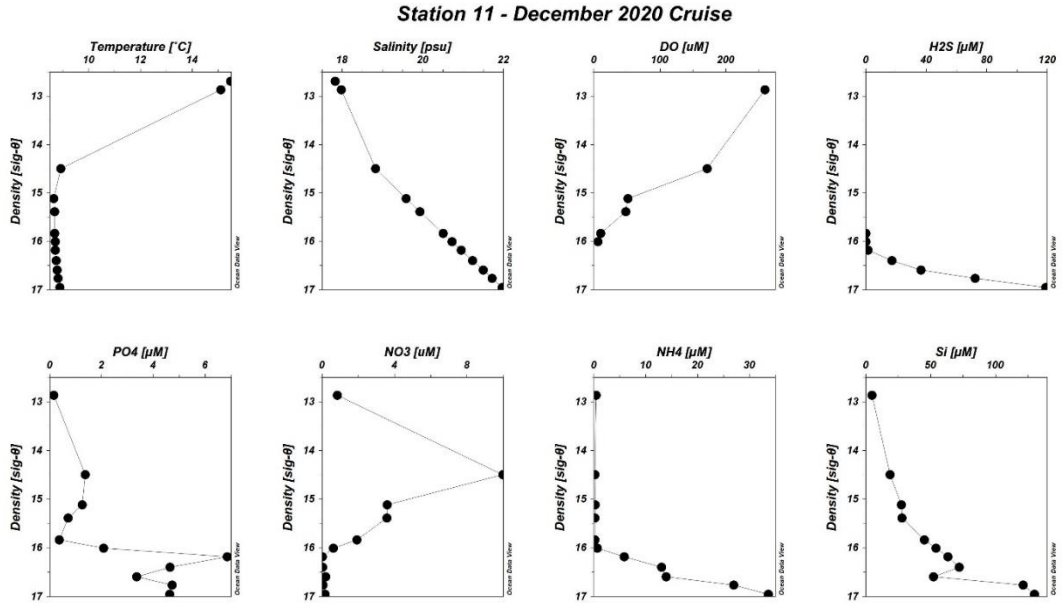

Figure 25: Station 11, December 2020 Black Sea R/V Bilim-2 Cruise: Water column physical and biogeochemical parameters vs. density graphs. Bottom depth: 448 m

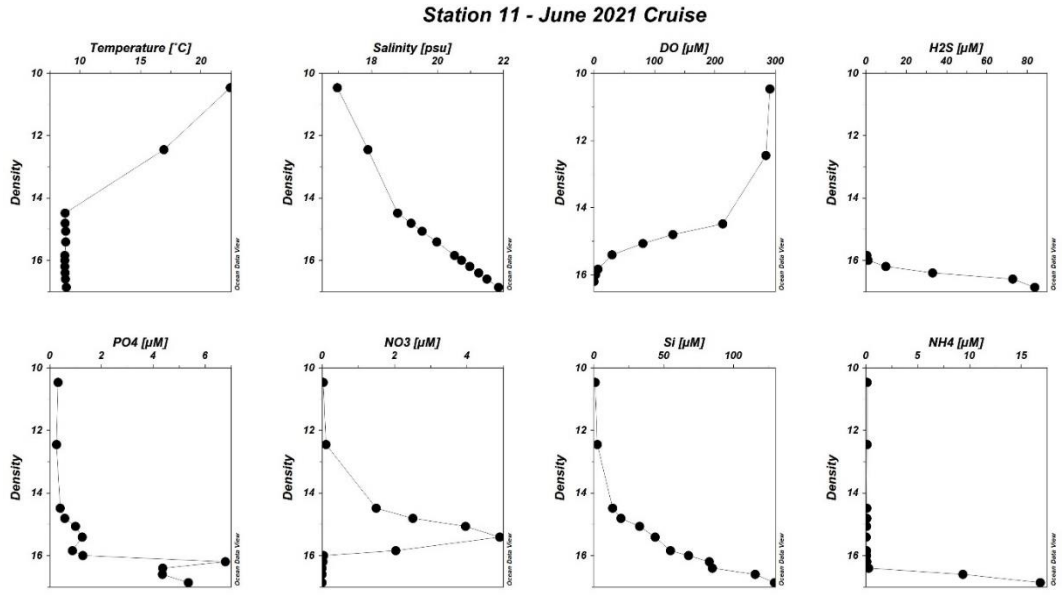

Figure 26: Station 11, June 2021 the Black Sea R/V Bilim-2 Cruise: Water column physical and biogeochemical parameters vs. density graphs. Bottom depth: 359 m

Sulfidic station 18 of the west of Bosphorus transect in Black Sea (Figure 27) was visited only during the June 2021 Cruise. Stations bottom waters had hydrogen sulfide at level of 202 µM H_2S at 16.88 σ_θ. Dissolved nitrate was below detection

and dissolved phosphate was 5.59 µM. Compared to other sulfidic station 11 in southwestern shelf result in June 2021, station 18 had higher H_2S values with similar nitrate, ammonia, and phosphate values at the bottom. In the water column, the phosphate and DO distributions are clearly affected by the oxygen rich water intrusion from Bosphorus, especially with 48 µM at 16.2 density layer. Related porewater results are given in section 3.1.2 Figure 34.

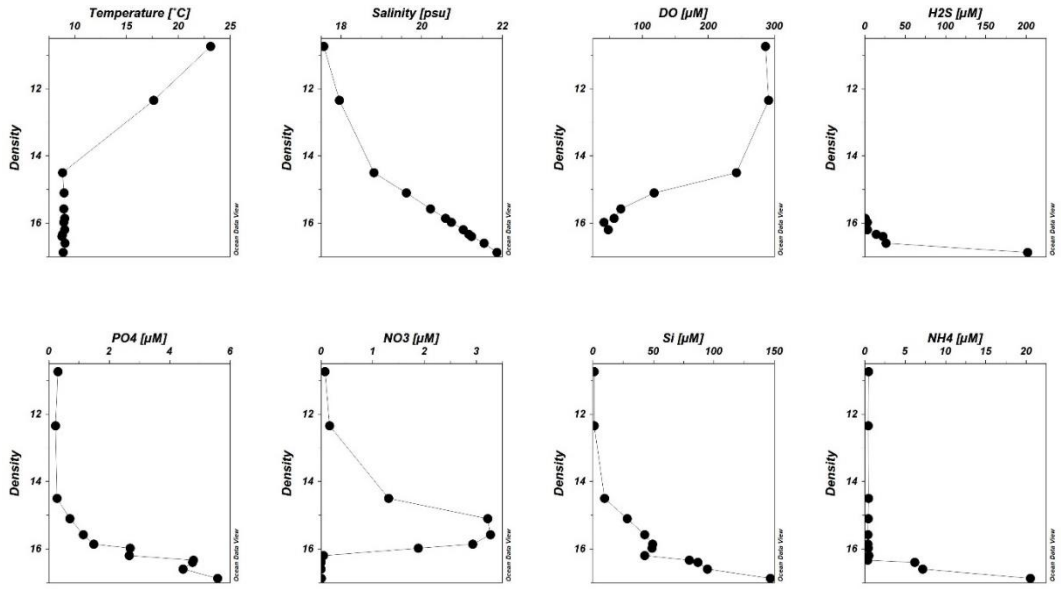

Figure 27: Station 18, June 2021 the Black Sea R/V Bilim-2 Cruise: Water column physical and biogeochemical parameters vs. density graphs. Bottom depth: 387 m

3.1.2 Results of sedimentary porewater profiles

3.1.2.1 Sedimentary Porewater Profiles of Oxic Stations

Porewater nitrate, ammonia, dissolved iron, and hydrogen sulfide distributions along the core of station 9 are given in Figure 28 for both cruises. The water column characteristics of station 9 are given in the section 3.1.1 in Figure 19 and Figure 20 for December 2020 and June 2021 results, respectively. The bottom conditions represented oxic in both sampling periods.

In December 2020, the interface water had 6 μM of nitrate which is higher than bottom nitrate values by a factor of 3. Nitrate decreased drastically in 1 cm surface layer to 1.9 μM and diminished at 10cm layer indicating high rates of denitrification at the very top of the sediment. Dissolved iron was 0.04 μM in the interface water and increased dramatically towards 2 cm layer to 138 μM levels indicating high activity of microbial iron reduction. Whole sediment profile exhibited high levels of dissolved iron higher than 15 μM for 1-25cm interval until 30cm layer to 3μM dFe value. Dissolved hydrogen sulfide was below detection limit at any layers.

In June 2021, the interface water had 1.37 μM of nitrate. Nitrate showed a decreasing trend on the top seen as in December 2020 results, however, did not become depleted and remained around 0.50 μM levels through whole profile. These results imply that the measurement of nitrate for this core had high percentages of error as nitrate would be expected to be absent in the reducing conditions of hydrogen sulfide presence. Dissolved iron was below detection limit in the interface water but denoted a maximum at 1cm with a value of 26 μM levels. At 10cm and deeper layers dFe was below 5 μM, and for 15-25 cm interval dropped up to nanomolar (nM) levels. Dissimilarly to December 2020, in June2021 hydrogen sulfide appeared at 10cm and increased to 10 μM at 20cm indicating microbial sulfate reduction activities.

Station 9 porewater nitrate, dFe and H_2S results indicated high levels of denitrification and mobilized iron on the surface of the sediment in both cruises. Redox condition quickly shifted from denitrification to iron reduction at the first 1-2cms. December 2020 and June 2021 results were found to be different mostly on the aspect of presence of hydrogen sulfide. June 2021 results showed stronger redox zonation with lower maxima of nitrate and dissolved iron.

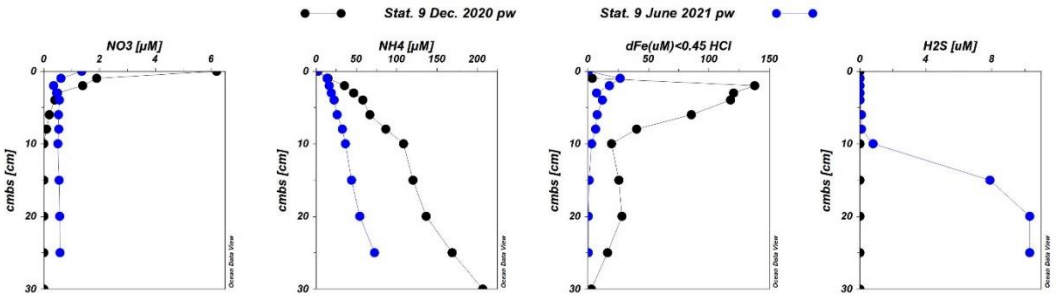

Figure 28: Station 9, December 2020 and June 2021 the Black Sea R/V Bilim-2 Cruise: Porewater redox-sensitive nutrients, dissolved hydrogen sulfide and dissolved iron (<0.45µm) distributions along the core.

Porewater nitrate, ammonia, dissolved iron, and hydrogen sulfide distributions along the core of station 16 are given in Figure 33. The water column characteristics of station 16 are given in the section 3.1.1 in Figure 21. The bottom water showed oxic conditions.

In station 16, nitrate ranged from 0.1 to 1 µM through the profile including the interface water, which was lower than bottom water values, indicating denitrification on the top of the sediment layer. Unexpected distribution of nitrate is related to June 2021 nutrient measurements error. Dissolved iron appeared after 1 cm and raised to 49 µM at 4cm layer. Dissolved iron decreased towards deeper to 0.15 µM at 30cm. Hydrogen sulfide measurements were not conducted during the cruise according to results of previous oxic station results.

Station 16 porewater results indicated high level of mobilized iron on the top part of the sediment being consistent with other oxic stations' porewater results.

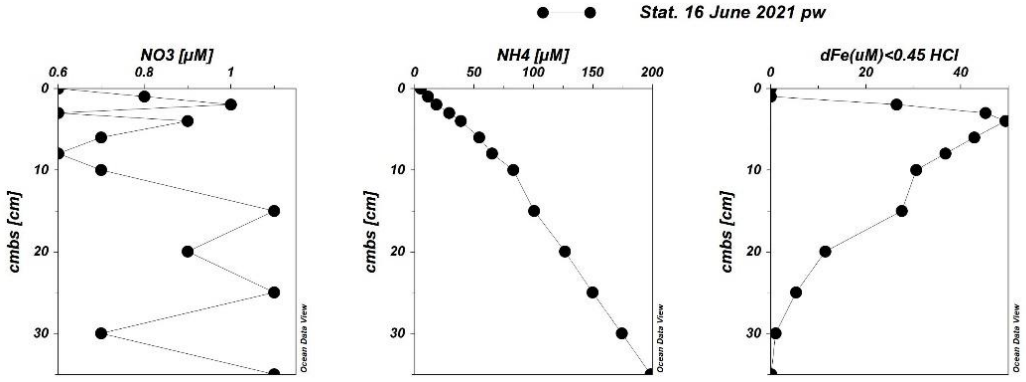

Figure 29: Station 16, June 2021 the Black Sea R/V Bilim-2 Cruise: Porewater redox-sensitive nutrients, dissolved hydrogen sulfide and dissolved iron (<0.45µm) distributions along the core.

3.1.2.2 Sedimentary Porewater Profiles of Hypoxic Stations

Porewater nitrate, ammonia, dissolved iron, and hydrogen sulfide distributions along the core of station 10 are given in Figure 30 for December 2020 cruise. The water column characteristics of station 10 are given in the section 3.1.1 in Figure 22 for December 2020. The bottom water exhibited hypoxic conditions in December 2020.

In December 2020, the interface water had 2.40 µM of nitrate which was lower than bottom nitrate values. Nitrate decreased towards 4cm layer and disappeared, indicating denitrification in the surface waters of sediment instead of sediment porewater. Dissolved iron was 0.36 µM in the interface water and increases towards 2 cm layer to 28 µM levels. Dissolved iron was lower than 5 µM between 10cm and 23cm reaching at a value of 1.82 µM at the bottom of the sediment core. Dissolved hydrogen sulfide detected only at 1cm layer with a concentration of 0.50 µM suggesting insufficient sulfate reduction for this sediment core.

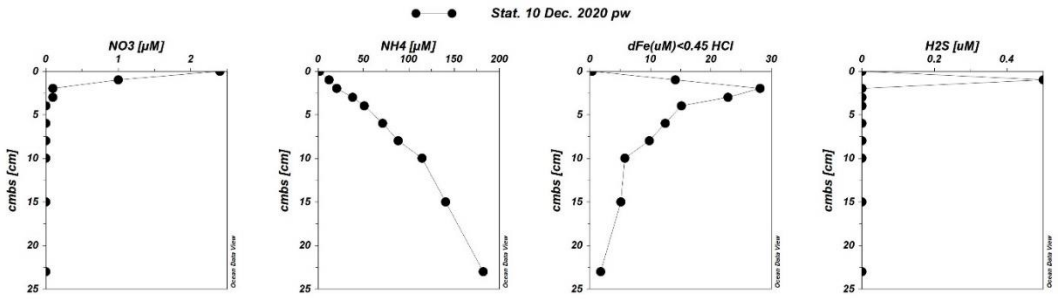

Figure 30: Station 10, December 2020 the Black Sea R/V Bilim-2 Cruise: Porewater redox-sensitive nutrients, dissolved hydrogen sulfide and dissolved iron (<0.45µm) distributions along the core.

Porewater nitrate, ammonia, dissolved iron, and hydrogen sulfide distributions along the core of station 17 are given in Figure 31. The water column characteristics of station 17 are given in the section 3.1.1 in Figure 23. The bottom water shows hypoxic conditions.

In station 17, nitrate was 0.40 µM in the interface waters which was lower than bottom water values. The whole profile couldn't be sampled for nutrients due to low volume of porewaters, so the nutrient data discontinues for 4-20cm interval. Until 8cm depth, nitrate increased to 8 µM unexpectedly. The increase in nitrate reflected to ammonia as decrease which might be indicating oxidation of ammonia during sampling. Dissolved iron concentrations were less than 2 µM until 10cm layer and maximized at 15cm at a level of 21 µM.

Station 17 porewater results indicated high positive error in nitrate measurements. Also, it differed from other Black Sea suboxic-hypoxic stations' results in terms of comparatively lower levels of mobilized iron at the surface of the sediment.

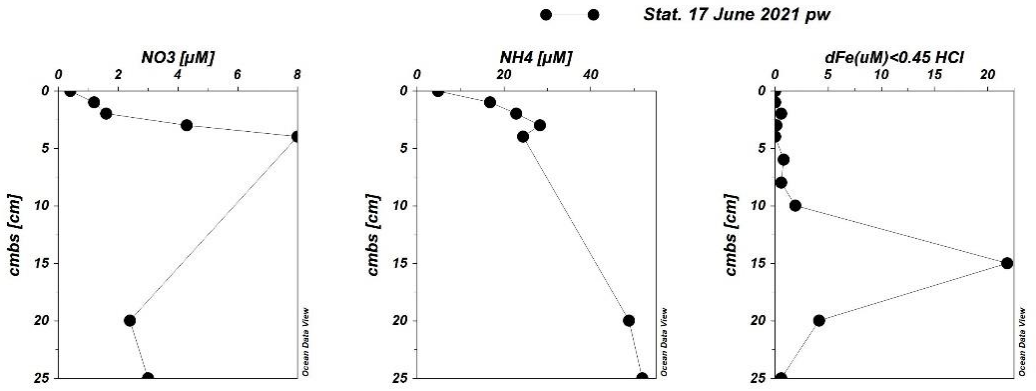

Figure 31: Station 17, June 2021 the Black Sea R/V Bilim-2 Cruise: Porewater redox-sensitive nutrients, dissolved hydrogen sulfide and dissolved iron (<0.45µm) distributions along the core

3.1.2.3 Sedimentary Porewater Profiles of Suboxic Stations

Porewater nitrate, ammonia, dissolved iron, and hydrogen sulfide distributions along the core of station 10 are given in Figure 32 for June 2021 Cruise. The water column characteristics of station 10 are given in the section 3.1.1 in Figure 24 for June 2021 results. The bottom water exhibited suboxic conditions in June 2021.

In June 2021, the interface water has 0.90 µM of nitrate which is higher than bottom waters, however the sediment profile of nitrate had a similar error as in station 9 in

June 2021. Nitrate varied between 0.4-0.8 µM through whole water column, even in hydrogen sulfide layer indicates a positive error in measurements. The error disables to deduce the exact sediment depth for denitrification layer in this core; however, the minimum levels are indicative of denitrification at the surface part of the sediment. Dissolved iron was 3.85 µM in the interface water and increases significantly to 110 µM at 2cm indicating high rates of microbial iron reduction. The iron reduction redox layer is narrower compared to December 2020, because dissolved iron decreases quickly to 19 µM at 3cm and remains below 1 µM until the bottom of sediment. Hydrogen sulfide was below 1 µM until 6cm but increased to 72 µM at 15cm which then decreased to levels around 2 µM below 25cm below seafloor. Dissimilarly to December 2020, in June2021 gives a mid-profile hydrogen sulfide peak and the trend indicates sulfate reduction below the iron reduction layer.

Station 10 porewater results pointed high levels of iron reduction in both cruises and sulfate reduction in June 2021. As in the comparison of cruises for station 9, June 2021 results indicates stronger redox zonation in the sediment, anyhow the dissolved iron peak was higher for June 2021 compared to December 2020.

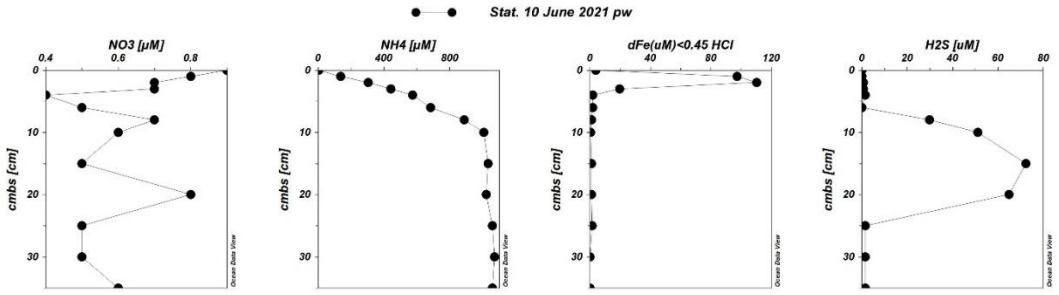

Figure 32: Station 10, June 2021 the Black Sea R/V Bilim-2 Cruise: Porewater redox-sensitive nutrients, dissolved hydrogen sulfide and dissolved iron (<0.45µm) distributions along the core.

3.1.2.4 Sedimentary Porewater Profiles of Sulfidic Stations

Porewater nitrate, ammonia, dissolved iron, and hydrogen sulfide distributions along the core of station 11 are given in Figure 33 for both cruises. The water column

characteristics of station 11 are given in the section 3.1.1 in Figure 25and Figure 26 for December 2020 and June 2021 results, respectively. The bottom waters were highly sulfidic conditions for both cruises.

In December 2020, nitrate was below detection limit due to highly reducing conditions in the sediment porewater. Dissolved iron was 0.33 µM within the first 1cm and remaining larger than 0.05uM throughout the sediment. Dissolved hydrogen sulfide was 215 µM at 1cm layer being higher than the bottom water values. Hydrogen sulfide increased towards deep in the profile up to 3 mM levels. Although hydrogen sulfide and dissolved iron did not display a redox zonation, the distribution trend of them pointed out a counteracting relation indicative of FeS precipitation.

In June 2021, porewater volume was so limited and only iron and hydrogen sulfide sub-samples were taken. Within these, only hydrogen sulfide could be measured. Dissolved iron measurements failed during the cruise due to complications with liquid wave guide capillary cell. As in December 2020 cruise results, hydrogen sulfide started to increase from 138 µM to about 3mM levels towards the bottom of sediment.

Station 11 porewater results showed that the presence of hydrogen sulfides hinders dissolved iron to nanomolar levels due to precipitation. The distribution trend was visible even at nanomolar levels. The distribution of iron through the profile appeared to be controlled by the amount of hydrogen sulfide, emphasizing the close coupling of Fe and S cycles in sediment porewaters.

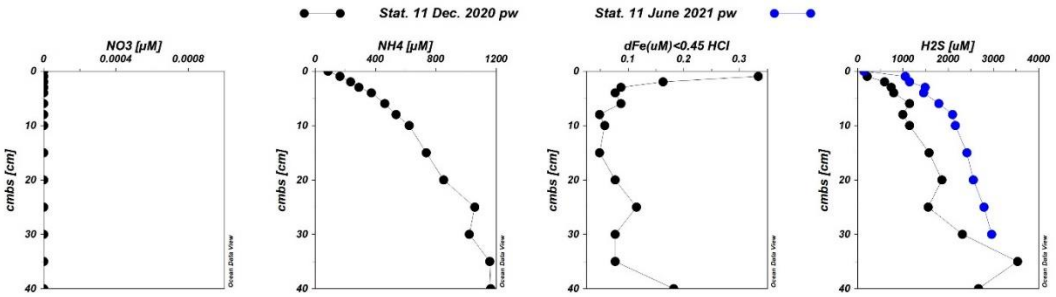

Figure 33: Station 11, December 2020 and June 2021 the Black Sea R/V Bilim-2 Cruise: Porewater redox-sensitive nutrients, dissolved hydrogen sulfide and dissolved iron (<0.45µm) distributions along the core.

Porewater nitrate, ammonia, dissolved iron, and hydrogen sulfide distributions along the core of station 18 are given in Figure 34. The water column characteristics of station 18 are given in the section 3.1.1 in Figure 27.

In station 18, nitrate showed measurement errors. Dissolved iron was not measured during the cruise because low levels of dissolved iron was shown in previous results.

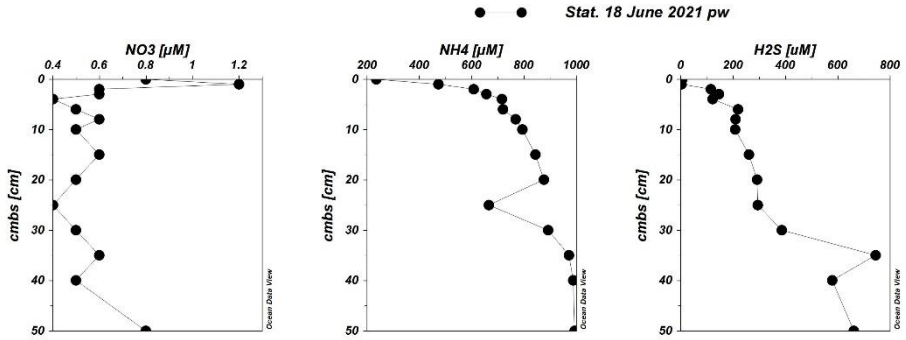

Figure 34: Station 18, June 2021 the Black Sea R/V Bilim-2 Cruise: Porewater redox-sensitive nutrients, dissolved hydrogen sulfide and dissolved iron (<0.45µm) distributions along the core

3.1.3 Profiles of carbon and nitrogen analysis in solid sediment samples

Analysis for elemental carbon (total and organic fraction) and nitrogen is given (Figure 35-Figure 37) for station s9,10 and 11 visited in December 2020 cruise.

Total carbon in station 9 sediments was higher than 3mmol/g for first 10cm and total organic carbon was higher than 1.5mmol/g. TOC/TN ratio increased towards 10cm indicating higher carbon content on the top part of the sediment.

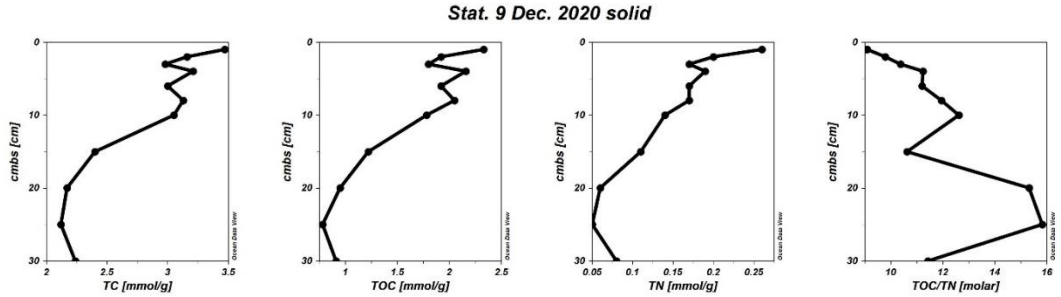

Figure 35: Station 9, December 2020 Black Sea R/V Bilim-2 Cruise: Sediment solid state total carbon and nitrogen distributions along the core

In station 10, 6cm sediment layer had significant change in total carbon and total organic carbon distributions that this layer consists of high amounts of deposited carbonate shells. Overall, total carbon was higher and, total organic carbon and total nitrogen was lower than TOC/TN of station 9.

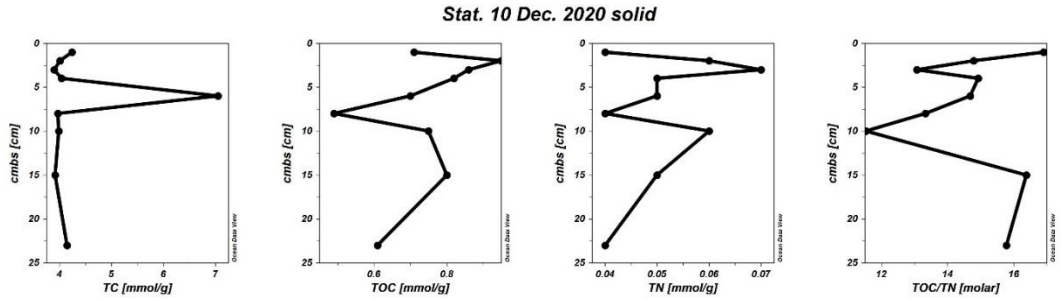

Figure 36: Station 10, December 2020 Black Sea R/V Bilim-2 Cruise: Sediment solid state total carbon and nitrogen distributions along the core

In station 11 was richer in terms of total organic carbon and total nitrogen content compared to the other stations. TOC/TN ratio was around 11 through the profile except for the depths of 20 and 25cm.

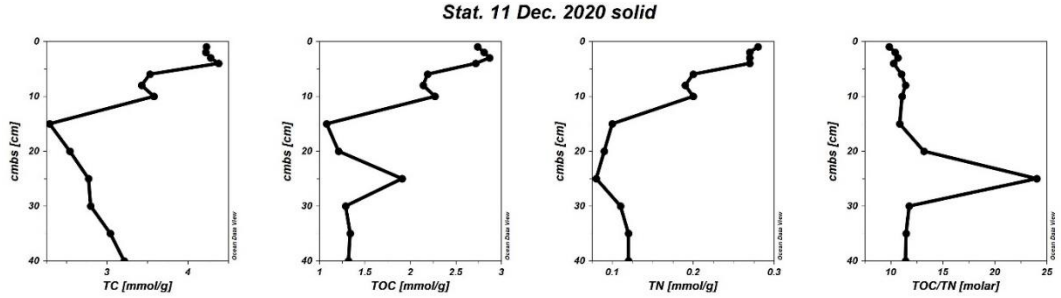

Figure 37: Station 11, December 2020 Black Sea R/V Bilim-2 Cruise: Sediment solid state total carbon and nitrogen distributions along the core

3.1.4 Profiles of size fraction in seawater and in porewater dFe

In station 9, high amount of dissolved iron result in porewater was promising for size fractionation analysis. The size fraction distribution along the core within the dissolved iroon pool is given in Figure 38. The fractions concentrations were obtained by subtracting from the larger pool and shown in size ranges. 0.02<dFe<0.20µm fraction represents colloidal iron and dFe<0.02µm one represents soluble iron. The dissolved iron pool was mostly dominated by soluble fraction and colloidal fraction was quite minor. However the collodial fraction was only found on the surface layer of the sediment. The results have obvious errors such as negative concentration values. In literature, such as Heyden et al. 2015, negative concentration values for size fractions was reported before. For the discussion of negative concentration results see section 4.2.

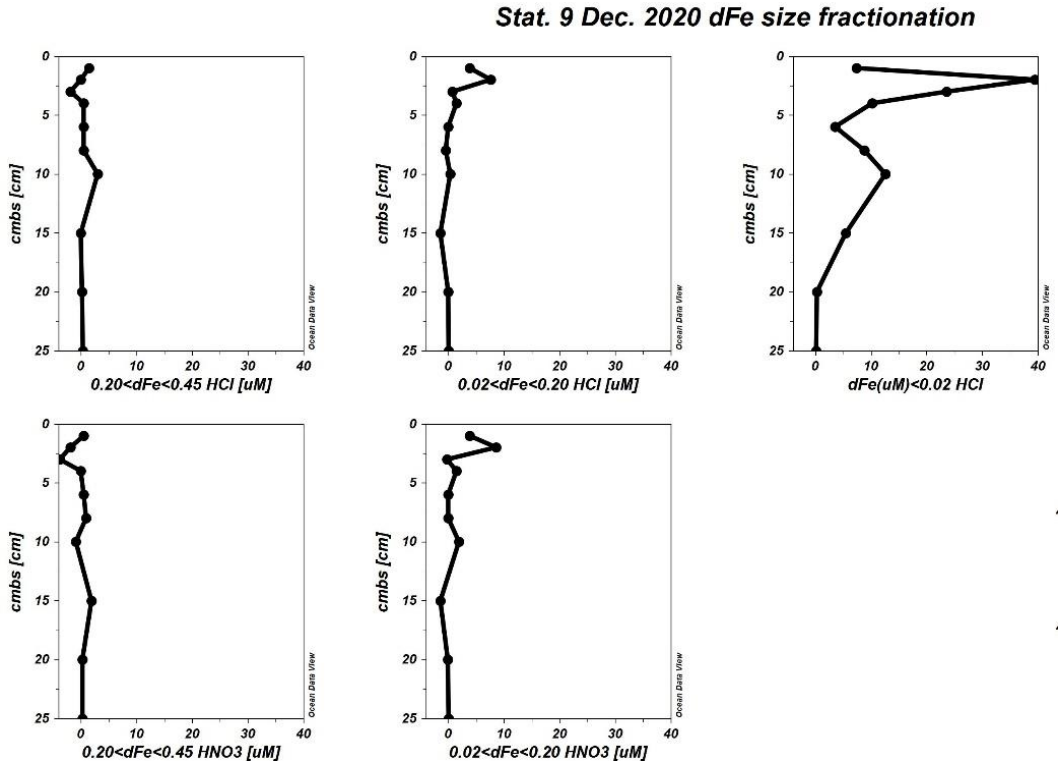

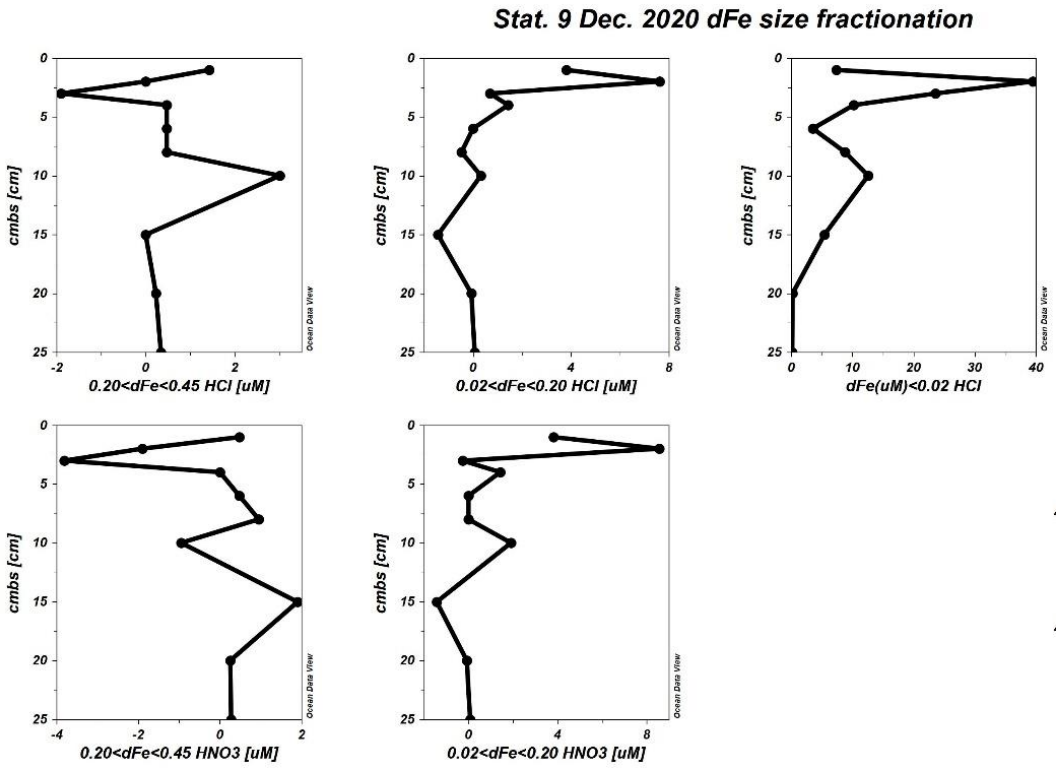

Figure 38: Station 9, December 2020 Black Sea R/V Bilim-2 Cruise: Porewater dissolved iron (<0.45μm) size fractions distributions along the core. (On top) the distributions over the same scale range of concentrations. (Below) the distributions are widened to observe the distribution trend.

In station 11, during December 2020 cruise, we sampled the seawater from suboxic layer at density depths of σ_θ= 15.84, 16.01, 16.19 for particulate iron analysis. The highest value was at 16.19 σ_θ with a concentration of 80nM at the onset of hydrogen sulfide layer. This was our preliminary results for seawater iron analysis.

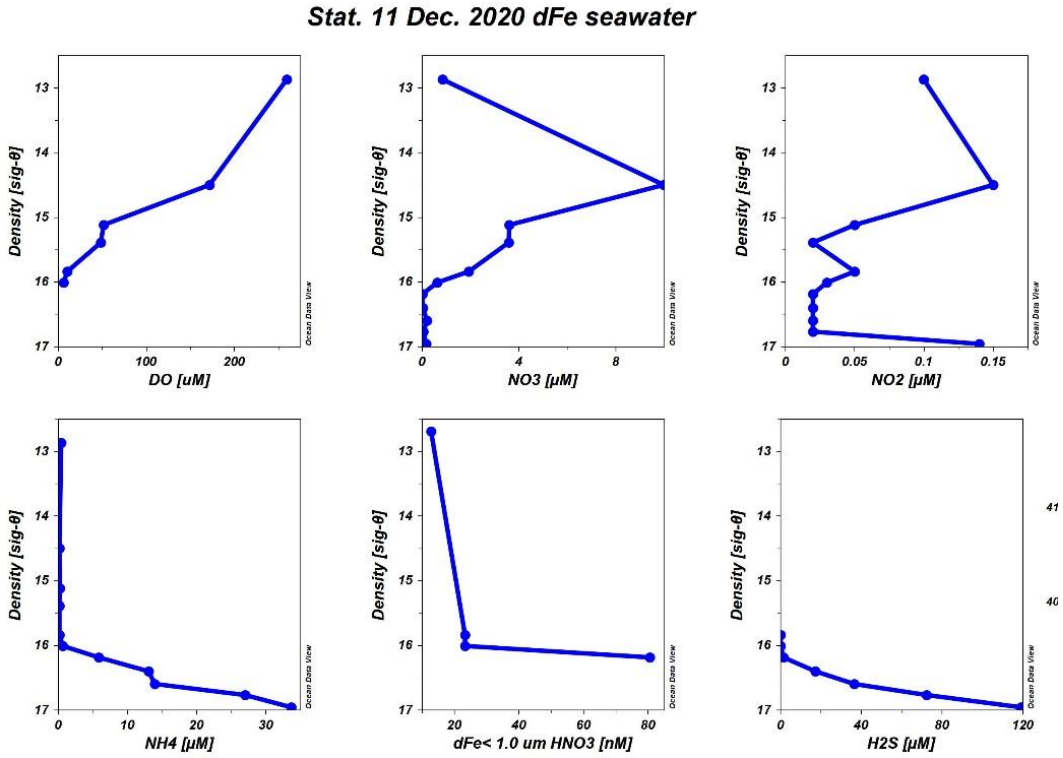

Figure 39: Station 11, December 2020 Black Sea R/V Bilim-2 Cruise: Seawater particulate iron (<1.0 µm), DO, redox sensitive nutrients and hydrogen sulfide distributions along the water column

Likewise, in station L56L10, we sampled the seawater along the whole water column for particulate iron analysis. The highest pFe value was 289nM at 16.60 σ_θ value on the upper boundary of hydrogen sulfide layer in the presence of 14.6uM H_2S.

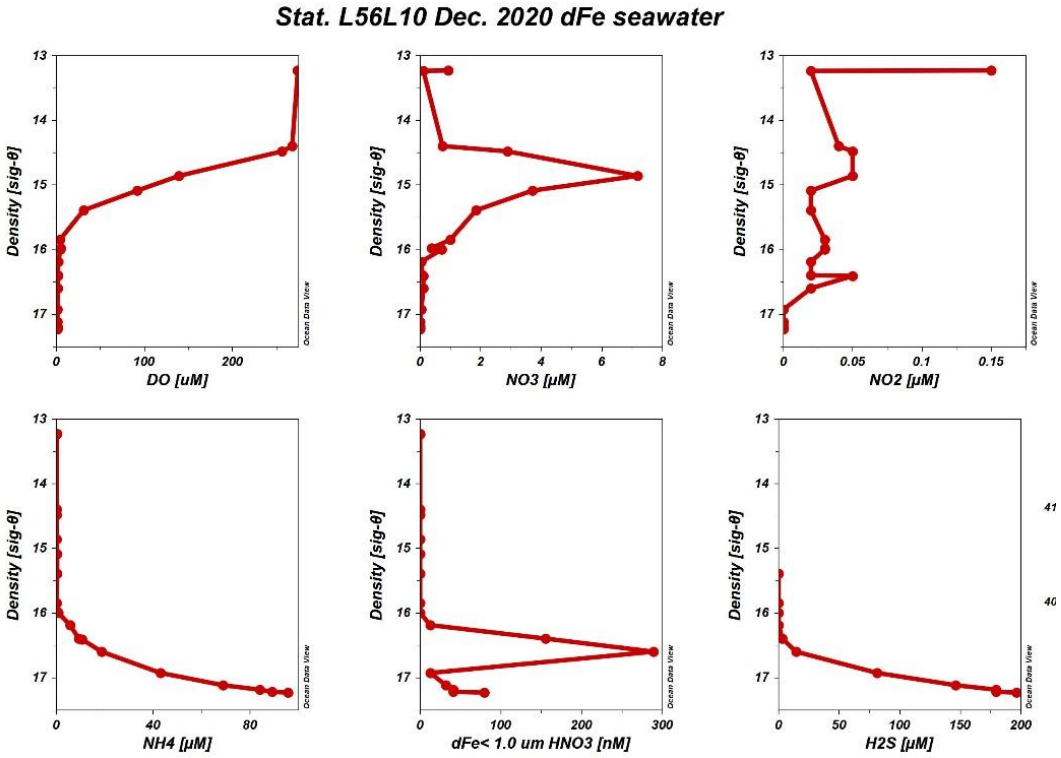

Figure 40: Station L56L10, December 2020 Black Sea R/V Bilim-2 Cruise: Seawater particulate iron (<1.0 µm), DO, redox sensitive nutrients and hydrogen sulfide distributions along the water column

After the preliminary results we obtained at nanomolar levels of iron in seawater during December 2020 cruise, in June 2021, we applied size fractionation in the depths of the highest dissolved iron in seawater. In station L43L10, in the off-shore of the southwestern transect, the dissolved iron distribution in watercolumn with other parameters are given on the top and size fractionation distribution of dissolved pool at σ_θ is given below in Figure 41. The suboxic layer showed high amounts of mobilized iron in the seawater to levels of 224nM. At 16.0 σ_θ value, dissolved iron was below detection limit. At 16.1 σ_θ value, the dissolved pool only consisted of colloidal fraction (29nM) and larger dissolved fraction (19nM). At 16.2 σ_θ depth, the dissolved pool only consisted of colloidal(38nM). There was no difference between nitric acid and hydrochloric acid treated samples for this station and no negative concentration result was obtained in this size fraction analysis.

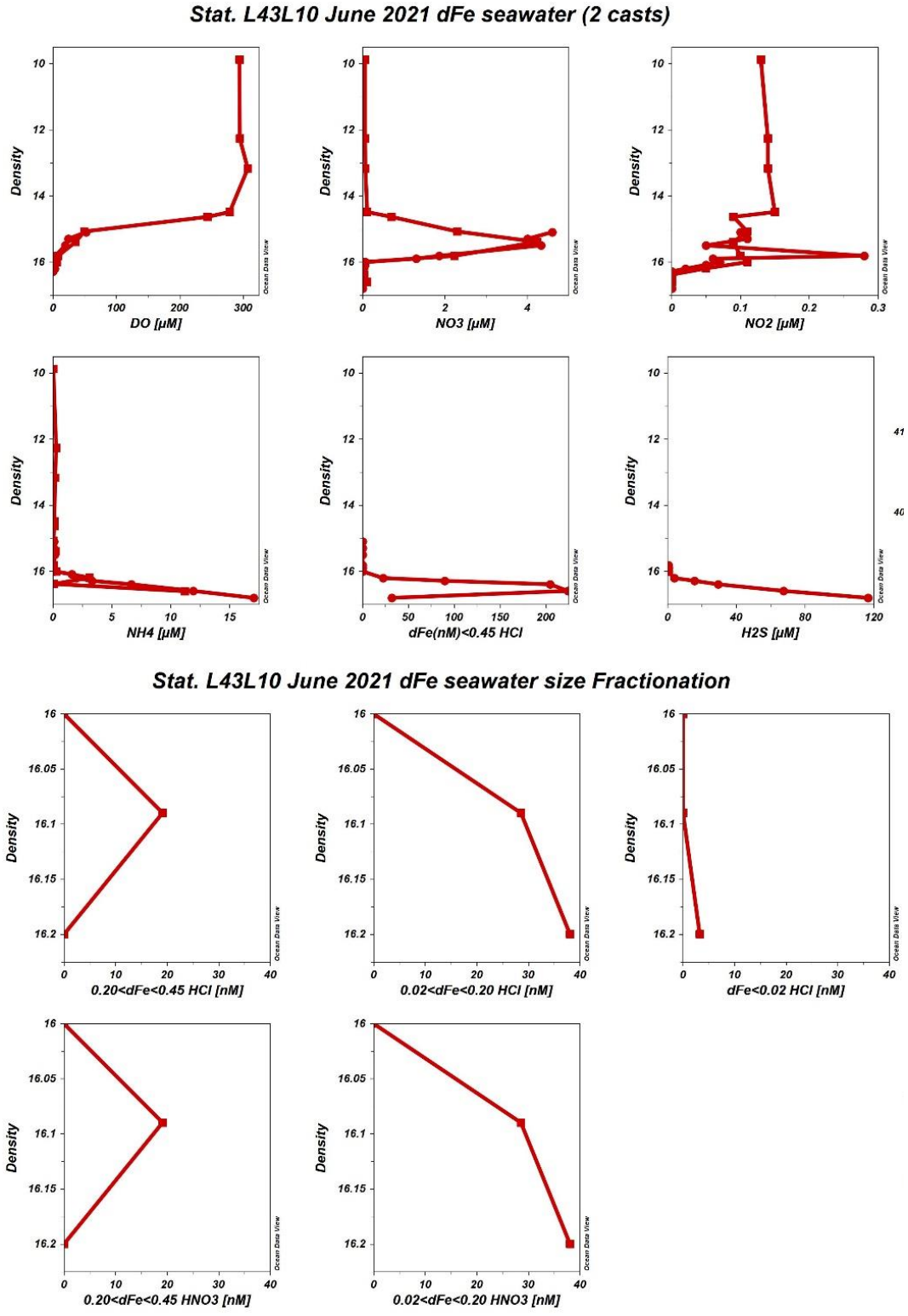

Figure 41: Station L43L10, June 2021 the Black Sea R/V Bilim-2 Cruise: (on top) Seawater dissolved iron (<0.45 µm), DO, redox sensitive nutrients and hydrogen

sulfide distributions along the water column. (below) Seawater dissolved iron (<0.45 μm) size fraction distributions along 3 density depths of σ_θ=16.0, 16.1, 16.2

In station L27L57, in the off-shore of the east of Bosphorus transect, the dissolved iron distribution in watercolumn with other parameters are given on the top and size fractionation distribution of dissolved pool at σ_θ is given below in Figure 42. The suboxic layer dissolved iron seawater was 89nM which were approximately half of the dissolved iron measured in L43L10. Selected σ_θ depths were 16.6,16.7 and 16.8, according to previous particulate iron results obtained in Black Sea. In this station, in addition to dissolved iron pool, particulate iron was also analyzed. 16.7 σ_θ depth had the highest particulate concentration as 176nM and colloidal concentration as 86nM. In this station, size fractionation results had negative values.

Overall, the negative concentration error was smaller in the seawater size fractionation results. The colloidal forms were found to be dominant for water column while soluble fraction was assessed to be dominant for porewater. These results exhibited that there was a difference in iron fractionation for seawater and porewater.

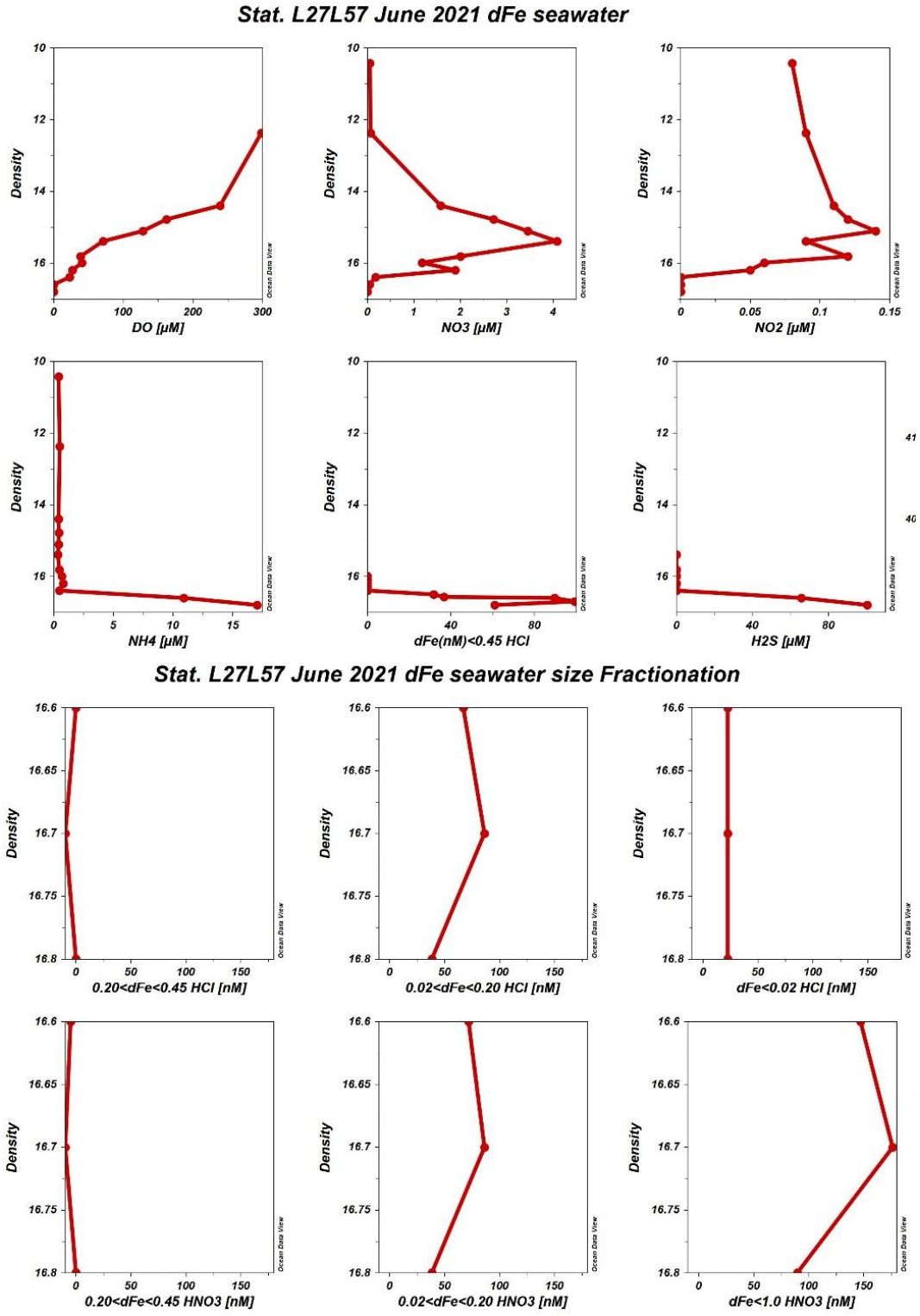

Figure 42: Station L27L57, June 2021 the Black Sea R/V Bilim-2 Cruise: (on top) Seawater dissolved iron (<0.45 µm), DO, redox sensitive nutrients and hydrogen

sulfide distributions along the water column. (below) Seawater dissolved iron (<0.45 μm) size fraction distribution along 3 density depths of σ_θ=16.6, 16.7, 16.8

3.2 The Sea of Marmara

3.2.1 Water column profiles of porewater stations

In this section, water column parameters are given over depth, exhibiting bottom water conditions for each station and temporal variability in between cruises.

Area	Cruise	Station	Bot. Depth (m)	Bot. DO [μM]	Redox Category
the sea of Marmara	December 2020	1	70	69	hypoxic
		3	286	11	hypoxic
		4	475	14	hypoxic
		5	84	39	hypoxic
		7	243	11	hypoxic
		8	381	17	hypoxic
	June 2021	1	67	49	hypoxic
		3	195	22	hypoxic
		4	649	7	suboxic
		IZMIT DEEP	206	0	sulfidic
		45-C	1214	5	suboxic

3.2.1.1 Hypoxic Water Column Profiles

Station 1 of the Izmit transect in the Sea of Marmara (Figure 43 in December 2020 and Figure 44 in June 2021), exhibited hypoxic conditions at the bottom with 69 μM DO in Dec. 2020 and 49 μM DO in June 2021. Dissolved nitrate was 6.6 μM in Dec. 2020 and it was higher in June 2021 as 9.57μM. Likewise, phosphate was 0.53μM during December 2020 and it was higher in June 2021 as 0.93μM. Overall, the nitrate levels of the bottom waters in the Sea of Marmara stations were higher than those of the Black Sea. Related porewater results are given in section 3.2.1.1 Figure 55.

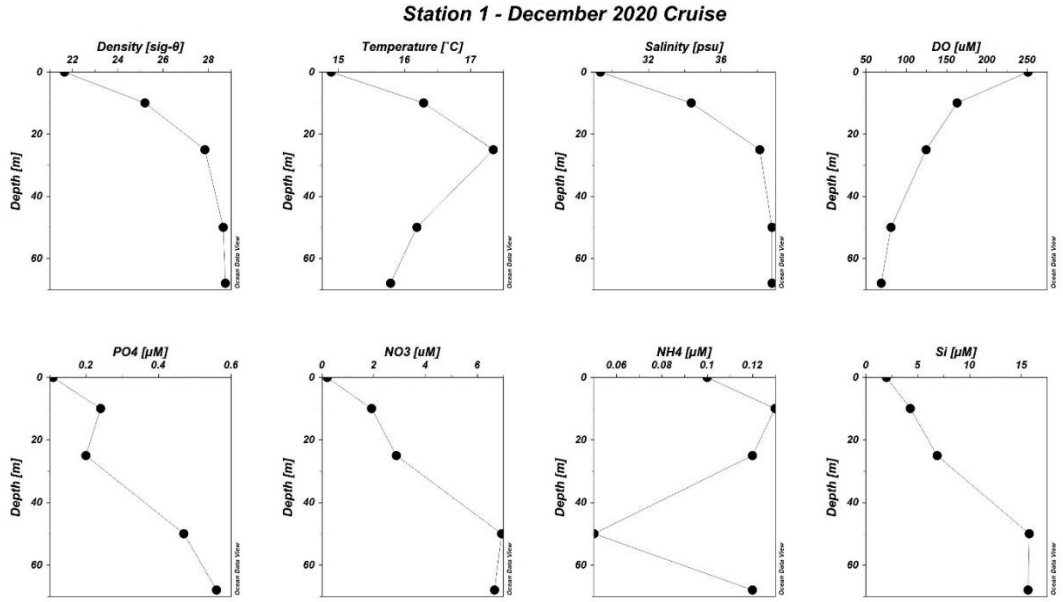

Figure 43: Station 1, December 2020 the Sea of Marmara R/V Bilim-2 Cruise: Water column physical and biogeochemical parameters vs. depth graphs. Bottom depth: 70m

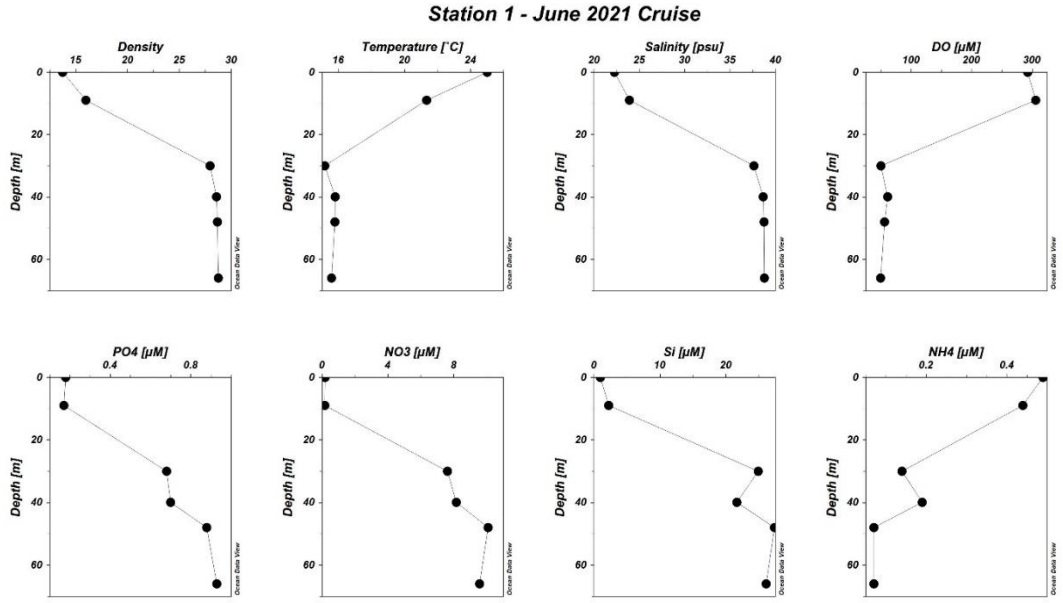

Figure 44: Station 1, June 2021 the Sea of Marmara R/V Bilim-2 Cruise: Water column physical and biogeochemical parameters vs. depth graphs. Bottom depth: 67m

Station 3 of the Izmit transect in the Sea of Marmara (Figure 45 in December 2020 and Figure 46 in June 2021), exhibited hypoxic conditions at the bottom with 21 µM

DO in Dec. 2020 and 11 µM DO in June 2021. Dissolved nitrate was 6.07 µM in Dec. 2020 and was higher in June 2021 as 8.18 µM. Likewise, phosphate was 0.74 µM during December 2020 and was higher in June 2021 as 0.99µM. Related porewater results are given in section 3.2.1.1 Figure 56.

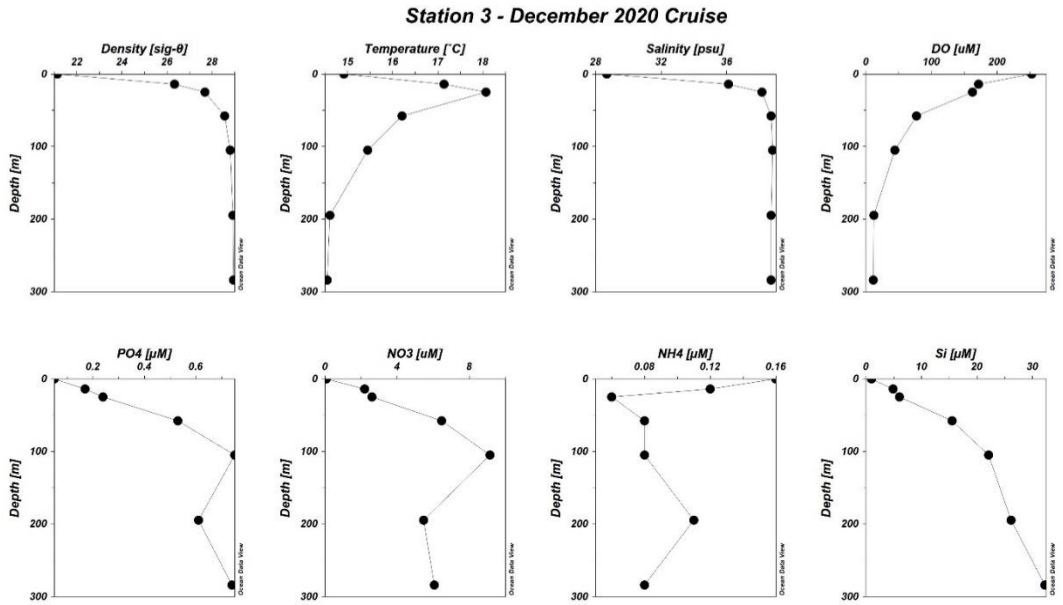

Figure 45: Station 3, December 2020 the Sea of Marmara R/V Bilim-2 Cruise: Water column physical and biogeochemical parameters vs. depth graphs. Bottom depth: 286m

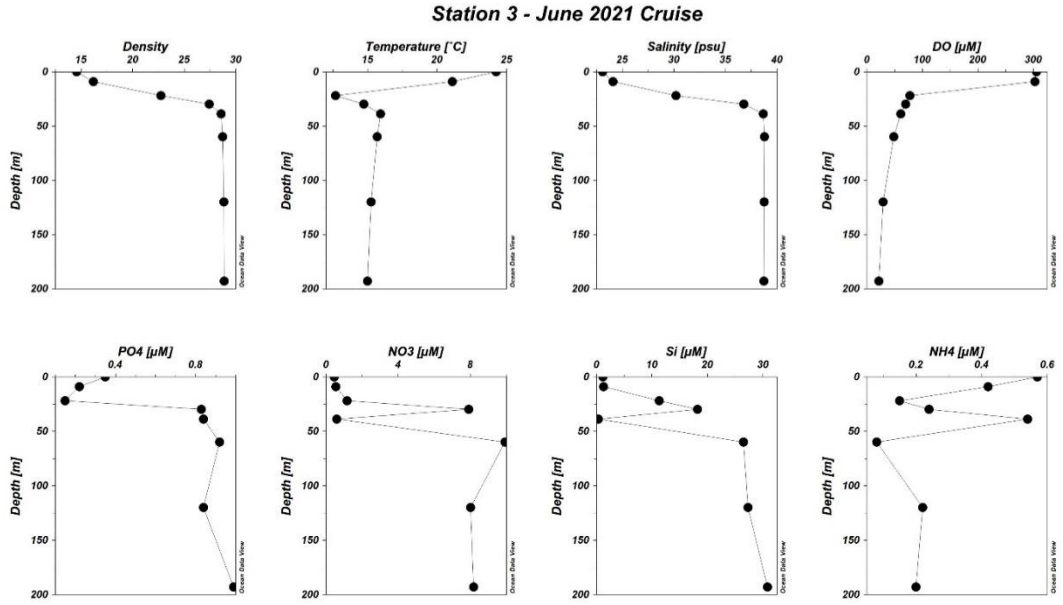

Figure 46: Station 3, June 2021 the Sea of Marmara R/V Bilim-2 Cruise: Water column physical and biogeochemical parameters vs. depth graphs. Bottom depth: 195 m

Station 4 of the Izmit transect in the Sea of Marmara (Figure 47 in December 2020), exhibited hypoxic conditions at the bottom with 13.5 µM DO in December 2020 cruise. Dissolved nitrate was 3.63 µM in Dec. 2020 and phosphate was 0.43 µM during December 2020. Related porewater results are given in section 3.2.1.1 Figure 57.

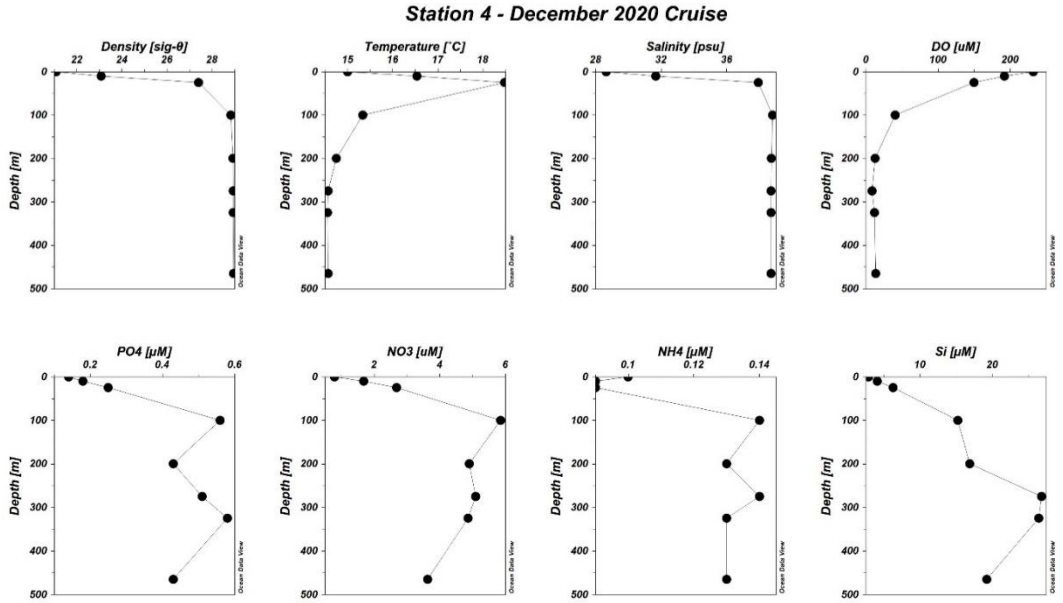

Figure 47: Station 4, December 2020 the Sea of Marmara R/V Bilim-2 Cruise: Water column physical and biogeochemical parameters vs. depth graphs. Bottom depth: 475 m

Station 5 of the Armutlu transect in the Sea of Marmara was visited only in December 2020 cruise (Figure 48), exhibited hypoxic conditions at the bottom with 39.3 µM DO. Dissolved nitrate was 13.36 µM while phosphate was 0.97 µM. Nitrate levels at the bottom of this area were significantly higher than the Black Sea transect and Izmit transect in the Sea of Marmara. Related porewater results are given in section 3.2.1.1 Figure 58.

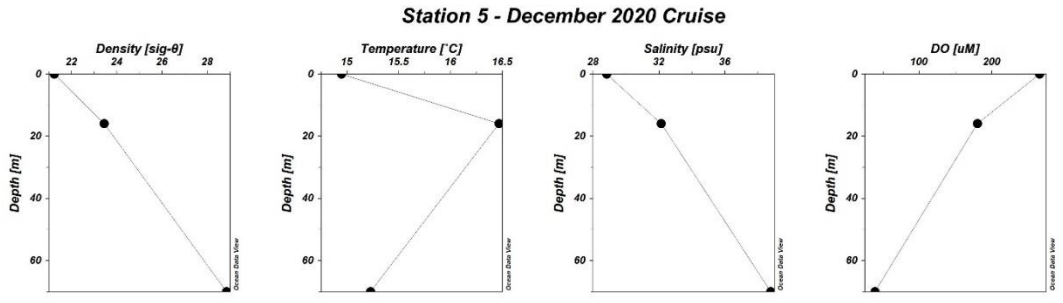

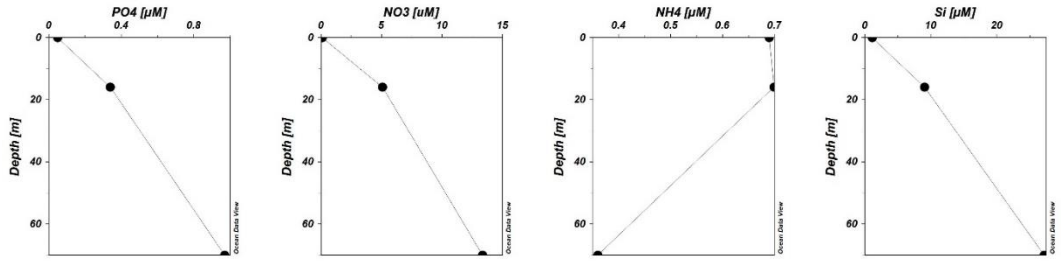

Figure 48: Station 5, December 2020 the Sea of Marmara R/V Bilim-2 Cruise: Water column physical and biogeochemical parameters vs. depth graphs. Bottom depth: 84 m

Station 7 of the Armutlu transect in the Sea of Marmara was visited only in December 2020 cruise (Figure 49), exhibited hypoxic conditions at the bottom with 11.10 µM DO. Dissolved nitrate was 14.62 µM while phosphate was 1.03 µM. Nitrate levels at the bottom are significantly higher than the Black Sea and Izmit transect in the Sea of Marmara. Related porewater results are given in section 3.2.1.1 Figure 59.

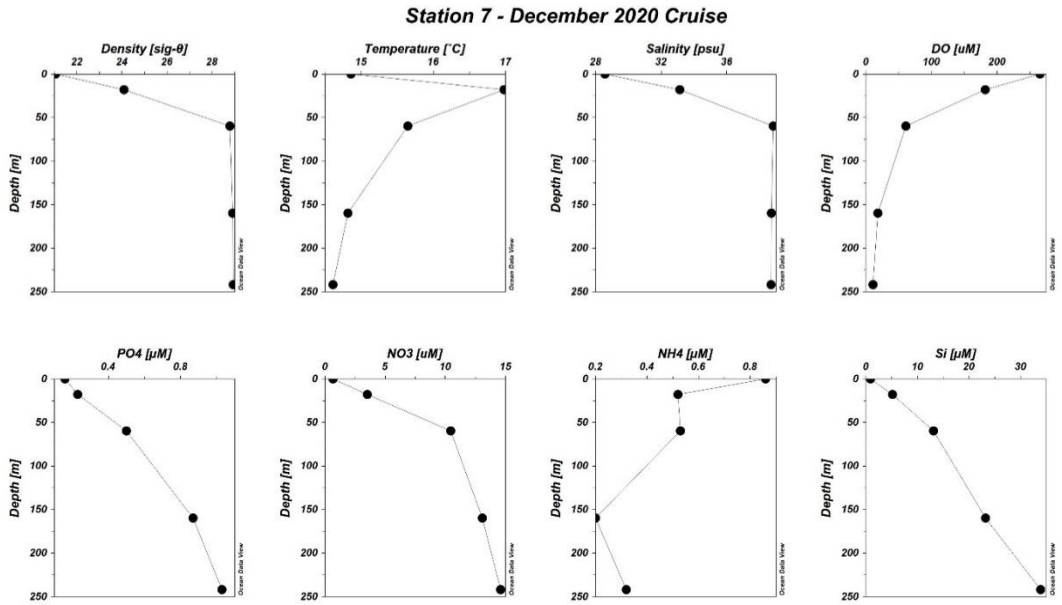

Figure 49: Station 7, December 2020 the Sea of Marmara R/V Bilim-2 Cruise: Water column physical and biogeochemical parameters vs. depth graphs. Bottom depth: 243 m

Station 8 of the Armutlu transect in the Sea of Marmara was visited only in December 2020 cruise (Figure 50), exhibited hypoxic conditions at the bottom with 17.30 µM DO. Dissolved nitrate was 12.75 µM while phosphate was 0.89 µM. Nitrate levels

at the bottom were significantly higher than the Black Sea and Izmit transect in the Sea of Marmara. Related porewater results are given in section 3.2.1.1 Figure 60.

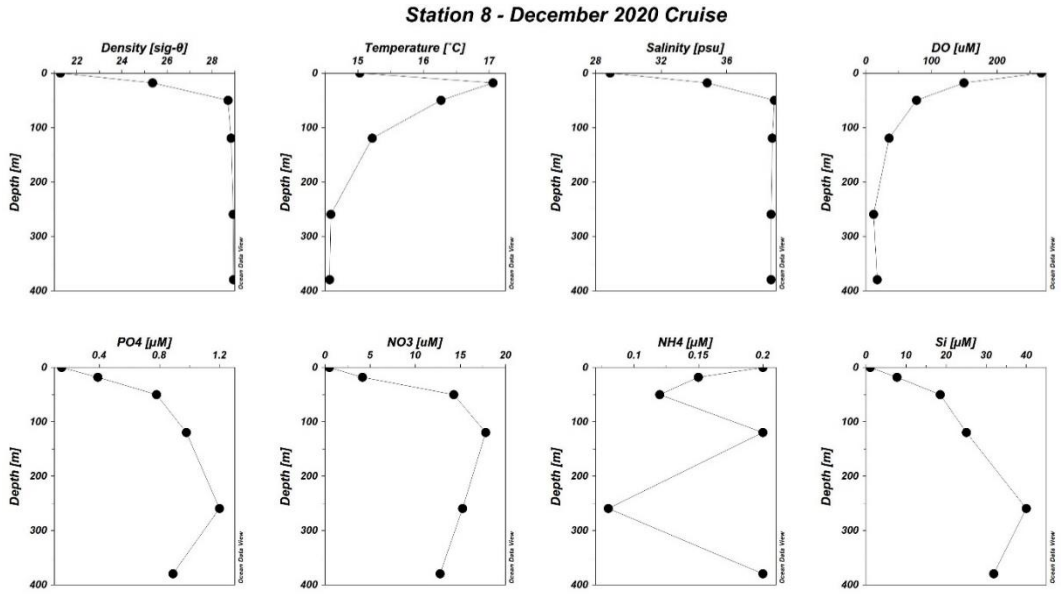

Figure 50: Station 8, December 2020 the Sea of Marmara R/V Bilim-2 Cruise: Water column physical and biogeochemical parameters vs. depth graphs. Bottom depth: 381 m

3.2.1.2 Suboxic Water Column Profiles

Station 4 of the Izmit transect in the Sea of Marmara (Figure 51 in June 2021), exhibited suboxic conditions with 7 µM DO in June 2021. Dissolved nitrate was 7.37 µM and phosphate was 1.33 µM. For station 4, in June 2021, a deeper area compared to December 2020 cruise was sampled due to drift during CTD operation which resulted in with lower DO and higher nutrient levels at the bottom. Related porewater results are given in section 3.2.1.1 Figure 57.

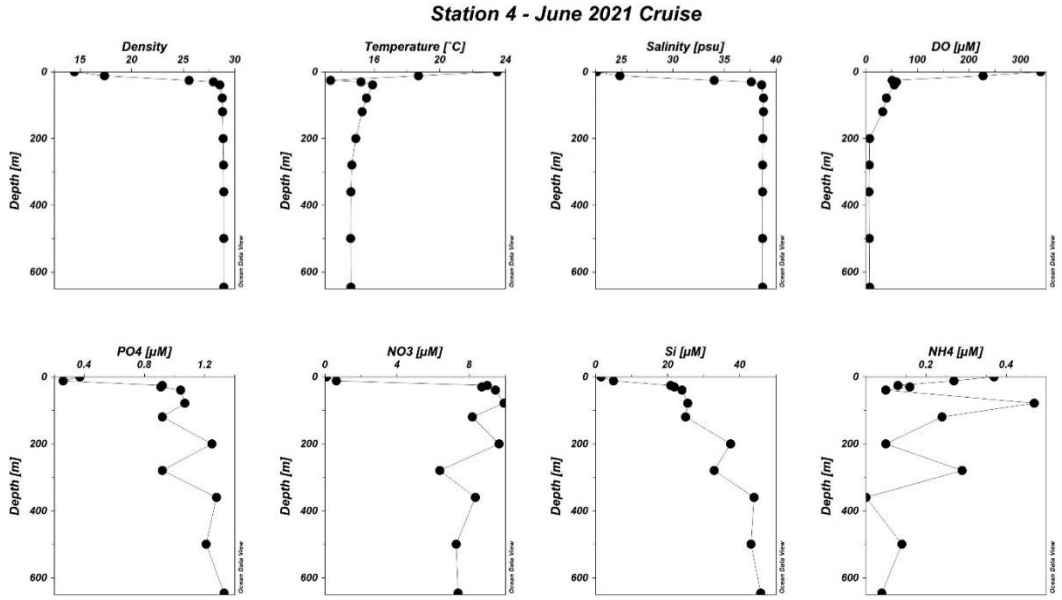

Figure 51: Station 4, June 2021 the Sea of Marmara R/V Bilim-2 Cruise: Water column physical and biogeochemical parameters vs. depth graphs. Bottom depth: 649 m

In addition to the shallow-deep transects around the rim of the Çınarcık Basin, we also collected samples for one time the Station 45-C (Çınarcık-Deep), deepest part in Çınarcık Basin in the Sea of Marmara, during the June 2021 cruise (Figure 52), exhibited nearly suboxic conditions at the bottom with 4.60 µM DO. In the bottom-most waters, dissolved nitrate was 4.29 µM which lower than other the Sea of Marmara stations while phosphate was 1.03 µM. In 45-C water column profile, general structure of the Sea of Marmara can be seen as drastically decreasing oxygen below pycnocline to 60µM levels and continues to decrease towards 350 m to levels of 10µM. 350-1000m interval exhibited DO levels around 10µM and below 1000m dissolved oxygen decreased to 5µM levels. 45-C water column represent an oxygen minimum zone (OMZ). Related porewater results are given in section 3.2.1.1 Figure 62.

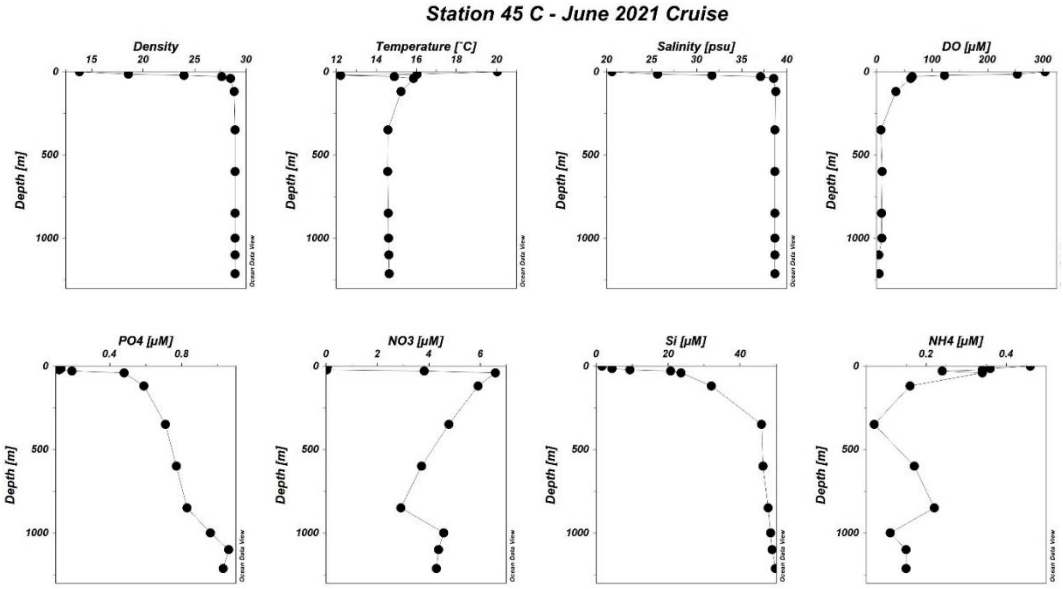

Figure 52: Station 45-C (Çınarcık-Deep), June 2021 the Sea of Marmara R/V Bilim-2 Cruise: Water column physical and biogeochemical parameters vs. depth graphs. Bottom depth: 1214 m

3.2.1.3 Sulfidic Water Column Profiles

Station IZMIT-DEEP, the deepest part of the İzmit Bay in the Sea of Marmara, was visited only in June 2021 cruise (Figure 53 and hydrogen sulfide profile in Figure 54), exhibited sulfidic conditions at the bottom with 33 µM H_2S. Bottom depth s 205m and below 118m appeared with 12µM and DO disappeared with 2.5µM, meaning bottom 87 meter water mass is sulfidic. Dissolved nitrate was close to detection limits as 0.4 µM at the bottom due to reducing conditions while phosphate was 1.98µM. Related porewater results are given in section 3.2.1.1 Figure 63.

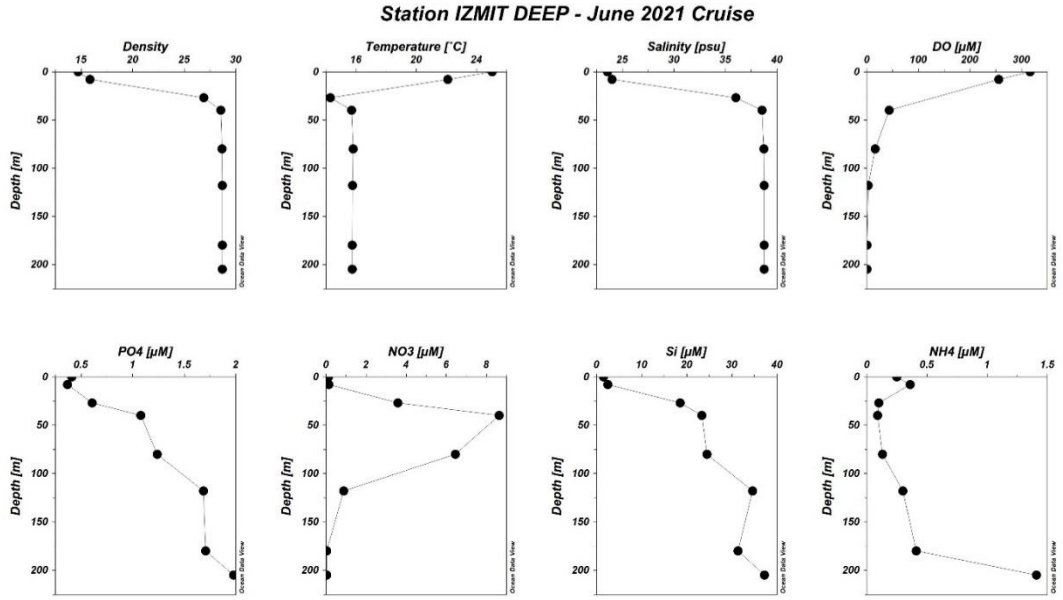

Figure 53: Station Izmit Deep, June 2021 the Sea of Marmara R/V Bilim-2 Cruise: Water column physical and biogeochemical parameters vs. depth graphs. Bottom depth: 206 m

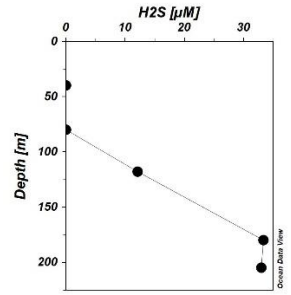

Figure 54: Station Izmit Deep, June 2021 the Sea of Marmara R/V Bilim-2 Cruise: dissolved hydrogen sulfide in water column.

In general, according to comparison of December and June cruises for the stations of 1, 3 and 4; June 2021 had higher nutrient values at the bottom. For the Sea of Marmara and the Black Sea bottom conditions comparison, the Sea of Marmara had significantly higher nitrate levels at the bottom in similar dissolved oxygen levels. This case suggests that the Sea of Marmara nutrient load is higher than the Black Sea for the periods we sampled.

3.2.2 Results of sedimentary porewater profiles

3.2.2.1 Sedimentary Porewater Profiles of Hypoxic Stations

Porewater nitrate, ammonia, dissolved iron, and hydrogen sulfide distributions along the core of station 1 are given in Figure 55 for both cruise legs in the Sea of Marmara. The water column characteristics of station 1 are given in the section 3.2.1 in Figure 43 and Figure 44 for December 2020 and June 2021 results, respectively. The bottom conditions represent hypoxia in both sampling periods.

In December 2020, the interface water had 10.10 μM of nitrate which was higher than bottom nitrate values. Nitrate decreased drastically in 1 cm surface layer to 2.10 μM indicating high denitrification activity at the very top of the sediment. Nitrate showed a decrease towards deeper with an increasing peak at 2cm and disappeared at 15cm layer. Dissolved iron was 1.78μM in the interface water and increased dramatically at 1 cm layer to 63.07 μM levels indicating high activity of microbial iron reduction. Nitrate and dissolved iron profile indicated high microbial anaerobic respiration within 1cm layer of the sediment. Dissolved iron reduction layer was quite narrow and dissolved iron decreased to 23.07 at 2cm and remained <1μM below 10cm except for 25 cm depth. Dissolved hydrogen sulfide was detected only in interface(2.3μM) and 3cm layer(0.8μM). The expected redox zonation order did not occur in this profile and no sulfate reduction layer appeared despite the very narrow iron reduction layer. This result might be related to small amount of TOC presence (Figure 64) in the core below 15cm (<0.80mmol/g).

In June 2021, the interface water had 1.60 μM of nitrate being remarkable lower than bottom water indicating denitrification on the sediment surface. Nitrate decreased to 0.40μM at 1cm, however, did not disappear and remains at 0.40-0.50 μM levels through whole profile. This result can be related to error in nitrate measurements and may be reflecting the contamination in distilled water used for measurements. Dissolved iron was 0.15μM in the interface water but exhibited a maxima at 1cm to

37µM levels. At 4 cm and deeper layers dFe varied from 3 to 5µM. As in December 2020, iron reduction appeared to be occurring at the top of the sediment within a narrow part. Dissolved hydrogen sulfide was detected only at 3cm layer (1.6µM) and 30cm layer(0.8µM).

Station 1 porewater nitrate, dFe and H_2S results indicated redox processes of denitrification and iron reduction is very intense in the surface sediments. December 2020 and June 2021 results looks similar interestingly especially for dissolved iron and dissolved hydrogen sulfide. Hydrogen sulfide appeared at 3cm in both cores and dissolved iron in corresponding layer did not show a significant increasing or decreasing trend.

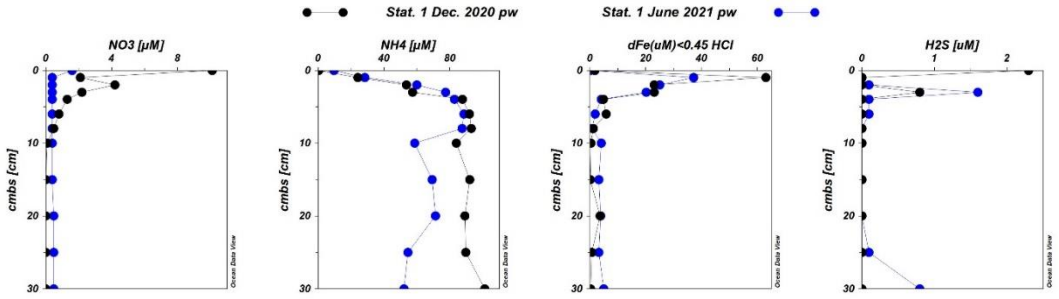

Figure 55: Station 1, December 2020 and June 2021 the Black Sea R/V Bilim-2 Cruise: Porewater redox-sensitive nutrients, dissolved hydrogen sulfide and dissolved iron (<0.45µm) distributions along the core.

Porewater nitrate, ammonia, dissolved iron, and hydrogen sulfide distributions along the core of station 3 are given in Figure 56 for both cruises. The water column characteristics of station 3 are given in the section 3.2.1 in Figure 45 and Figure 46 for December 2020 and June 2021 results, respectively. The bottom conditions represent hypoxia in both sampling periods.

In December 2020, the interface water had 6.40 µM of nitrate which was nearly the bottom water levels. Nitrate started to decrease from the surface towards 8cm and disappeared. Dissolved iron was 1.11µM in the interface water and increased dramatically at 1 cm layer to 87 µM levels indicating high activity of microbial iron reduction. Differently the nitrate profile indicated larger redox zonation compared to

station 1 and present below the iron reduction layer. Denitrification and iron reduction zones appeared to coincide. Dissolved hydrogen sulfide was detected only at 2-4cm range with maxima at 3cm as 4µM.

In June 2021, the interface water had 1.20 µM of nitrate which was substantially lower the nitrate concentrations of the bottom waters. Nitrate remained at 0.5-1.0 µM levels through whole profile except for 40cm layer with 1.9µM. Dissolved iron was 0.15µM in the interface water but maximized at 1cm to a concentration of 27µM. At 10 cm and deeper layers dFe was lower than 15µM, after 25cm decreased to 5µM levels and for the deeper part than 40cm remained in levels close to detection. Dissolved hydrogen sulfide was detected only 2-6 cm layer range (maxima=1.6µM).

Similar to station 1, station 3 porewater nitrate, dFe and H_2S results indicated a strong imprint of denitrification and iron reduction processes on the surface sediments. For both stations in December 2020 and June 2021 results looks similar and 3-5cm layer shows presence of hydrogen sulfide.

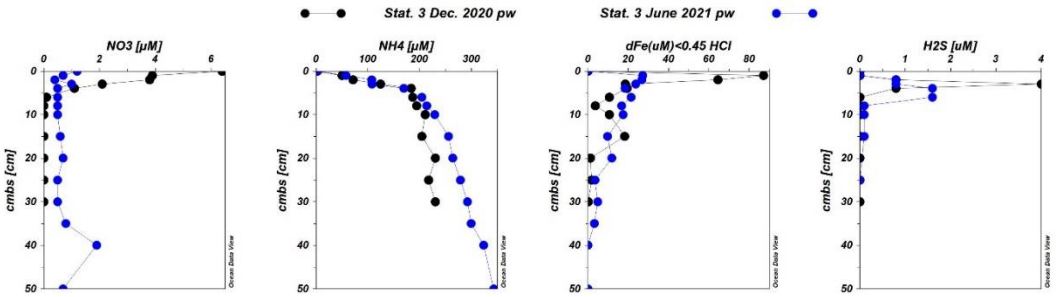

Figure 56: Station 3, December 2020 and June 2021 the Black Sea R/V Bilim-2 Cruise: Porewater redox-sensitive nutrients, dissolved hydrogen sulfide and dissolved iron (<0.45µm) distributions along the core.

Porewater nitrate, ammonia, dissolved iron, and hydrogen sulfide distributions along the core of station 4 are given in Figure 57 for December 2020 Cruise which exhibited hypoxic conditions at the bottom. The water column characteristics of station 4 are given in the section 3.2.1 Figure 47Figure 51 for December 2020.

In December 2020, the interface water had 9.5 µM of nitrate which was higher than bottom water levels. Nitrate started to decrease from the surface and disappears at

first 3 cm. Dissolved iron was 1.64µM in the interface water and increased at 3 cm layer to 26µM levels. Dissolved iron decreased after 3cm and gave a second peak at 8cm as 22µM. Dissolved hydrogen sulfide was detected only at 2-6cm range which remains to be 0.80µM. The hydrogen sulfide layer coincided with the decrease layer in dissolved iron before the second peak.

Station 1, 3 and 4 indicated that redox zonation in the Sea of Marmara is quite near the surface and dominated by denitrification and iron reduction. Surface 10 cm of the sediment was more prone to form redox zonation might be related to those general low levels of TOC below 10cm (section 0) in the Sea of Marmara restricted high respiration activities. Even though presence of hydrogen sulfide appeared only in some sediment layers and, especially around 3-5cm layers in the Sea of Marmara, it might be an indicative of sulfate reduction below the iron reduction zone. Disordered distribution of the hydrogen might be due to precipitation reactions between iron and sulfur which inhibits dissolved hydrogen sulfide in porewater.

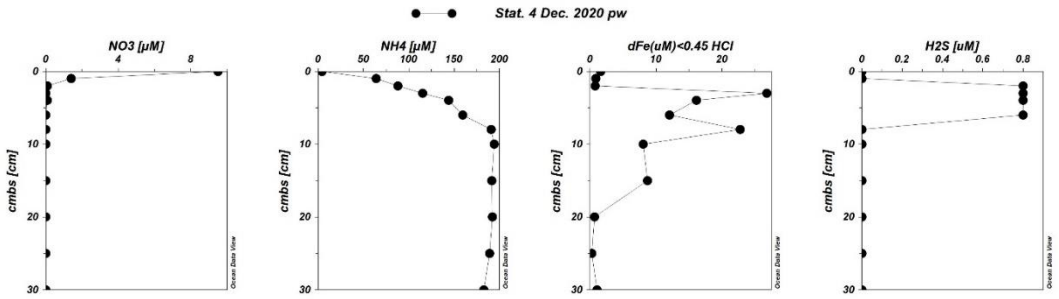

Figure 57: Station 4, December 2020 the Black Sea R/V Bilim-2 Cruise: Porewater redox-sensitive nutrients, dissolved hydrogen sulfide and dissolved iron (<0.45µm) distributions along the core

Porewater nitrate, ammonia, dissolved iron, and hydrogen sulfide distributions along the core of station 5 are given in Figure 58, which was visited only in December 2020 cruise. The water column characteristics of station 5 are given in the section 3.2.1 in Figure 48. The bottom conditions represented hypoxic.

In station 5, the interface water had 11.3 µM of nitrate, despite the nitrate concentration was high, the bottom water still had higher nitrate concentrations.

Nitrate started to decrease from the surface and disappeared at first 4 cm and lower level at the interface indicated the denitrification occurs above the sediment. Dissolved iron was 0.07µM in the interface water and increased at 1 cm layer to 11.5 µM levels. Dissolved iron remained around 10µM along the core (30cm) except for 4.87µM at 8cm. Ammonia distribution mirrored nitrate profile and was similar to the iron profile, indicating the release of both NH_4^+ and Fe to porewaters during sedimentary organic matter respiration. Dissolved hydrogen sulfide was below detection limit throughout the core.

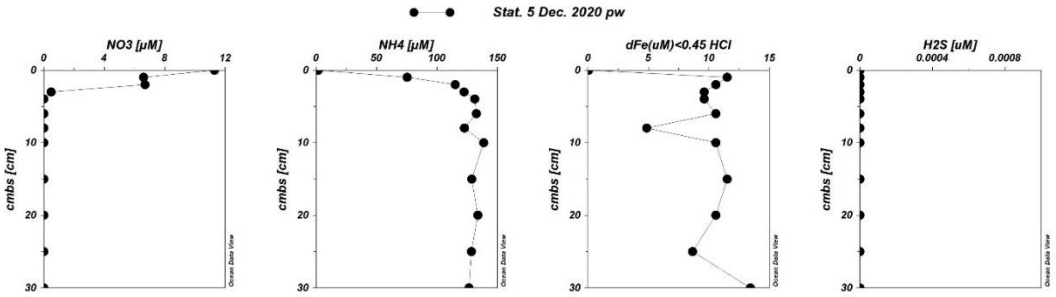

Figure 58: Station 5, December 2020 the Sea of Marmara R/V Bilim-2 Cruise: Porewater redox-sensitive nutrients, dissolved hydrogen sulfide and dissolved iron (<0.45µm) distributions along the core

Porewater nitrate, ammonia, dissolved iron, and hydrogen sulfide distributions along the core of station 7 are given in Figure 59, which was visited only in December 2020 cruise. The water column characteristics of station 7 are given in the section 3.2.1 in Figure 49. The bottom conditions represent hypoxic.

In station 7, the interface water had 1.40 µM of nitrate, the bottom water had significantly higher nitrate concentrations. Nitrate started to decrease from the surface and disappeared at first 4 cm and lower level at the interface indicated the denitrification occurs above the sediment. Dissolved iron was 0.11µM in the interface water and increases at 1 cm layer to 12.43 µM levels. Dissolved iron remained around 10µM down to 25cm and decreases to <5µM levels below 25cm. As in station 5, ammonia accumulated with depth except for the 10-14 cm interval. Dissolved hydrogen sulfide was only detected at the range of 4-8cm as 0.80µM.

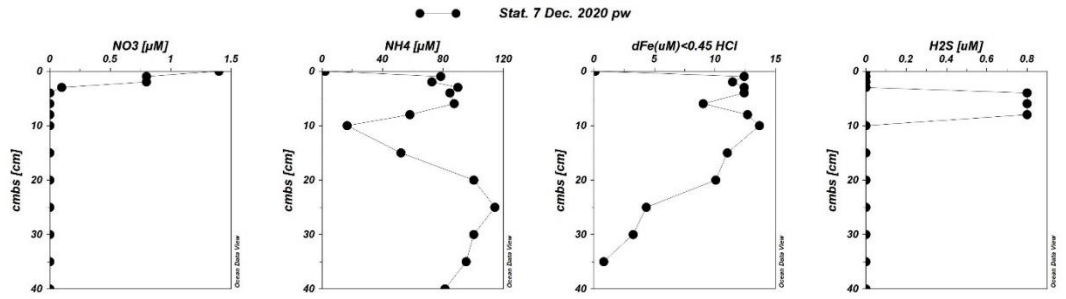

Figure 59: Station 7, December 2020 the Sea of Marmara R/V Bilim-2 Cruise: Porewater redox-sensitive nutrients, dissolved hydrogen sulfide and dissolved iron (<0.45µm) distributions along the core

Porewater nitrate, ammonia, dissolved iron, and hydrogen sulfide distributions along the core of station 8 are given in Figure 60, which was visited only in December 2020 cruise. The water column characteristics of station 8 are given in the section 3.2.1 in Figure 50. The bottom conditions represent hypoxic.

In station 8, the interface water had 9.80 µM of nitrate, the bottom water had higher nitrate concentrations. Nitrate started to decrease from the surface towards 2cm to 0.10µM and and disappeared at first 4 cm. Lower level at the interface indicates the denitrification occurs above the sediment. Dissolved iron was 0.86µM in the interface water and increased drastically at 1 cm layer to 60.37 µM levels. Dissolved iron showed disordered distribution with strong twists along the core, which was not the case in the station 5 and 7. Dissolved iron decreased to 8 µM at 2cm from 60µM at 1cm; increased at 3-4cm to 30-35µM levels and decreased again in the range of 4-10cm to 0.43µM levels. Below 10cm the layers had maximum and minimum points within 0-10µM concentration range. Dissolved hydrogen sulfide was only detected at the range of 3-10cm as 0.80µM. Ammonia distribution indicated a different increasing trend below 10cm and did not show coupled distribution with dissolved iron, a different trend from the station 5 and 7.

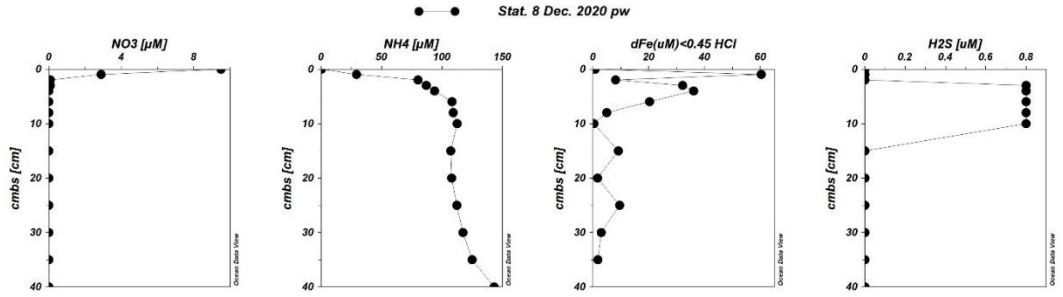

Figure 60: Station 8, December 2020 the Sea of Marmara R/V Bilim-2 Cruise: Porewater redox-sensitive nutrients, dissolved hydrogen sulfide and dissolved iron (<0.45µm) distributions along the core.

3.2.2.2 Sedimentary Porewater Profiles of Suboxic Stations

Porewater nitrate, ammonia, dissolved iron, and hydrogen sulfide distributions along the core of station 4 are given in Figure 61 for June 2021 cruise. The water column characteristics of station 4 are given in the section 3.2.1 in Figure 51 for June 2021 results which exhibited suboxic conditions at the bottom.

In June 2021, the interface water had 1.10 µM of nitrate which was lower than nitrate levels in the bottom water. Nitrate remained at 0.5-1.0 µM levels throughout whole profile, resembling the pattern of station 3 June 2021 profile. Dissolved iron was 0.58µM in the interface water and gave a maxima at 4cm to 50µM levels. Differently from other the Sea of Marmara stations, dissolved iron layer was larger as between 6-15cm dFe was around 30µM and only after 20cm decreased to 15µM. Dissolved hydrogen sulfide appeared at 1cm as 5 µM and discontinued along the core with presence at 2 and 6cm depths as 0.80µM.

In June 2021, the bottom water nutrients are quite higher than of December 2020, especially for nitrate, and dissolved oxygen levels are lower. The change in the water column towards less oxygenated state is seen as denitrification above the sediment surface instead of first 1-2cm of the sediment.

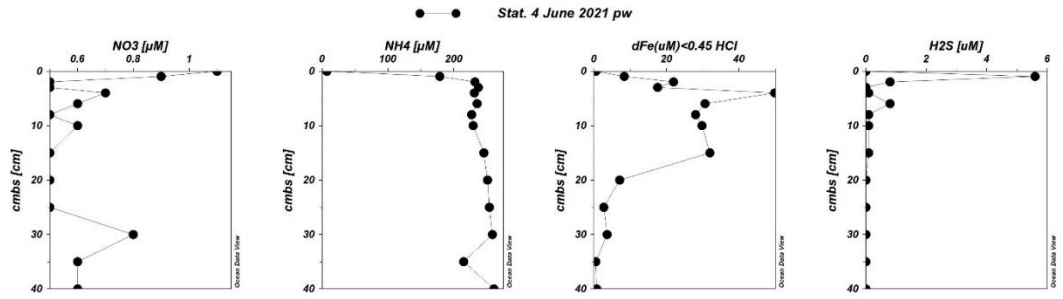

Figure 61: Station 4, June 2021 the Black Sea R/V Bilim-2 Cruise: Porewater redox-sensitive nutrients, dissolved hydrogen sulfide and dissolved iron (<0.45µm) distributions along the core

After presenting the results of the two transects, below the results of the two special stations in the Sea of Marmara 45-C and Izmit-Deep are given.

Porewater nitrate, ammonia, dissolved iron, and hydrogen sulfide distributions along the core of station 45-C are given in Figure 62 for both core results, which was visited only in June 2021 cruise but sampled two cores in the sample multi-corer operation. The water column characteristics of station 45-C are given in the section 3.2.1 in Figure 52. The bottom conditions were suboxic.

In station 45-C, the interface water had 1.40 µM of nitrate, lower than the bottom water levels. Nitrate decreased and remained in the range of 0.40-1.2µM along the core. June 2021 nutrient measurement errors masks the distribution of nitrate along the core however compared to bottom water conditions, sediment porewater levels were lower indicating the denitrification occurs above the sediment layer. Only dissolved iron and dissolved hydrogen sulfide was measured for both cores and nutrient were measured only in 45-1 numbered core. The data points for 6, 8 and 25cm layers was missing due to problems during sample handling for dissolved iron of the 45-1 core. These data points coincided the decreasing ranges within dissolved iron layer and thus the profile of dissolved iron distribution appeared differently for 45-1 core because of missing data points. The expectation was to have similar distribution for both cores since they were sampled during the same operation although the sediment layer was not expected to be fully homogenous. The most apparent difference was the amount of the dissolved iron. The dissolved hydrogen

sulfide, however, was sampled for all sampling depths and the distributions showed similarity with slight shift downward in the 45-2 core. Thus, the dissolved iron descriptions in this section refers to 45-2 core dFe values even though the nutrient data is coming from the 45-1 core. Dissolved iron was below detection limit in the interface water however appeared at the surface layer and remained around 5µMm until 4cm. Peaks at 6cm as 25µM, a second peak appears at 15cm as 27µM, and the third peak was at 30-35cm interval as 28-29µM. At 10cm a minima appeared as 18µM, second minima was at 25cm as 5.34 µM and for below 40cm layer, dFe remained in the range of 0.5-1.5µM. Dissolved iron showed disordered distribution with shifts in trend along the core at 10 and 25cm layers. Dissolved hydrogen sulfide was only detected at the range of 1-8cm with absence at 4cm, thus 2 peaks as 1.60µM at 1-2cm and as 0.80 at 6-8cm. Ammonia distribution did not show coupled distribution with dissolved iron, differently from the station 5 and 7.

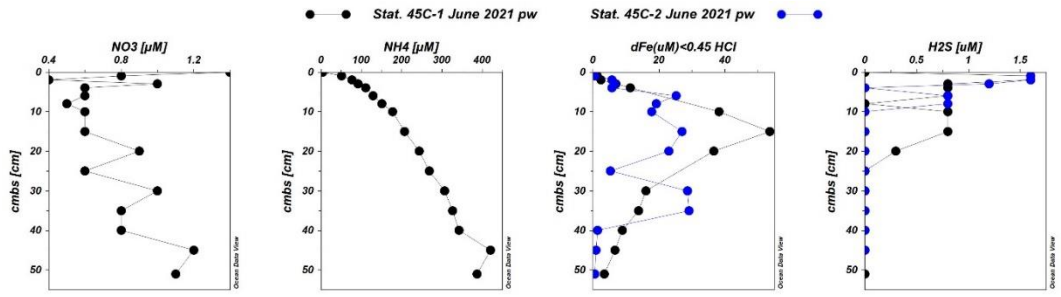

Figure 62: Station 45-C (Çınarcık-Deep), June 2021 the Sea of Marmara R/V Bilim-2 Cruise: Porewater redox-sensitive nutrients, dissolved hydrogen sulfide and dissolved iron (<0.45µm) distributions along the core.

3.2.2.3 Sedimentary Porewater Profiles of Sulfidic Stations

İzmit-Deep station is the deepest point (200m depth) in the İzmit Bay and was the most anoxic part of the Sea of Marmara. Porewater nitrate, ammonia, dissolved iron, and hydrogen sulfide distributions along the core of station IZMIT-DEEP are given in Figure 63, which was visited only in June 2021 cruise. The water column characteristics of station IZMIT-DEEP are given in the section 3.2.1 in Figure 53 and Figure 54. The bottom conditions were sulfidic in the deepest 87 meter of the

water column, indicating high microbial sulfate reduction activity in the water column.

In station IZMIT-DEEP, the interface water was sampled only for dissolved iron and dissolved hydrogen sulfide thus there is no data for nitrate in interface water. Nitrate remained in the range of 0.5-1.0µM for whole profile which might be related to measurement error. At 50cm, nitrate appeared as 3.6µM unexpectedly at the bottom of the core. Dissolved iron was 0.15µM in the interface water and remained in the range of 0.15-0.6µM for most of the part of the core (0-40cm) with an exceptional peak at 8cm as 3.20µM. Below 40cm, dFe increased towards 50cm to 2.55µM. Increase in dissolved iron and nitrate at the bottom of the core might be indicating the redox state was different at the bottom in addition to the regard of absence of hydrogen sulfide. Dissolved hydrogen sulfide was 32.3µM in the interface water which was the same levels as bottom water. Dissolved hydrogen sulfide increased towards 6cm and gives a maxima point as 182 µM. At 8 cm, coinciding the dFe peak, H_2S decreased to 51.60µM and increased again to 66µM at 10 cm layer. Below 10cm, H_2S remained to be 0.10µM. Ammonia distribution indicated a different increasing trend below 10cm. The shifts below 10 cm might be indicating less reducing conditions below 10 cm might be signifying that the reducing condition on the upper part of the sediment and water column is a recent change.

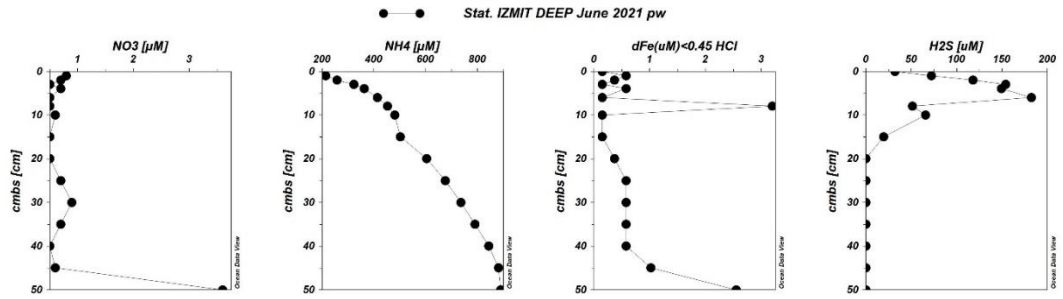

Figure 63: Station IZMIT-DEEP, June 2021 the Sea of Marmara R/V Bilim-2 Cruise: Porewater redox-sensitive nutrients, dissolved hydrogen sulfide and dissolved iron (<0.45µm) distributions along the core

Overall, except for IZMIT-DEEP station, the Sea of Marmara benthic characteristics is storngly similar to those of the Black Sea's oxic and suboxic bottoms considering

the high amounts of mobilized dissolved iron at the surface of the sediment. IZMIT-DEEP station resembles to sulfidic bottom of the Black Sea, however, IZMIT-DEEP has higher dFe values due to lower reducing conditions compared to sulfidic stations of the Black Sea. Also, the higher dFe values might be due to a recent change in the redox conditions and the sulfate reduction and iron reduction competition is not overwhelmingly won by sulfate reduction as it is in the Black Sea. In general, the Sea of Marmara redox state is mostly dominated by denitrification and iron reduction zone on the upper sediment and bottom waters; and compensates sulfate reduction at this moment.

3.2.3 Profiles of carbon and nitrogen analysis in solid sediment samples

Analysis for elemental carbon (total and organic fraction) and nitrogen is given (Figure 64-Figure 69) for station 1,3,4,5,7 and 8 visited in December 2020 cruise.

Total carbon in station 1 sediments is in the range of 2-3mmol/g and total organic carbon is in the range of 1-2mmol/g for first 10cm. Below 10cm, the range of TC drops to 1.7-1.8mmol/g and the range of TOC drops to 0.6-0.8mmol/g. TN is in the range of 0.07-0.19mmol/g for first 8cm and below it drops to 0.05-0.07 mmol/g range. TOC/TN ratio exhibits increasing trend towards 10-15cm as value of 18 and drops to levels of 14 below 15cm. Higher TOC content in the first 10cm shows stronger redox zonation on the upper part (Figure 55). Below 10cm, lower organic carbon content may not be adequate to support high anaerobic activities thus does not induce products of anaerobic processes at μM levels.

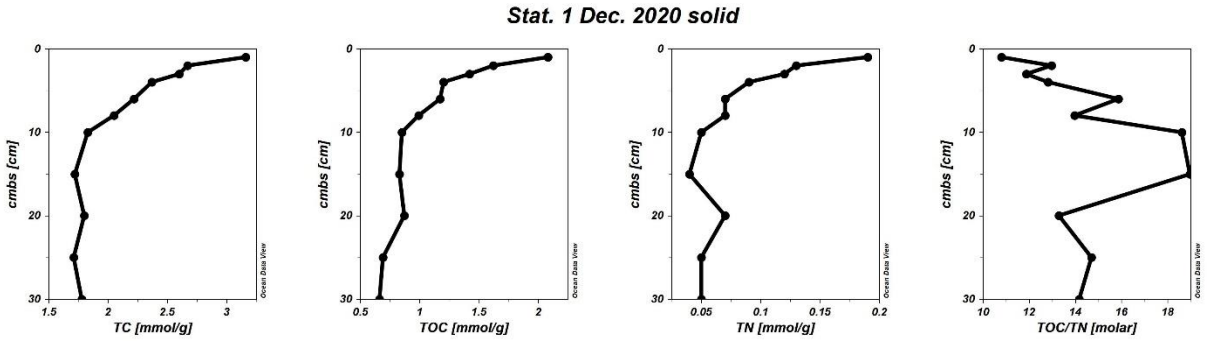

Figure 64: Station 1, December 2020 the Sea of Marmara R/V Bilim-2 Cruise: Sediment solid state total carbon and nitrogen distributions along the core.

Total carbon in station 3 sediments is in the range of 2-2.6mmol/g and total organic carbon is in the range of 1-1.5mmol/g for first 10cm. Below 10cm, the range of TC drops to 2-1.9mmol/g and the range of TOC drops to 1.0-0.7 mmol/g. TN is in the range of 0.06-0.12mmol/g for most of the profile with a minima of 0.03mmol/g at 30cm.

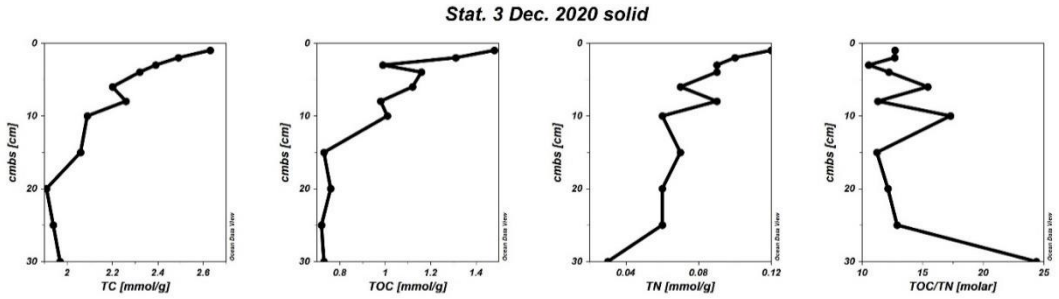

Figure 65: Station 3, December 2020 the Sea of Marmara R/V Bilim-2 Cruise: Sediment solid state total carbon and nitrogen distributions along the core.

Total carbon in station 4 sediments is in the range of 2-2.4mmol/g and total organic carbon is in the range of 0.9-1.29mmol/g for first 10cm. Below 10cm, the range of TC drops to 1.85-1.95mmol/g and the range of TOC drops to 0.8-0.9 mmol/g. TN is in the range of 0.07-0.11mmol/g for first 10cm and below 10cm it is in the range of 0.05-0.07mmol/g.

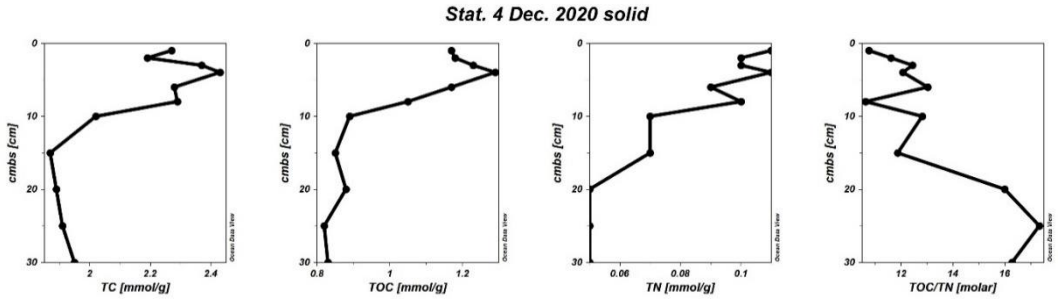

Figure 66: Station 4, December 2020 the Sea of Marmara R/V Bilim-2 Cruise: Sediment solid state total carbon and nitrogen distributions along the core.

Total carbon in station 5 sediments is in the range of 1.5-2.0mmol/g and total organic carbon is in the range of 0.4-0.8mmol/g for first 10cm. Below 10cm, the range of TC drops to 1.3-1.5mmol/g and the range of TOC drops to 0.3-0.5 mmol/g. TN is significantly low in the sediment solid as 0.04-0.03mmol/g for only the first 6cm.

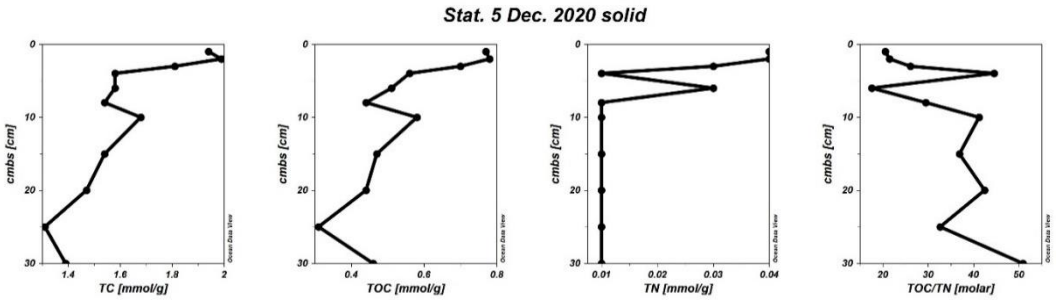

Figure 67: Station 5, December 2020 the Sea of Marmara R/V Bilim-2 Cruise: Sediment solid state total carbon and nitrogen distributions along the core.

Total carbon in station 7 sediments is in the range of 2.0-3.0mmol/g through whole profile except for 20cm with 3.93mmol/g. the difference between total carbon and total organic carbon is higher compared to other stations indicating high carbonate content. Total organic carbon decouples especially at 20cm signifies high amount of carbonate deposition.

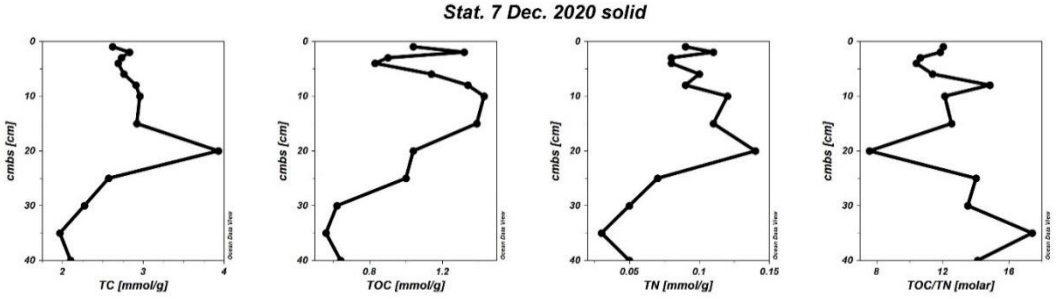

Figure 68: Station 7, December 2020 the Sea of Marmara R/V Bilim-2 Cruise: Sediment solid state total carbon and nitrogen distributions along the core.

Total carbon in station 8 sediments is in the range of 2.0-2.7mmol/g and total organic carbon is in the range of 0.5-1.5mmol/g for the first 20cm, differently than other stations 10 cm organic rich part. Below 20cm, the range of TC drops around 1.5mmol/g and the range of TOC drops around 0.2mmol/g. TN is in the range of

0.04-0.1 mmol/g for first 20cm and below 20cm it is in the range of 0.01-0.02mmol/g.

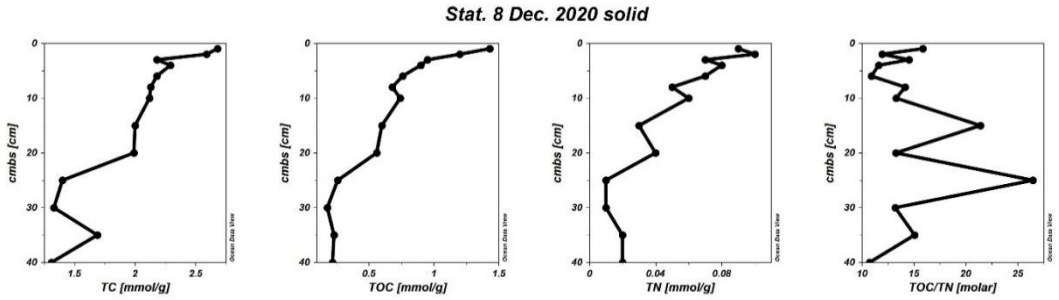

Figure 69: Station 8, December 2020 the Sea of Marmara R/V Bilim-2 Cruise: Sediment solid state total carbon and nitrogen distributions along the core

3.2.4 Profiles of size fraction in porewater dFe

In station 3 and 7, high amount of dissolved iron result in porewater was promising for size fractionation analysis. The size fraction distribution along the core within the dissolved iron pool is given in Figure 70 for station 3 and Figure 71 for station 7. The results has higher negative concentration error in fractions than for the Black Sea size fractions in porewater. Higher error and absence of colloids indicates the nature of the fractions different than Black Sea benthic fractions.

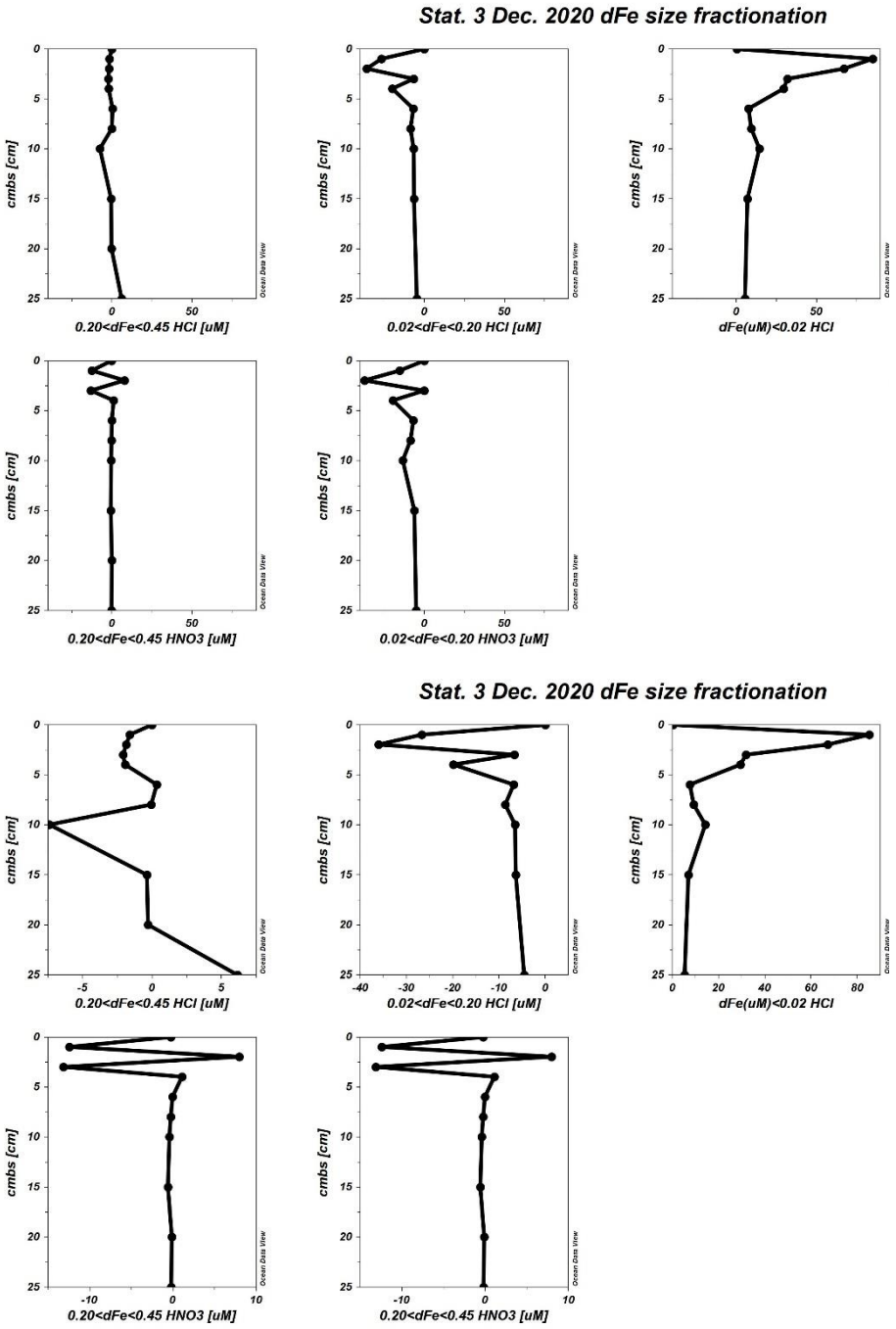

Figure 70: Station 3, December 2020 the Sea of Marmara R/V Bilim-2 Cruise: Porewater dissolved iron (<0.45µm) size fractions distributions along the core. (On top) the distributions over the same scale range of concentrations. (Below) the distributions are widened to observe the distribution trend.

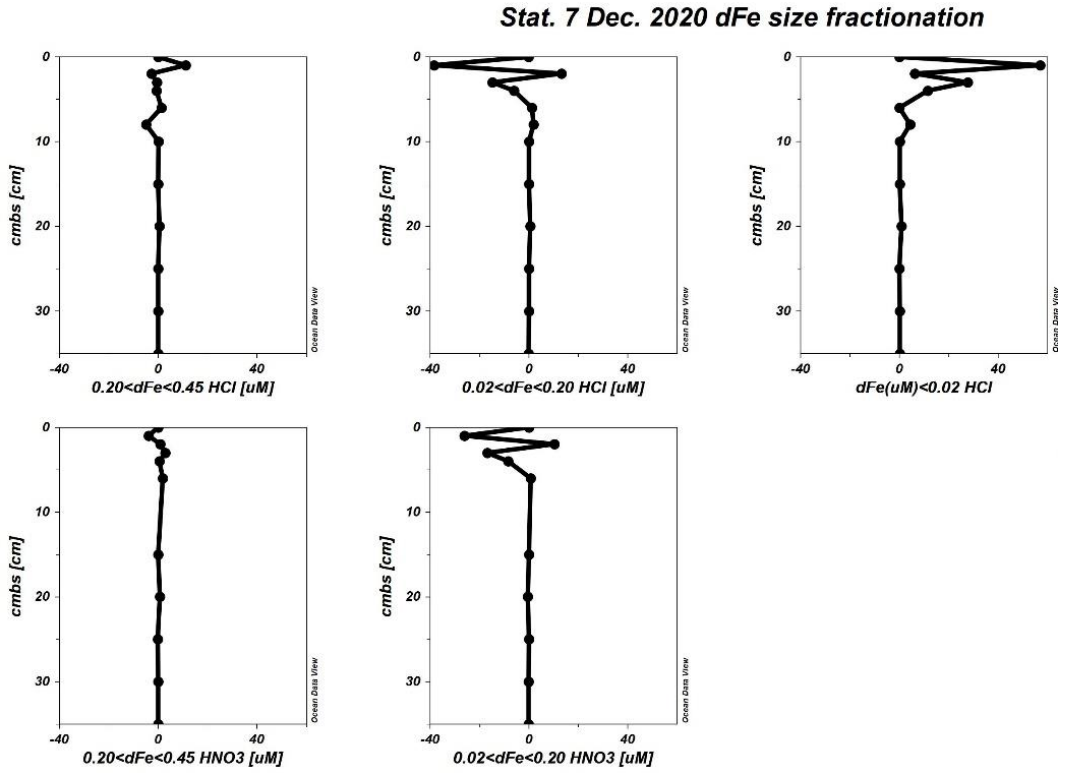
Stat. 7 Dec. 2020 dFe size fractionation
cmbs [cm]
0.20<dFe<0.45 HCl [uM]
0.02<dFe<0.20 HCl [uM]
dFe(uM)<0.02 HCl
0.20<dFe<0.45 HNO3 [uM]
0.02<dFe<0.20 HNO3 [uM]
Ocean Data View

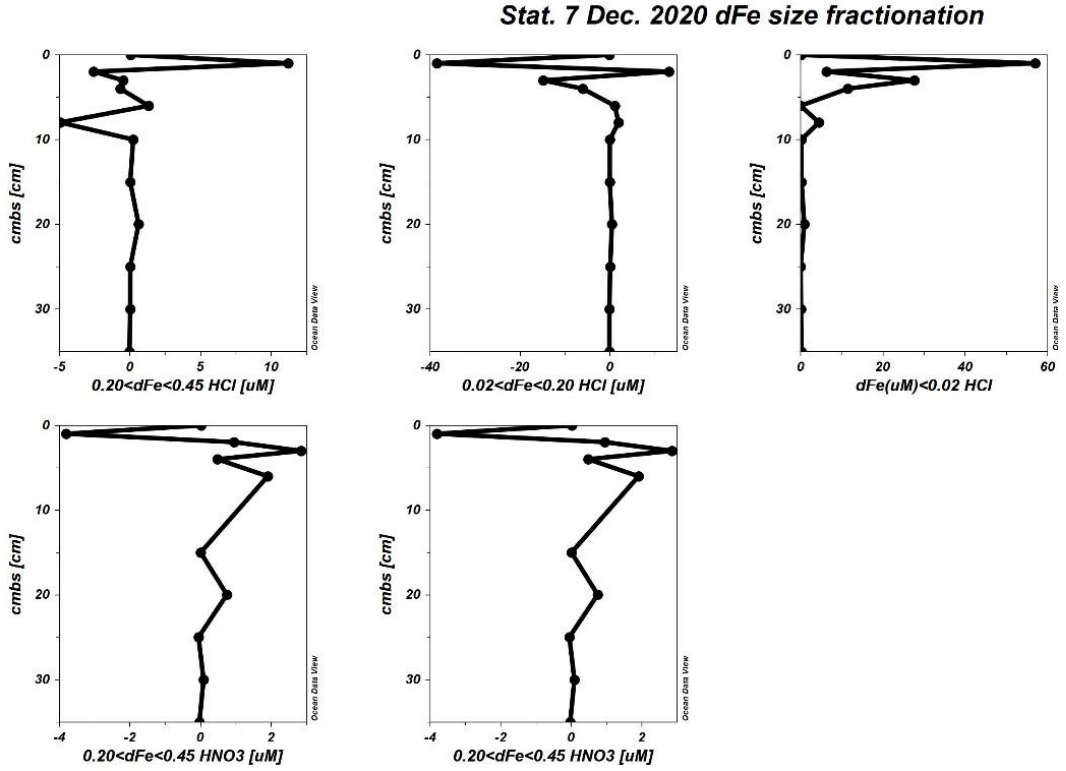
Stat. 7 Dec. 2020 dFe size fractionation
cmbs [cm]
0.20<dFe<0.45 HCl [uM]
0.02<dFe<0.20 HCl [uM]
dFe(uM)<0.02 HCl
0.20<dFe<0.45 HNO3 [uM]
0.20<dFe<0.45 HNO3 [uM]
Ocean Data View

Figure 71: Station 7, December 2020 the Sea of Marmara R/V Bilim-2 Cruise: Porewater dissolved iron (<0.45μm) size fractions distributions along the core. (On top) the distributions over the same scale range of concentrations. (Below) the distributions are widened to observe the distribution trend.

CHAPTER 4

DISCUSSION

4.1 Comparison of the Black Sea vs. the Sea of Marmara

In the Black Sea, the porewater profiles are consistent with the typical organic matter respiration pathways and their expected zonation in the literature (D. E. Canfield et al., 1993). For oxic/hypoxic conditions in Black Sea, denitrification occurs at the very surface of the sediment or even above the sediment layer, extending well into the bottom deep waters. Below the denitrification layer the redox zone shifts to iron reduction layer in the range of 2-4 cm of the sediment surface, yielding a sharp dissolved iron peak. The finding that in the uppermost centimeters of the sediment layer we encountered signs of microbial iron respiration indicates that redox transitions are rapid and fast on the surface sediments, primarily driven by high rates of organic carbon oxidation rates because lower carbon oxidation rates would cause metal cycles to appear much lower layers in the sediment (Y. Wang & Van Cappellen, 1996). Sedimentary iron reduction occurs mainly by two mechanisms: reductive iron dissolution by organic matter respiration (biotic) and reduction by hydrogen sulfide (mostly abiotic) (Burdige, 1993; A J Pyzik et al., 1992; Albert J Pyzik & Sommer, 1981). Reduction by hydrogen sulfide immobilizes iron to precipitate as Fe-S minerals (Rickard & Luther, 2007). According to Burdige (1993), the production of dissolved iron in the sediments porewater is mainly controlled by reductive dissolution of iron coupled to organic matter degradation. In Black Sea results, high amounts of dissolved iron at the surface sediments indicates high levels of overall organic matter degradation and reductive iron respiration under oxic and suboxic conditions. In the sulfidic conditions, as expected according to literature,

low levels of dissolved iron are present due to strongly reducing conditions that is fully dominated by sulfate reduction. Here, iron reduction is only taking place concurrently with sulfate reduction (Donald E. Canfield et al., 1996) and iron is immobilized down to nanomolar levels. In general, the sedimentary organic matter degradation is dominated by anaerobic process in the absence of oxygen (D. E. Canfield et al., 1993).

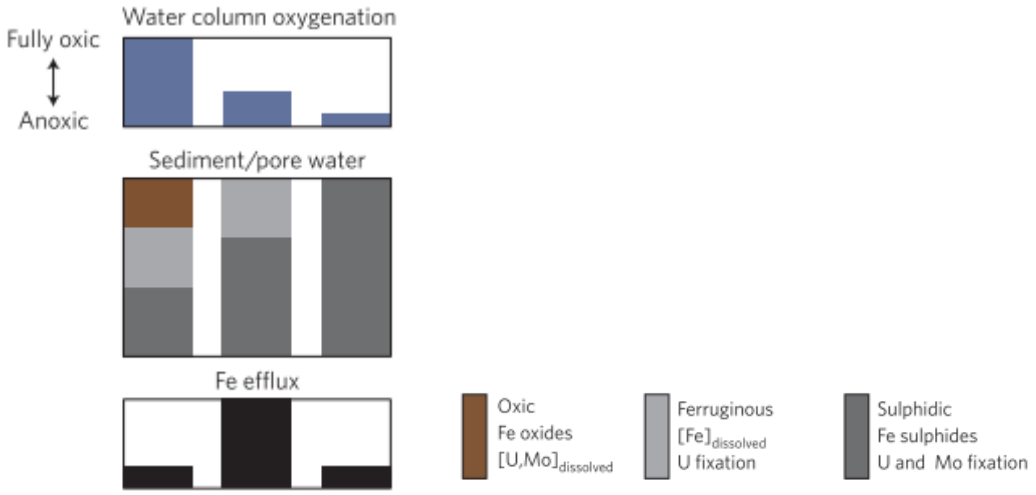

Figure 72: The relation between Fe efflux and bottom water oxygen levels (Scholz et al., 2014.)

The most favorable condition for iron dissolution is a narrow redox window with low-oxygen and non-sulfidic condition on the surface of the sediment (W. B. Homoky et al., 2011; Pakhomova et al., 2007; Scholz et al., 2014b), which is consistent with our Black Sea transects results. the Sea of Marmara experiencing a recent deoxygenation due to recent anthropogenic stress and eutrophication (Akçay, 2022), represents an oxygen-depleted bottom which suitable for high dissolved iron efflux at the bottom. The stations selected in the eastern part of the Sea of Marmara , due to remoteness from the Mediterranean oxygenated water input and high impact of urban areas, exhibits low-oxygen and hypoxic conditions at the sea floor (see section 3.2.1) and (Yucel et al., 2020; 2021; Akçay, 2022). Thus, the Sea of Marmara is a promising spot to find high levels of dissolved iron in sediments. However, the benthic iron in sedimentary porewater studies in the Sea of Marmara was missing

while the iron speciation in sediment solids were studied (Yang et al., 2018a). So far, the porewater of the Sea of Marmara was mostly studied within the aim of understand the gas hydrate related processes and not included iron dynamics of porewaters (Ruffine et al., 2015). On top of this, the Sea of Marmara differs from the suboxic areas of Black Sea in terms of the redox history. The Black Sea's redox conditions are quite profound and well-structured while the Sea of Marmara is experiencing a recent deoxygenation and changes in its redox regimens. Hence, the comparison between the Black Sea and the Sea of Marmara provides a novel approach and an additional perspective for investigating the benthic iron dynamics under recent redox changes.

According to bottom water results of the Sea of Marmara, nitrate concentrations were generally higher than Black Sea's bottom waters which indicates higher levels of availability of a higher energy-yielding electron acceptor compared to iron. The dominant microbial respiration pathways were denitrification and iron reduction on the surface of the sediment, with absence of hydrogen sulfide layer indicating no significant activity of sulfate reduction along the sampled sediment depths. Also, due to lower organic carbon content of the deeper sediments, the carbon oxidation activity was mostly restricted to surface 10 cm layers of the sediment. Despite the lack of a significant sulfate reduction, just below the iron reduction zone a low level of dissolved hydrogen sulfide was detected for 3-5cm layers in most of the station. This pattern might be indicative of low activity of sulfate reduction just below the iron reduction zone which could be a consequence of tight redox zonation created by narrow organic carbon layer. The hydrogen sulfide accumulation cannot be taking place in the occupation of dissolved iron.

4.1.1 Flux Calculations

The porewater dissolved iron concentrations and their distributions among the stations were presented in the result section (see section 3.1.2 and 3.2.1.1). To understand their potential scale of being a sedimentary source, dissolved iron fluxes

based on diffusion calculation upon concentrations gradients are needed to be assessed.

Porewater dissolved iron fluxes based on diffusion for each station visited in R/V Bilim-2 December 2020 cruise was calculated by using Fick's first law of diffusion (Boudreau, 1996; Yücel, 2009). According to Fick's first law of diffusion (Eq.1), the flux, J, is calculated by the parameters of effective diffusivity (D^{eff}) and the concentration gradient(∂C) over the depth interval(∂z). The depth intervals for concentration gradient are preferred according to surface peak values (Table 3).

$$J = D^{eff}\left(\frac{\partial C}{\partial z}\right) \qquad \text{(Eq.1)}$$

Effective diffusivity coefficients are adjusted molecular diffusivity (D_0) coefficients accordingly for porous media (Eq.2).

$$D^{eff} = D_0 - [1 - 2\ln(ø)] \quad \text{(Eq.2)}$$

Porosity(ø) of the sediment over the depth interval is calculated by the ratio of voids over total weight of the sediment (Eq.3).

$$ø = \frac{wet - dry\ weight}{wet\ weight} \qquad \text{(Eq.3)}$$

Molecular diffusivity values were also corrected according to salinity, temperature and pressure conditions at the bottom for each station and values are obtained by using R programming "marelac" package by Karline Soetaert and Thomas Petzoldt (2020) which is based on (Boudreau, 1996).

Dale and coworkers (2015) suggested that to improve the estimations for benthic inputs to marine iron cycle, carbon oxidation rate and bottom water oxygen levels are crucial parameters to include, and previous models were underestimating the benthic fluxes. For this reason, with estimation approaches, carbon oxidation rate and the relation of the bottom water oxygen levels are discussed below.

Flux calculations were done to infer and investigate: I) sediment-water interface diffusive flux of iron to interpret the benthic iron source; II) depth integrated flux for

NH_4^+ and Fe compared to interpret the total carbon oxidation and the contribution of iron respiration.

The carbon content of the sediment solid phases was only analyzed for the samples of December 2020 Cruise. So, the porosity data required for the flux calculation of June 2021 cruise samples was taken from the December 2020 cruise.

Table 3: Diffusive iron flux at sediment-water interface with redox conditions and physical parameters affecting the molecular diffusivity. Orange cells: porosity data

Area	Cruise	Station	dFe [µM]	dZ (cm)	Molecular Diffusivity D_0 ($m^2.d^{-1}$)	porosity ø	JFe ($\mu mol.m^{-2}d^{-1}$)	Bottom Depth (m)	Bottom Temp (°C)	Bot. Salinity (psu)	Bottom DO [µM]	Bottom NO_3^- [µM]	TOC at dZ (mmol/g)
the Sea of Marmara	December 2020	1	63	1	4.54E-05	0.14	**56**	70	15.8	38.8	69	6.7	2.1
		3	87	1	4.40E-05	0.14	**78**	286	14.6	38.7	11	6.1	1.5
		4	27	3	4.40E-05	0.11	**7**	475	14.6	38.7	14	3.6	1.2
		5	12	1	4.47E-05	0.10	**9**	84	15.2	38.8	39	13.4	0.8
		7	12	1	4.40E-05	0.16	**12**	243	14.6	38.7	11	14.6	1.0
		8	60	1	4.40E-05	0.11	**48**	381	14.6	38.7	17	12.8	1.4
	June 2021	1	37	1	4.51E-05	0.14 *	**34**	67	15.6	38.8	49	9.6	
		3	27	1	4.44E-05	0.14 *	**24**	195	15.0	38.8	22	8.2	
		4	22	2	4.41E-05	0.11 *	**9**	649	14.6	38.7	7	7.4	
		IZMIT	0.6	1	4.54E-05	0.14 *	**0.4**	206	15.8	38.8	0	0.0	
		45-C	6	2	4.43E-05	0.11 *	**2**	1214	14.7	38.7	5	4.3	
the Black Sea	Dec. 2020	9	138	2	3.87E-05	0.13	**53**	81	8.9	19.4	157	2.2	1.9
		10	28	2	3.84E-05	0.10	**9**	107	8.7	20.3	57	3.8	0.9
		11	0	1	3.86E-05	0.16	**0**	448	8.9	22.0	0	0.2	2.7
	June 2021	9	27	1	3.86E-05	0.15 *	**22**	87	8.9	19.8	181	1.0	
		10	110	2	3.84E-05	0.10 *	**36**	142	8.8	21.0	8	0.1	
		16	27	2	3.88E-05	0.13 *	**10**	83	9.0	19.6	195	2.0	
		17	0.6	2	3.87E-05	0.10 *	**0.2**	120	8.9	20.7	65	3.4	

is taken from the same stations of December 2020 Cruise. (*: porosity data is taken from the similar regions' porosity data from December 2020 Cruise)

The highest benthic dFe flux was calculated for station 3 in the Sea of Marmara of December 2020 cruise as 78 $\mu mol.m^{-2}d^{-1}$ within all stations. Despite the highest dFe levels were found in the oxic sea floor of the Black Sea, the highest flux was calculated for the Sea of Marmara. The average flux for only the hypoxic stations is 28 $\mu mol.m^{-2}d^{-1}$ for the Sea of Marmara and 22 $\mu mol.m^{-2}d^{-1}$ for the Black Sea. The major reason for this difference is due to molecular diffusion coefficients are calculated specifically for station conditions and the coefficients are higher with warmer and more saline media (Boudreau, 1996). Thus, according to diffusive flux calculations, the Sea of Marmara is more prone to release the dissolved iron due to faster diffusion mechanisms. The relation between the amount of dissolved iron in the iron reduction layer and the calculated flux can be seen in Figure 73. The slope of the line for the Sea of Marmara is two times higher than of the Black Sea suggesting that even a recent redox change in warmer seafloors can cause higher impacts in the bottom waters compared to less warm iron rich environments due to faster diffusion mechanism. Keeping mind that the calculated diffusive flux is an approach to estimate the flux however does not represent exact flux values which can be detected by in-situ chamber measurements. It is known that the concentration gradient diffusive flux calculations can under/overestimate compared to in-situ analysis by up to factor of 0.01-50 (Pakhomova et al., 2007), depending on the other controls of bio irrigation, resuspension and redox reactions.

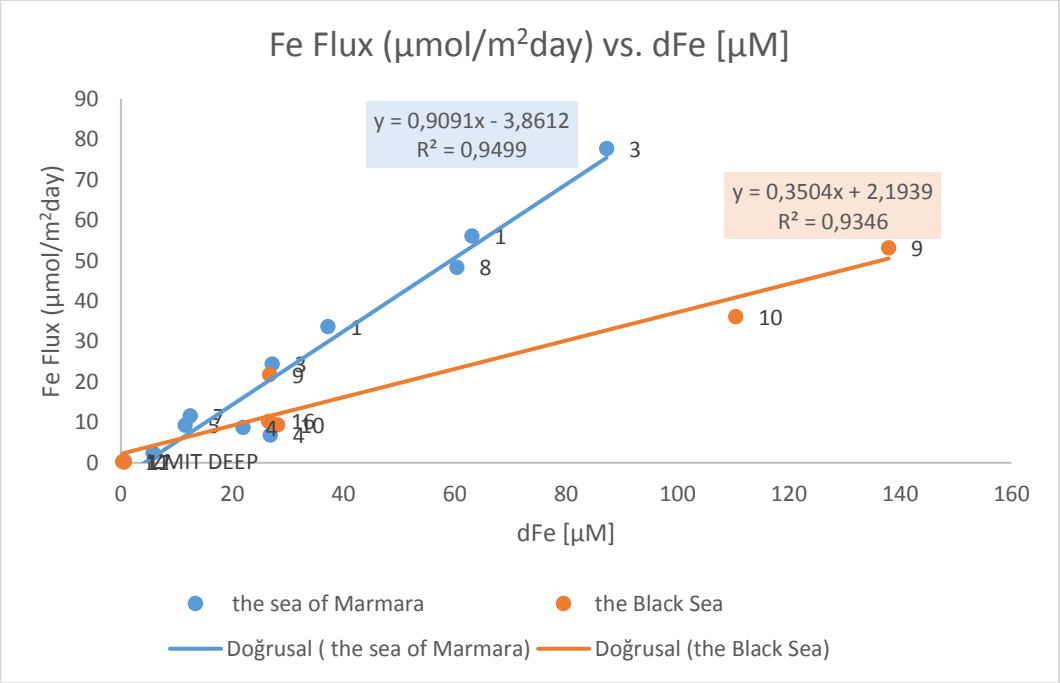

Figure 73: Graph of diffusive iron flux vs. dissolved iron concentration in porewaters for the Black Sea and the Sea of Marmara. Blue: The Sea of Marmara (n=11). Orange: The Black Sea(n=7).

On contrary to the relation between bottom water oxygen and benthic iron fluxes are reversely correlated suggested by Dale (2015), our data shows different trends within different oxygen ranges and possible coupling to TOC content acting as a compensating factor. However, for The Black Sea, the result seems consistent with Dale (2015) bottom oxygen and iron flux reflects the reverse correlation when grouped as “oxic” and “suboxic” stations of their transect.

As indicated by Crémière (2017), Ruffine (2018) and Yang (2018), higher TOC contents creates more reducing and acidic conditions in the sediment which might induce upward transition of redox zonation and tight interconnections between zones. Thus, higher TOC content might act as a compensating factor for higher oxygen levels at the bottom. However, the higher TOC content can also make the sediment much reducing that the iron reduction and sulfate reduction zones overlap.

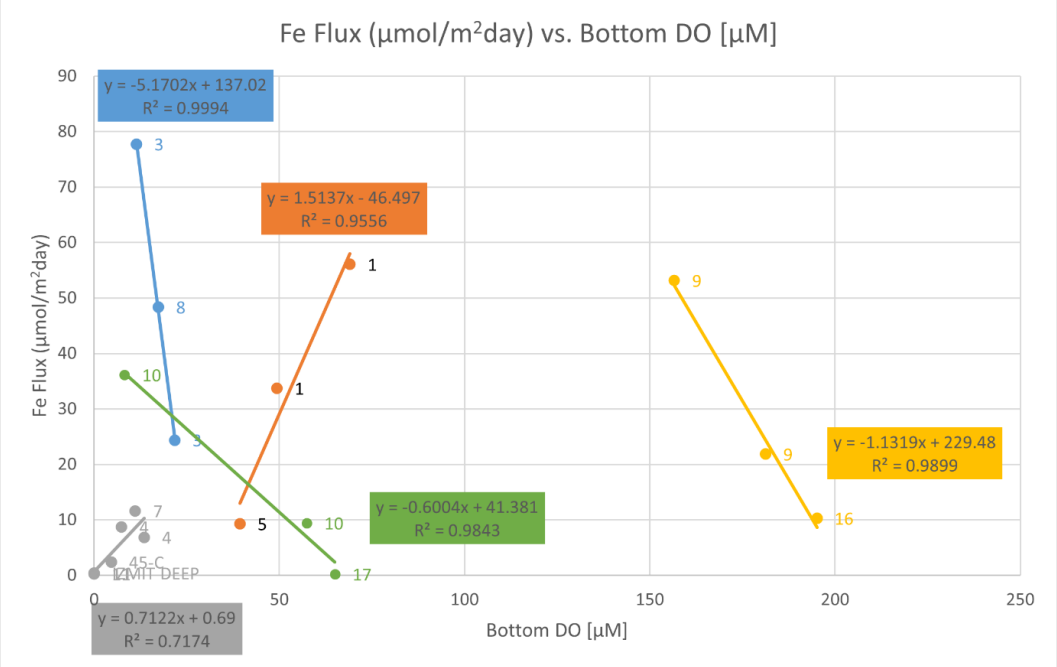

Figure 2: Graph of diffusive iron flux vs. bottom water dissolved oxygen concentrations for the stations of December 2020 Cruise for the Black Sea and the Sea of Marmara. Blue: The Sea of Marmara. Orange: The Black Sea

In non-sulfidic stations, total organic carbon content at the dissolved iron peak layers is correlated with diffusive Fe fluxes indicating the higher organic carbon content induces higher levels of iron mobilization. The relation between the TOC content and iron fluxes are correlated while the bottom oxygen levels exhibit distinctly reverse and correlated relations.

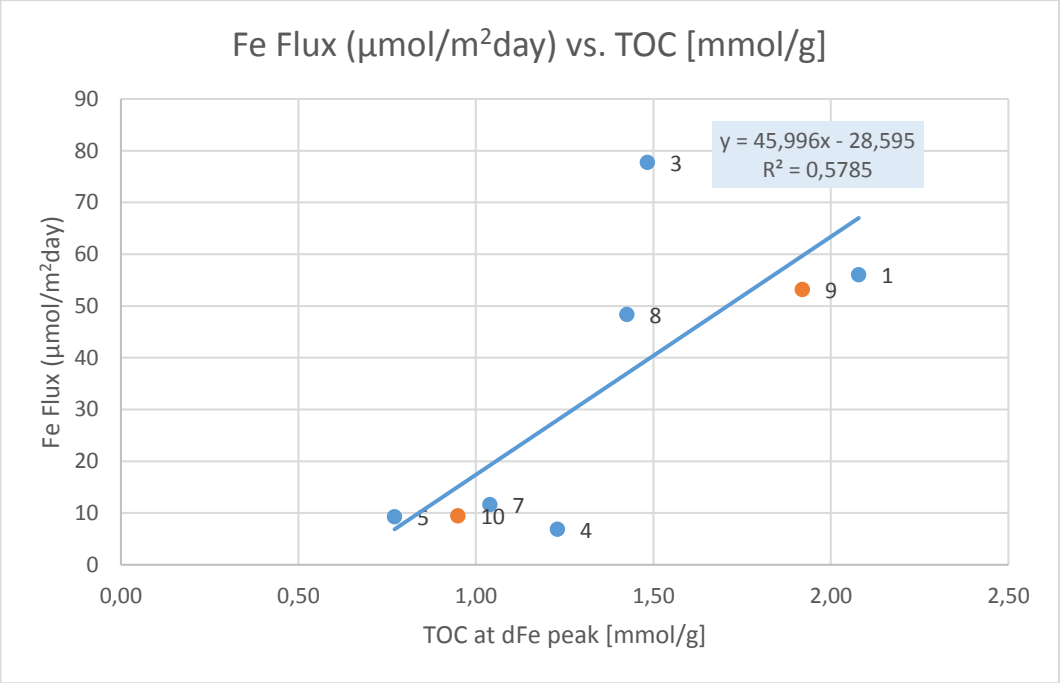

Figure 3: Graph of diffusive iron flux vs. total organic carbon content in sediment solids for the hypoxic/low-oxygen stations of December 2020 Cruise for the Black Sea and the Sea of Marmara. Blue: The Sea of Marmara. Orange: The Black Sea

The low TOC bearing stations (4, 5, 7) might be indicating that the iron respiration cannot be supported adequately by the electron donors thus the iron respiration is low. However, the iron respiration ratios are significantly small among the total estimated carbon oxidation. These results might be related that sulfate reduction occurring just below the iron reduction zone might trapping both the dissolved iron and dissolved hydrogen, thus the calculated iron respiration rate is underestimated.

Station 3 and 8 distinguishes with higher iron fluxes which has intermediate TOC content and low oxygen compared to other stations. Iron flux and the iron respiration ratio from station 3 was decreased in June 2021 which might be indicating that redox conditions becoming more reducing and likewise for stations 4,5, and 7, iron respiration was calculated to have negative error.

Table 4: Contribution of microbial Fe reductive organic matter respiration to estimated total carbon respiration in sediment porewaters for each station.

Area	Cruise	Station	J_{Fe}-depth integrated ($\mu mol.m^{-1}d^{-1}$)	J_{NH4}-depth integrated ($\mu mol.m^{-1}d^{-1}$)	Cox rate ($\mu mol.m^{-1}d^{-1}$)	Fe resp. / Total C ox. (%)	Bot. DO [µM]
the Sea of Marmara	December 2020	1	1.06	2.35	20.8	20	69
		3	1.51	5.53	48.9	12	11.4
		4	0.15	3.99	35.3	2	13.5
		5	0.15	2.77	24.5	2	39.3
		7	0.22	2.82	24.9	3	11.1
		8	0.77	2.33	20.6	15	17.3
	June 2021	1	0.59	0.97	8.6	28	49.3
		3	0.48	8.27	73.2	3	21.7
		4	0.79	5.66	50.1	6	7.4
		IZMIT DEEP	0.05	15.46	136.8	0	0
		45-C	0.42	9.36	82.8	2	4.6
the Black Sea	Dec. 2020	9	2.02	4.21	37.2	22	156.6
		10	0.37	3.51	31.0	5	57.4
		11	0.00	24.61	217.8	0	0
	June 2021	9	0.39	1.44	12.7	12	181.2
		10	1.48	20.50	181.4	3	8.2
		16	0.74	4.28	37.9	8	195.1
		17	0.32	0.92	8.1	16	65

Moreover, a recent accumulation of higher TOC (see section 3.1.2.1 and 0) causes shallower redox zonation which complicates the redox species interplay. Thus, to understand the interplay between bottom oxygen levels, organic carbon content of the sediment and the diffusive flux of iron can be more complicated than presumed especially in recently deoxygenation and eutrophic environments. This point of view is crucial to understand future of benthic iron dynamics and patterns regarding the expansion of hypoxic areas.

4.1.2 Comparison of the Sea of Marmara with other hypoxic systems

According to model estimations that includes carbon oxidation rates and bottom oxygen levels (Dale et al., 2015), benthic dFe flux in the global ocean is 109±55

Gmol/yr, with components of 72 Gmol/yr from the shelf sediments(<200m) and 37 Gmol/yr by slope sediments (200–2000m).

Calculated mean benthic dFe flux according to (Dale et al., 2015) is 7.3 μmol.$m^{-2}d^{-1}$ for shelf (<200m depth) margins and 3.5 μmol.$m^{-2}d^{-1}$ for upper slope margins (200<depth<1000m). And specifically, for oxygen depleted seafloors the average is estimated to be 35 μmol.$m^{-2}d^{-1}$ in recognition that this can be an underestimation and they can be up to 3 factors higher. the Sea of Marmara flux values, that were measured for the first time in this study, are comparable to other global oceanic areas with high benthic iron fluxes, particularly similar to the range detected in the oxygen minimum zones of the Peruvian, California and Oregon margins of the Pacific Ocean. The Sea of Marmara fluxes are not as high as that seen in Baltic Sea bays and fjords, which may support the notion that the Sea of Marmara oxygen minimum zonation displays a more oceanic/continental shelf character than small/enclosed bay character. an aspect which may render a more accurate analogue of the Proterozoic iron-rich oceans of the geologic past.

Table 5: Benthic iron flux ranges from other margins. Edited after *Dale et al. (2015), Pakhomova et al. (2007)*

Study	**Area**	**JFe from pw concentration [μmol.$m^{-2}d^{-1}$]**	**JFe from incubations in situ or ex situ [μmol.$m^{-2}d^{-1}$]**
This study	the Sea of Marmara	0.4 - 78	NA
This study	Southwestern shelf of the Black Sea	0.25 - 53	NA
(Pakhomova et al., 2007)	Golubaya Bay in Black Sea, the Vistula Lagoon in the Baltic Sea, the Gulf of Finland in the Baltic Sea	3 – 400	5 – 1000
(Mcmanus et al., 1997)	Californian margin Borderland Basins	NA	-0.18 –18
(Berelson et al., 2003)	Monterey Bay (California)	NA	1.3–10.8
(Severmann et al., 2010)	Oregon-California shelf Californian Borderland Basins	NA	12–568

Table 5. (cont.)

(Noffke et al., 2012)	Peruvian margin	NA	0–316
(Friedl et al., 1998)	Northwestern shelf of the Black Sea	NA	0-18.7
(William B. Homoky et al., 2012)	the California and Oregon shelves	73-103	3.5-8.3

Proterozoic oceans experienced a redox shift during the Great Oxidation Event, and the surface waters were oxygenated while the deep oceans were governed by anoxia. The deep waters are known to be Fe^{+2} rich where some areas were in the sulfidic phase (Planavsky et al., 2011). The competition between the iron and sulfide was dominated by reduced iron for deep waters (Donald E. Canfield et al., 2008). The strong redoxcline at the seafloor and iron rich character implicates that the Sea of Marmara represents an ideal analogue environment for Proterozoic ocean dynamics among the other proposed analogue environments for Proterozoic Oceans by Rico & Sheldon (2019), especially considering the Sea of Marmara benthic mobilized iron patterns represents a global OMZ character. The interplay between the carbon, nitrogen, phosphorus, and sulfur in the sediment layer can give clues about the biogeochemical dynamics during the Proterozoic Era's oceans.

4.2 Nature of colloidal and soluble phases of benthic iron

Regarding the differences of durability and longevity of between iron species, size fractionation is one of the key applications to understand better the dissolved iron pool and its further implications on ocean iron cycle. Among different methods of separation of size fractionations in seawater (Fitzsimmons & Boyle, 2014), we applied porewater centrifugation and sequential filtration with membranes to obtain colloidal(20nm<dFe<200nm) and soluble(dFe<20nm) fractions, which was previously applied to hydrothermal vent fluids to investigate colloidal fraction in

vent fluids (Yücel et al., 2011). The future directions in the aim of understanding differences of longevity and durability of the iron species will be focusing on chemical speciation of iron within size fractions and the strong interplay between organic ligand speciation (P. W. Boyd & Ellwood, 2010a; von der Heyden & Roychoudhury, 2015). Organic ligands are known to be forming complexes with iron and stabilizes the iron in dissolved form that enhances the residence time of the iron in the water column(P. W. Boyd & Ellwood, 2010b). In this section, comparison of size fraction results within I) the porewater vs. seawater, II) the Sea of Marmara vs. the Black Sea benthic areas.

The negative concentration results of size fractions were reported in the data compilation of (von der Heyden & Roychoudhury, 2015) paper as 57 data points of the 1320 total data within 11 of 29 studies they compiled corresponding to 7.9% of the open ocean euphotic zone data. The error is claimed to be due to several reasons (von der Heyden & Roychoudhury, 2015); I) multiple filtrations increases the manipulation of the sample by introducing air, changing the pH and temperature which can result in disequilibrium between fraction and repartitioning in between separating the sub-samples ((Chin et al., 1998; Fitzsimmons & Boyle, 2012; Thuróczy et al., 2011). II) colloid disaggregation and particle adsorption on filters (Boye et al., 2010).

Comparing the benthic size fraction results (ref results section), the size fraction in station 9 in the Black Sea exhibits smaller error percentages compared to the Sea of Marmara stations. This difference can be due to two possible reasons: I) the colloid fraction is actually a smaller pool that a recent dissolution of iron cannot feed colloid formation yet. II) the bottom temperature of the Sea of Marmara is higher than the Black Sea might be acting on faster repartitioning of fractions and creates larger errors during sampling handling.

Comparing the seawater and benthic size fractions, only benthic size fractionation shows negative concentrations while in seawater there was none. According to our size fractionation in seawater data the dominant fraction within the dissolved iron

pool was colloidal fraction which is consistent with 37–51% on average colloidal fraction in southern ocean (Boye et al., 2010). Benthic fractionation exhibits negative concentration error might be due to seawater colloids are more durable to filtration and do not transfer material to smaller size pool during filtration.

4.3 Colloidal and soluble phases of benthic vs. hydrothermal fluids

As stated by the studies shown that the organic complexation (Bennett et al., 2008; Hawkes et al., 2013) and colloidal nanoparticle formation (Findlay et al., 2019; Yücel et al., 2011, 2021) of dissolved iron from hydrothermal vent fluids, hydrothermal vent iron input to global ocean cycle is more promising than was thought. In this section, I compare the potential impact scale of hydrothermal vent and benthic iron inputs, two iron sources which was thought to be effective only in deep ocean. H. Wang (2019) compares the size fractions of iron and organic ligands in the fluids from the Longqi hydrothermal plumes on the Southwest Indian Ridge. The colloids were around 70% of the dissolved iron while the soluble phase was around 30%. The major fractions of colloidal iron were iron oxyhydroxides and sulfide colloids 86.4 ± 6.2% and organically complexed iron formed the 65.7 ± 5.4% of the soluble phase. The results indicate that the ligands are most likely to stabilize the soluble phase while the colloids are stabilized by the inorganic formations. In (Yücel et al., 2011), the pyrite nanoparticles within the colloidal fraction was 10% and the formation on these fractions were proposed to be occur before the discharge of the fluid. Followed by the study (Yücel et al., 2021) the inorganic colloids is shown to be stable around the vent area bearing the potential to be effective in long-distances. Thus, the major controls on the colloid phase stabilization in vent fluids seems to be the dependent on the inorganic processes before fluid discharge in high temperature and mineral-rich environment. And the organic complexation within the deep ocean might be acting on the soluble phase and labile ligands. DOC is being used as a parametrization for ligand in the global iron cycle models based on the assumption that the ligands are produced by the remineralization of organic matter

(Somes et al., 2021; Völker & Tagliabue, 2015). According to study by Burdige & Gardner (1998), the porewater DOC is dominated by the molecular weight species that are smaller than 3kDa by 60-90%. Hence, the stabilization of iron especially the soluble phase might be controlled by the organic complexation in the porewaters. On top of the fact that the organically complexed iron from hydrothermal vent fluids is dominantly the soluble fraction, the sedimentary iron might be more prone to be in the form of soluble fraction in organically stabilized form. This approach would approve our size fractionation results from the porewater because our results mostly consisted of soluble phase. However, since the ligand size fractions and functional group speciation are understudied, more studies is needed for a more comprehensive view.

CHAPTER 5

CONCLUSION

On the basis of iron's biogeochemical importance for the Earth system, it is apparent that iron studies considering the niches of iron, coupling and interplay with other elements and the impact of various redox conditions on these dynamics is understudied and need to be understood better. This thesis work contributes to studies of iron for establishment of new understandings of iron dynamics in a recently changing environment, the Sea of Marmara, and, in a well-established redox stable area hosting different conditions, the Black Sea. According to our results, the high activity of benthic iron mobilization in the sea floor of the Sea of Marmara is now evident. This results indicates that antropogenic stress, on top of its unique structure, induces deoxygenation and consequently high activity of anaerobic respiration processes at the bottom of the basin. The current redox state indicates that the denitrification and iron reductive respiration is the most dominant process in the upper sediments resulting in high amounts of dissolved iron release within the first centimeters of the sediment.

To approach the sedimentary iron sources by keeping in mind that new improvements made for the understanding of retention and stability of different iron pools, we applied the physical categorization of iron to further investigate the potential outcome of the detected benthic iron input. The size fractionation application was done for the first time in the sedimentary porewaters of the Sea of Marmara and the Black Sea. The size fractionation also applied to seawater of the Black Sea which is already known to have high levels of dissolved and particulate iron in the sub oxic water column. The results indicates the size partitioning of iron in porewater and seawaters have different characteristics imlpying different controls might be acting on. The results are also compared with the hydrothermal vent sourced size fractions to undertand differences between the deep ocean iron sources.

Methodologically, fast on board detection of iron enables to avoid most of the challenges with iron analysis such as oxidation which will contribute to further analytical studies of reduced and oxidized iron forms.

In summary, a more detailed view of iron dynamics needed to be understood to depict the whole biogeochemical cycle of iron comprehensively. And to do so, more detailed and multi-dependent approaches is required.

REFERENCES

Adelson, J. M., Helz, G. R., & Miller, C. V. (2001). Reconstructing the rise of recent coastal anoxia; molybdenum in Chesapeake Bay sediments. *Geochimica et Cosmochimica Acta*, *65*(2), 237–252. https://doi.org/10.1016/S0016-7037(00)00539-1

Akçay, İ. (2022). *COASTAL EUTROPHICATION AND HYPOXIA UNDER FOCUS: REDOX DEPENDENT BENTHIC NUTRIENT FLUXES ACROSS SEA BOUNDARIES IN THE NORTHEASTERN MEDITERRANEAN AND MARMARA SEA IN PARTIAL FULFILLMENT OF THE REQUIREMENTS FOR THE DEGREE OF DOCTOR OF PHILOSOPHY IN OCEANOGRAP*.

Algan, A. O., Çağatay, M. N., Sarikaya, H. Z., Balkis, N., & Sari, E. (1999). Pollution monitoring using marine sediments: A case study on the Istanbul metropolitan area. *Turkish Journal of Engineering and Environmental Sciences*, *23*(1), 39–48.

Algan, O., Balkis, N., Çağatay, M. N., & Sari, E. (2004). The sources of metal contents in the shelf sediments from the Marmara Sea, Turkey. *Environmental Geology*, *46*(6–7), 932–950. https://doi.org/10.1007/S00254-004-1104-2/TABLES/5

Algeo, T. J., & Li, C. (2020). Redox classification and calibration of redox thresholds in sedimentary systems. *Geochimica et Cosmochimica Acta*, *287*, 8–26. https://doi.org/10.1016/J.GCA.2020.01.055

Balkis, N., & Çağatay, M. N. (2001). Factors controlling metal distributions in the surface sediments of the Erdek Bay, Sea of Marmara, Turkey. *Environment International*, *27*(1), 1–13. https://doi.org/10.1016/S0160-4120(01)00044-7

Bennett, S. A., Achterberg, E. P., Connelly, D. P., Statham, P. J., Fones, G. R., &

German, C. R. (2008). The distribution and stabilisation of dissolved Fe in deep-sea hydrothermal plumes. *Earth and Planetary Science Letters*, *270*(3–4), 157–167. https://doi.org/10.1016/J.EPSL.2008.01.048

Berelson, W., McManus, J., Coale, K., Johnson, K., Burdige, D., Kilgore, T., Colodner, D., Chavez, F., Kudela, R., & Boucher, J. (2003). A time series of benthic flux measurements from Monterey Bay, CA. *Continental Shelf Research*, *23*(5), 457–481. https://doi.org/10.1016/S0278-4343(03)00009-8

Berner, R. A. (1984). Sedimentary pyrite formation: An update. *Geochimica et Cosmochimica Acta*, *48*(4), 605–615. https://doi.org/10.1016/0016-7037(84)90089-9

Beşiktepe, Ş. T., Sur, H. I., Özsoy, E., Latif, M. A., Oğuz, T., & Ünlüata, Ü. (1994). The circulation and hydrography of the Marmara Sea. In *Progress in Oceanography* (Vol. 34, Issue 4, pp. 285–334). Pergamon. https://doi.org/10.1016/0079-6611(94)90018-3

Bethke, C. M., Sanford, R. A., Kirk, M. F., Jin, Q., & Flynn, T. M. (2011). The thermodynamic ladder in geomicrobiology. *American Journal of Science*, *311*(3), 183–210. https://doi.org/10.2475/03.2011.01

Boudreau, B. P. (1996). Diagenetic models and their implementation: modelling transport and reactions in aquatic sediments. *Diagenetic Models and Their Implementation: Modelling Transport and Reactions in Aquatic Sediments*. https://www.researchgate.net/publication/235335761

Boyd, P. W., & Ellwood, M. J. (2010a). The biogeochemical cycle of iron in the ocean. *Nature Geoscience*, *3*(10), 675–682. https://doi.org/10.1038/ngeo964

Boyd, P. W., & Ellwood, M. J. (2010b). The biogeochemical cycle of iron in the ocean. *Nature Geoscience 2010 3:10*, *3*(10), 675–682. https://doi.org/10.1038/ngeo964

Boyd, Philip W., Watson, A. J., Law, C. S., Abraham, E. R., Trull, T., Murdoch,

R., Bakker, D. C. E., Bowie, A. R., Buesseler, K. O., Chang, H., Charette, M., Croot, P., Downing, K., Frew, R., Gall, M., Hadfield, M., Hall, J., Harvey, M., Jameson, G., … Zeldis, J. (2000). A mesoscale phytoplankton bloom in the polar Southern Ocean stimulated by iron fertilization. *Nature*, *407*(6805), 695–702. https://doi.org/10.1038/35037500

Boye, M., Nishioka, J., Croot, P., Laan, P., Timmermans, K. R., Strass, V. H., Takeda, S., & de Baar, H. J. W. (2010). Significant portion of dissolved organic Fe complexes in fact is Fe colloids. *Marine Chemistry*, *122*(1–4), 20–27. https://doi.org/10.1016/J.MARCHEM.2010.09.001

Broderick, J. B. (2015). *Coenzymes and Cofactors*. 206–224. https://doi.org/10.1016/B978-0-12-384947-2.00181-1

Burdige, D. J. (1993). The biogeochemistry of manganese and iron reduction in marine sediments. *Earth Science Reviews*, *35*(3), 249–284. https://doi.org/10.1016/0012-8252(93)90040-E

Burdige, D. J., & Gardner, K. G. (1998). Molecular weight distribution of dissolved organic carbon in marine sediment pore waters. *Marine Chemistry*, *62*(1–2), 45–64. https://doi.org/10.1016/S0304-4203(98)00035-8

Canfield, D. E., Jørgensen, B. B., Fossing, H., Glud, R., Gundersen, J., Ramsing, N. B., Thamdrup, B., Hansen, J. W., Nielsen, L. P., & Hall, P. O. J. (1993). Pathways of organic carbon oxidation in three continental margin sediments. *Marine Geology*, *113*(1–2), 27–40. https://doi.org/10.1016/0025-3227(93)90147-N

Canfield, Donald E., Lyons, T. W., & Raiswell, R. (1996). A model for iron deposition to euxinic Black Sea sediments. *American Journal of Science*, *296*(7), 818–834. https://doi.org/10.2475/ajs.296.7.818

Canfield, Donald E., Poulton, S. W., Knol, A. H., Narbonne, G. M., Ross, G., Goldberg, T., & Strauss, H. (2008). Ferruginous conditions dominated later neoproterozoic deep-water chemistry. *Science*, *321*(5891), 949–952.

https://doi.org/10.1126/science.1154499

Canfield, Donald E., Thamdrup, B., & Hansen, J. W. (1993). The anaerobic degradation of organic matter in Danish coastal sediments: Iron reduction, manganese reduction, and sulfate reduction. *Geochimica et Cosmochimica Acta*, *57*(16), 3867–3883. https://doi.org/10.1016/0016-7037(93)90340-3

Chever, F., Bucciarelli, E., Sarthou, G., Speich, S., Arhan, M., Penven, P., & Tagliabue, A. (2010). Physical speciation of iron in the Atlantic sector of the Southern Ocean along a transect from the subtropical domain to the Weddell Sea Gyre. *Journal of Geophysical Research: Oceans*, *115*(C10), 10059. https://doi.org/10.1029/2009JC005880

Chin, W. C., Orellana, M. V., & Verdugo, P. (1998). Spontaneous assembly of marine dissolved organic matter into polymer gels. *Nature*, *391*(6667), 568–572. https://doi.org/10.1038/35345

Chu, N.-C., Johnson, C. M., Beard, B. L., German, C. R., Nesbitt, R. W., Frank, M., Bohn, M., Kubik, P. W., Usui, A., & Graham, I. (2006). Evidence for hydrothermal venting in Fe isotope compositions of the deep Pacific Ocean through time. *Earth and Planetary Science Letters*, *245*, 202–217. https://doi.org/10.1016/j.epsl.2006.02.043

CLINE, J. D. (1969). SPECTROPHOTOMETRIC DETERMINATION OF HYDROGEN SULFIDE IN NATURAL WATERS. In *Limnology and Oceanography* (Vol. 14, Issue 3, pp. 454–458). https://doi.org/10.4319/lo.1969.14.3.0454

Coale, K. H., Worsfold, P., & De Baar, H. (1999). Iron age in oceanography. *Eos*, *80*(34), 377–382. https://doi.org/10.1029/EO080i034p00377-02

Codispoti, L. A., Friederich, G. E., Murray, J. W., & Sakamoto, C. M. (1991). Chemical variability in the Black Sea: implications of continuous vertical profiles that penetrated the oxic/anoxic interface. *Deep-Sea Research, Part A*, *38*(Suppl. 2A), S691–S710. https://doi.org/10.1016/s0198-0149(10)80004-4

Crémière, A., Strauss, H., Sebilo, M., Hong, W. L., Gros, O., Schmidt, S., Tocny, J., Henry, F., Gontharet, S., & Laverman, A. M. (2017). Sulfur diagenesis under rapid accumulation of organic-rich sediments in a marine mangrove from Guadeloupe (French West Indies). *Chemical Geology*, *454*, 67–79. https://doi.org/10.1016/J.CHEMGEO.2017.02.017

Dale, A. W., Nickelsen, L., Scholz, F., Hensen, C., Oschlies, A., & Wallmann, K. (2015). A revised global estimate of dissolved iron fluxes from marine sediments. *Global Biogeochemical Cycles*, *29*(5), 691–707. https://doi.org/10.1002/2014GB005017

de Baar, H. J. W., Boyd, P. W., Coale, K. H., Landry, M. R., Tsuda, A., Assmy, P., Bakker, D. C. E., Bozec, Y., Barber, R. T., Brzezinski, M. A., Buesseler, K. O., Boyé, M., Croot, P. L., Gervais, F., Gorbunov, M. Y., Harrison, P. J., Hiscock, W. T., Laan, P., Lancelot, C., … Wong, C. S. (2005). Synthesis of iron fertilization experiments: From the iron age in the age of enlightenment. In *Journal of Geophysical Research C: Oceans* (Vol. 110, Issue 9, pp. 1–24). John Wiley & Sons, Ltd. https://doi.org/10.1029/2004JC002601

Deuser, W. G. (1974). Evolution of Anoxic Conditions in Black Sea During Holocene. *The Black Sea—Geology, Chemistry, and Biology*. https://doi.org/10.1306/M20377C41

Diaz, R. J., & Rosenberg, R. (2008). Spreading dead zones and consequences for marine ecosystems. *Science*, *321*(5891), 926–929. https://doi.org/10.1126/science.1156401

Dodd, M. S., Papineau, D., Grenne, T., Slack, J. F., Rittner, M., Pirajno, F., O'Neil, J., & Little, C. T. S. (2017). Evidence for early life in Earth's oldest hydrothermal vent precipitates. *Nature*, *543*(7643), 60–64. https://doi.org/10.1038/nature21377

Ediger, D., Beken, Ç., Yüksek, A., & Tuğrul, S. (2016). Eutrophication in the Sea of Marmara. In *The Sea of Marmara: Marine Biodiversity, Fisheries,*

Conservation and Governance (pp. 723–736). www.tudav.org

Elrod, V. A., Berelson, W. M., Coale, K. H., & Johnson, K. S. (2004). The flux of iron from continental shelf sediments: A missing source for global budgets. *Geophysical Research Letters*, *31*(12). https://doi.org/10.1029/2004GL020216

Ergin, M., Saydam, C., Baştürk, Ö., Erdem, E., & Yörük, R. (1991). Heavy metal concentrations in surface sediments from the two coastal inlets (Golden Horn Estuary and İzmit Bay) of the northeastern Sea of Marmara. *Chemical Geology*, *91*(3), 269–285. https://doi.org/10.1016/0009-2541(91)90004-B

Findlay, A. J., Estes, E. R., Gartman, A., Yücel, M., Kamyshny, A., & Luther, G. W. (2019). Iron and sulfide nanoparticle formation and transport in nascent hydrothermal vent plumes. *Nature Communications*, *10*(1), 1–7. https://doi.org/10.1038/s41467-019-09580-5

Fitzsimmons, J. N., & Boyle, E. A. (2012). An intercalibration between the GEOTRACES GO-FLO and the MITESS/Vanes sampling systems for dissolved iron concentration analyses (and a closer look at adsorption effects). *Limnology and Oceanography: Methods*, *10*(6), 437–450. https://doi.org/10.4319/LOM.2012.10.437

Fitzsimmons, J. N., & Boyle, E. A. (2014). Assessment and comparison of Anopore and cross flow filtration methods for the determination of dissolved iron size fractionation into soluble and colloidal phases in seawater. *Limnology and Oceanography: Methods*, *12*(4), 246–263. https://doi.org/10.4319/LOM.2014.12.246

Fitzsimmons, J. N., Boyle, E. A., & Jenkins, W. J. (2014). Distal transport of dissolved hydrothermal iron in the deep South Pacific Ocean. *Proceedings of the National Academy of Sciences of the United States of America*, *111*(47), 16654–16661. https://doi.org/10.1073/pnas.1418778111

Friedl, G., Dinkel, C., & Wehrli, B. (1998). Benthic fluxes of nutrients in the northwestern Black Sea. *Marine Chemistry*, *62*(1–2), 77–88.

https://doi.org/10.1016/S0304-4203(98)00029-2

Garcia, A. K., McShea, H., Kolaczkowski, B., & Kaçar, B. (2020). Reconstructing the evolutionary history of nitrogenases: Evidence for ancestral molybdenum-cofactor utilization. *Geobiology*, *18*(3), 394–411. https://doi.org/10.1111/gbi.12381

Glazer, B. T., Luther, G. W., Konovalov, S. K., Friederich, G. E., Trouwborst, R. E., & Romanov, A. S. (2006). Spatial and temporal variability of the Black Sea suboxic zone. *Deep-Sea Research Part II: Topical Studies in Oceanography*, *53*(17–19), 1756–1768. https://doi.org/10.1016/j.dsr2.2006.03.022

Gordon, R. M., Martin, J. H., & Knauer, G. A. (1982). Iron in north-east Pacific waters. *Nature*, *299*(5884), 611–612. https://doi.org/10.1038/299611a0

Gran, H. H. (1931). II. On the Conditions for the Production of Plankton in the Sea. *Rapports et Procès-Verbaux Des Réunions*, *75*, 35–46. http://www.ices.dk/sites/pub/Publication Reports/Marine Science Symposia/Phase 2/Rapport et Proces-Verbaux des Reunions - Volume 75 - 1931 - Partie 04 de 08.pdf

Haraldsson, C., & Westerlund, S. (1988). Trace metals in the water columns of the Black Sea and Framvaren Fjord. *Marine Chemistry*, *23*(3–4), 417–424. https://doi.org/10.1016/0304-4203(88)90108-9

Hawkes, J. A., Connelly, D. P., Gledhill, M., & Achterberg, E. P. (2013). The stabilisation and transportation of dissolved iron from high temperature hydrothermal vent systems. *Earth and Planetary Science Letters*, *375*, 280–290. https://doi.org/10.1016/J.EPSL.2013.05.047

Hélène, O., Karine, O., Stéphanie, D., Carla, S., Anne-Sophie, A., Clément, G., & Livio, R. (2020). Geological and biological diversity of seeps in the Sea of Marmara. *Deep-Sea Research Part I: Oceanographic Research Papers*, *161*(April), 103287. https://doi.org/10.1016/j.dsr.2020.103287

Homoky, W. B., Hembury, D. J., Hepburn, L. E., Mills, R. A., Statham, P. J., Fones, G. R., & Palmer, M. R. (2011). Iron and manganese diagenesis in deep sea volcanogenic sediments and the origins of pore water colloids. *Geochimica et Cosmochimica Acta*, *75*(17), 5032–5048. https://doi.org/10.1016/J.GCA.2011.06.019

Homoky, William B., Severmann, S., McManus, J., Berelson, W. M., Riedel, T. E., Statham, P. J., & Mills, R. A. (2012). Dissolved oxygen and suspended particles regulate the benthic flux of iron from continental margins. *Marine Chemistry*, *134–135*, 59–70. https://doi.org/10.1016/J.MARCHEM.2012.03.003

Johnson, K. S., Michael Gordon, R., & Coale, K. H. (1997). What controls dissolved iron concentrations in the world ocean? *Marine Chemistry*, *57*(3–4), 137–161. https://doi.org/10.1016/S0304-4203(97)00043-1

Jorgensen, B. B. (2006). Bacteria and marine biogeochemistry. In *Marine Geochemistry* (pp. 169–206). https://doi.org/10.1007/3-540-32144-6_5

K. Grasshoff, M. Ehrhardt, K. K. (1983). Methods of Seawater Analysis. Second, Revised and Extended Edition.–Weinheim/Deerfield Beach, Florida: Verlag Chemie 1983. *Internationale Revue Der Gesamten Hydrobiologie Und Hydrographie*, *70*(2), 302–303. https://doi.org/10.1002/iroh.19850700232

Kappler, A., Bryce, C., Mansor, M., Lueder, U., Byrne, J. M., & Swanner, E. D. (2021). An evolving view on biogeochemical cycling of iron. *Nature Reviews Microbiology 2021 19:6*, *19*(6), 360–374. https://doi.org/10.1038/s41579-020-00502-7

Klunder, M. B., Laan, P., Middag, R., De Baar, H. J. W., & Bakker, K. (2012). Dissolved iron in the Arctic Ocean: Important role of hydrothermal sources, shelf input and scavenging removal. *Journal of Geophysical Research: Oceans*, *117*(C4), 4014. https://doi.org/10.1029/2011JC007135

Konovalov, S. K., Luther, G. W., Friederich, G. E., Nuzzio, D. B., Tebo, B. M.,

Murray, J. W., Oguz, T., Glazer, B., Trouwborst, R. E., Clement, B., Murray, K. J., & Romanov, A. S. (2003). Lateral injection of oxygen with the Bosporus plume-fingers of oxidizing potential in the Black Sea. *Limnology and Oceanography*, *48*(6), 2369–2376. https://doi.org/10.4319/LO.2003.48.6.2369

Konovalov, S. K., Luther, G. W., & Yücel, M. (2007). Porewater redox species and processes in the Black Sea sediments. *Chemical Geology*, *245*(3–4), 254–274. https://doi.org/10.1016/j.chemgeo.2007.08.010

Konovalov, S. K., Murray, J. W., & Luther, G. W. (2005). Basic processes of Black Sea biogeochemistry. *Oceanography*, *18*(SPL.ISS.2), 24–35. https://doi.org/10.5670/oceanog.2005.39

Kraal, P., Yücel, M., & Slomp, C. P. (2019). Turbidite deposition and diagenesis in the southwestern Black Sea: Implications for biogeochemical cycling in an anoxic basin. *Marine Chemistry*, *209*, 48–61. https://doi.org/10.1016/j.marchem.2019.01.001

Lenstra, W. K., Hermans, M., Séguret, M. J. M., Witbaard, R., Behrends, T., Dijkstra, N., van Helmond, N. A. G. M., Kraal, P., Laan, P., Rijkenberg, M. J. A., Severmann, S., Teacă, A., & Slomp, C. P. (2019). The shelf-to-basin iron shuttle in the Black Sea revisited. *Chemical Geology*, *511*, 314–341. https://doi.org/10.1016/j.chemgeo.2018.10.024

Lenstra, Wytze K., Hermans, M., Séguret, M. J. M., Witbaard, R., Severmann, S., Behrends, T., & Slomp, C. P. (2021). Coastal hypoxia and eutrophication as key controls on benthic release and water column dynamics of iron and manganese. *Limnology and Oceanography*, *66*(3), 807–826. https://doi.org/10.1002/LNO.11644

Lewis, B. L., & Landing, W. M. (1991a). The biogeochemistry of manganese and iron in the Black Sea. *Deep-Sea Research, Part A*, *38*(Suppl. 2A). https://doi.org/10.1016/s0198-0149(10)80009-3

Lewis, B. L., & Landing, W. M. (1991b). The biogeochemistry of manganese and iron in the Black Sea. *Deep-Sea Research, Part A*, *38*(Suppl. 2A), S773–S803. https://doi.org/10.1016/s0198-0149(10)80009-3

Lohan, M. C., & Tagliabue, A. (2018). Oceanic micronutrients: Trace metals that are essential for marine life. *Elements*, *14*(6), 385–390. https://doi.org/10.2138/gselements.14.6.385

Lyons, T. W., & Severmann, S. (2006). A critical look at iron paleoredox proxies: New insights from modern euxinic marine basins. *Geochimica et Cosmochimica Acta*, *70*(23 SPEC. ISS.), 5698–5722. https://doi.org/10.1016/j.gca.2006.08.021

Mark Moore, C., Mills, M. M., Achterberg, E. P., Geider, R. J., Laroche, J., Lucas, M. I., McDonagh, E. L., Pan, X., Poulton, A. J., Rijkenberg, M. J. A., Suggett, D. J., Ussher, S. J., & Woodward, E. M. S. (2009). Large-scale distribution of Atlantic nitrogen fixation controlled by iron availability. *Nature Geoscience 2009 2:12*, *2*(12), 867–871. https://doi.org/10.1038/ngeo667

Martin, J. H., & Fitzwater, S. E. (1988). Iron deficiency limits phytoplankton growth in the north-east pacific subarctic. *Nature*, *331*(6154), 341–343. https://doi.org/10.1038/331341a0

Martin, J. H., & Michael Gordon, R. (1988). Northeast Pacific iron distributions in relation to phytoplankton productivity. *Deep Sea Research Part A, Oceanographic Research Papers*, *35*(2), 177–196. https://doi.org/10.1016/0198-0149(88)90035-0

Martin, W., Baross, J., Kelley, D., & Russell, M. J. (2008). Hydrothermal vents and the origin of life. In *Nature Reviews Microbiology* (Vol. 6, Issue 11, pp. 805–814). https://doi.org/10.1038/nrmicro1991

Mcmanus, J., Berelson, W. M., Coale, K. H., Johnson, K. S., & Kilgore, T. E. (1997). Phosphorus regeneration in continental margin sediments. *Geochimica et Cosmochimica Acta*, *61*(14), 2891–2907. https://doi.org/10.1016/S0016-

7037(97)00138-5

Moore, E. K., Jelen, B. I., Giovannelli, D., Raanan, H., & Falkowski, P. G. (2017). Metal availability and the expanding network of microbial metabolisms in the Archaean eon. *Nature Geoscience*, *10*(9), 629–636. https://doi.org/10.1038/ngeo3006

Moore, J. K., Doney, S. C., Glover, D. M., & Fung, I. Y. (2001). Iron cycling and nutrient-limitation patterns in surface waters of the world ocean. *Deep-Sea Research Part II: Topical Studies in Oceanography*, *49*(1–3), 463–507. https://doi.org/10.1016/S0967-0645(01)00109-6

MOORE, R., MILLEY, J., & CHATT, A. (1984). The potential for biological mobilization of trace elements from aeolian dust in the ocean and its importance in the case of iron. *Oceanologica Acta*, *7*(2), 221–228.

Mülayim, A., Balkis, N., Balkis, H., & Aksu, A. (2012). Distributions of total metals in the surface sediments of the Bandirma and Erdek Gulfs, Marmara Sea, Turkey. *Toxicological and Environmental Chemistry*, *94*(1), 56–69. https://doi.org/10.1080/02772248.2011.633914

Murray, J. W., Top, Z., & Ozsoy, E. (1991). Hydrographic properties and ventilation of the Black Sea. *Deep-Sea Research, Part A*, *38*(Suppl. 2A), S663–S689. https://doi.org/10.1016/s0198-0149(10)80003-2

Murray, James W., Lee, B.-S., Bullister, J., & Luther, G. W. (1999). The Suboxic Zone of the Black Sea. In *Environmental Degradation of the Black Sea: Challenges and Remedies* (pp. 75–91). Springer, Dordrecht. https://doi.org/10.1007/978-94-011-4568-8_6

Murray, James W., & Yakushev, E. (2006). the Suboxic Transition Zone in the Black Sea. *Past and Present Water Column Anoxia*, 105–138. https://doi.org/10.1007/1-4020-4297-3_05

Noffke, A., Hensen, C., Sommer, S., Scholz, F., Bohlen, L., Mosch, T., Graco, M.,

& Wallmann, K. (2012). Benthic iron and phosphorus fluxes across the Peruvian oxygen minimum zone. *Limnology and Oceanography*, *57*(3), 851–867. https://doi.org/10.4319/lo.2012.57.3.0851

Oguz, T., La Violette, P. E., & Unluata, U. (1992). The upper layer circulation of the Black Sea: its variability as inferred from hydrographic and satellite observations. *Journal of Geophysical Research*, *97*(C8). https://doi.org/10.1029/92jc00812

Oguz, T., Latif, M. A., Sur, H. I., Ozsoy, E., & Unluata, U. (1991). On the Dynamics of the Southern Black Sea. In *Black Sea Oceanography* (pp. 43–63). Springer Netherlands. https://doi.org/10.1007/978-94-011-2608-3_3

Oguz, T., Latun, V. S., Latif, M. A., Vladimirov, V. V., Sur, H. I., Markov, A. A., Özsoy, E., Kotovshchikov, B. B., Eremeev, V. V., & Ünlüata, Ü. (1993). CIRCULATION IN THE SURFACE AND INTERMEDIATE LAYERS OF THE BLACK-SEA. *Deep-Sea Research Part I*, *40*(8), 1597–1612. https://doi.org/10.1016/0967-0637(93)90018-X

Okay, O. S., Pekey, H., Morkoç, E., Başak, S., & Baykal, B. (2008). Metals in the surface sediments of Istanbul Strait (Turkey). *Journal of Environmental Science and Health - Part A Toxic/Hazardous Substances and Environmental Engineering*, *43*(14), 1725–1734. https://doi.org/10.1080/10934520802330412

Özsoy, E., & Ünlüata, Ü. (1997). Oceanography of the Black Sea: A review of some recent results. *Earth-Science Reviews*, *42*(4), 231–272. https://doi.org/10.1016/S0012-8252(97)81859-4

Pakhomova, S. V., Hall, P. O. J., Kononets, M. Y., Rozanov, A. G., Tengberg, A., & Vershinin, A. V. (2007). Fluxes of iron and manganese across the sediment-water interface under various redox conditions. *Marine Chemistry*, *107*(3), 319–331. https://doi.org/10.1016/j.marchem.2007.06.001

Piper, D. Z. (2016). Geochemistry of the Black Sea during the last 15 kyr: A

protracted evolution of its hydrography and ecology. *Paleoceanography*, *31*(8), 1117–1137. https://doi.org/10.1002/2016PA002949

Piper, D. Z., & Calvert, S. E. (2011). Holocene and late glacial palaeoceanography and palaeolimnology of the Black Sea: Changing sediment provenance and basin hydrography over the past 20,000years. *Geochimica et Cosmochimica Acta*, *75*(19), 5597–5624. https://doi.org/10.1016/j.gca.2011.07.016

Planavsky, N. J., McGoldrick, P., Scott, C. T., Li, C., Reinhard, C. T., Kelly, A. E., Chu, X., Bekker, A., Love, G. D., & Lyons, T. W. (2011). Widespread iron-rich conditions in the mid-Proterozoic ocean. *Nature 2011 477:7365*, *477*(7365), 448–451. https://doi.org/10.1038/nature10327

Pyzik, A J, Sommer, S. E., Rickard, D. T., Canfield, D. E., & Berner, R. A. (1992). Reductive Dissolution of Iron(III) (Hydr)oxides by Hydrogen Sulfide The experimental data are compatible with the constants ke = 30 h"1 and ke' = 400 h"1 and surface complex formation constants for =FeS" (=FeOH + H2S(g) j=t =FeS" + H+ + H20) and =FeSH (=FeOH + H2S(g) f* =FeSH + H20) of log Xs =-2.70 and. *In Aquatic Chemical Kinetics·*, *8*(1), 645. https://pubs.acs.org/sharingguidelines

Pyzik, Albert J, & Sommer, S. E. (1981). Sedimentary iron monosulfides: Kinetics and mechanism of formation. *Geochimica et Cosmochimica Acta*, *45*(5), 687–698. https://doi.org/10.1016/0016-7037(81)90042-9

Raiswell, R., & Canfield, D. E. (2012). The iron biogeochemical cycle past and present. *Geochemical Perspectives*, *1*(1), 1–232. https://doi.org/10.7185/geochempersp.1.1

Rickard, D., & Luther, G. W. (2007). Chemistry of Iron Sulfides. *Chemical Reviews*, *107*(2), 514–562. https://doi.org/10.1021/CR0503658

Rico, K. I., & Sheldon, N. D. (2019). Nutrient and iron cycling in a modern analogue for the redoxcline of a Proterozoic ocean shelf. *Chemical Geology*, *511*(July 2018), 42–50. https://doi.org/10.1016/j.chemgeo.2019.02.032

Ruffine, L., Donval, J. P., Croguennec, C., Burnard, P., Lu, H., Germain, Y., Legoix, L. N., Bignon, L., Çağatay, M. N., Marty, B., Madre, D., Pitel-Roudaut, M., Henry, P., & Géli, L. (2018). Multiple gas reservoirs are responsible for the gas emissions along the Marmara fault network. *Deep Sea Research Part II: Topical Studies in Oceanography*, *153*, 48–60. https://doi.org/10.1016/J.DSR2.2017.11.011

Ruffine, L., Germain, Y., Polonia, A., De Prunelé, A., Croguennec, C., Donval, J. P., Pitel-Roudaut, M., Ponzevera, E., Caprais, J. C., Brandily, C., Grall, C., Bollinger, C., Géli, L., & Gasperini, L. (2015). Pore water geochemistry at two seismogenic areas in the Sea of Marmara. *Geochemistry, Geophysics, Geosystems*, *16*(7), 2038–2057. https://doi.org/10.1002/2015GC005798

Russell, M. J., & Hall, A. J. (2006). The onset and early evolution of life. In *Evolution of Early Earth's Atmosphere, Hydrosphere, and Biosphere - Constraints from Ore Deposits*. Geological Society of America. https://doi.org/10.1130/2006.1198(01)

Saito, M. A., Noble, A. E., Tagliabue, A., Goepfert, T. J., Lamborg, C. H., & Jenkins, W. J. (2013). Slow-spreading submarine ridges in the South Atlantic as a significant oceanic iron source. *Nature Geoscience 2013 6:9*, *6*(9), 775–779. https://doi.org/10.1038/ngeo1893

Scholz, F., Mcmanus, J., Mix, A. C., Hensen, C., & Schneider, R. R. (2014a). The impact of ocean deoxygenation on iron release from continental margin sediments. *Nature Geoscience*, *7*(6), 433–437. https://doi.org/10.1038/ngeo2162

Scholz, F., Mcmanus, J., Mix, A. C., Hensen, C., & Schneider, R. R. (2014b). The impact of ocean deoxygenation on iron release from continental margin sediments. *Nature Geoscience*, *7*(6), 433–437. https://doi.org/10.1038/ngeo2162

Severmann, S., McManus, J., Berelson, W. M., & Hammond, D. E. (2010). The

continental shelf benthic iron flux and its isotope composition. *Geochimica et Cosmochimica Acta*, *74*(14), 3984–4004. https://doi.org/10.1016/J.GCA.2010.04.022

Slomp, C. P., Malschaert, J. F. P., Lohse, L., & Van Raaphorst, W. (1997). Iron and manganese cycling in different sedimentary environments on the North Sea continental margin. *Continental Shelf Research*, *17*(9), 1083–1117. https://doi.org/10.1016/S0278-4343(97)00005-8

Somes, C. J., Dale, A. W., Wallmann, K., Scholz, F., Yao, W., Oschlies, A., Muglia, J., Schmittner, A., & Achterberg, E. P. (2021). Constraining Global Marine Iron Sources and Ligand-Mediated Scavenging Fluxes With GEOTRACES Dissolved Iron Measurements in an Ocean Biogeochemical Model. *Global Biogeochemical Cycles*, *35*(8). https://doi.org/10.1029/2021GB006948

Stookey, L. L. (1970). Ferrozine-A New Spectrophotometric Reagent for Iron. *Analytical Chemistry*, *42*(7), 779–781. https://doi.org/10.1021/ac60289a016

Tagliabue, A., Aumont, O., & Bopp, L. (2014a). The impact of different external sources of iron on the global carbon cycle. *Geophysical Research Letters*, *41*(3), 920–926. https://doi.org/10.1002/2013GL059059

Tagliabue, A., Aumont, O., & Bopp, L. (2014b). The impact of different external sources of iron on the global carbon cycle. *Geophysical Research Letters*, *41*(3), 920–926. https://doi.org/10.1002/2013GL059059

Tagliabue, A., Barrier, N., Du Pontavice, H., Kwiatkowski, L., Aumont, O., Bopp, L., Cheung, W. W. L., Gascuel, D., & Maury, O. (2020). An iron cycle cascade governs the response of equatorial Pacific ecosystems to climate change. *Global Change Biology*, *26*(11), 6168–6179. https://doi.org/10.1111/GCB.15316

Tagliabue, A., Bopp, L., Dutay, J. C., Bowie, A. R., Chever, F., Jean-Baptiste, P., Bucciarelli, E., Lannuzel, D., Remenyi, T., Sarthou, G., Aumont, O., Gehlen,

M., & Jeandel, C. (2010). Hydrothermal contribution to the oceanic dissolved iron inventory. *Nature Geoscience*, *3*(4), 252–256. https://doi.org/10.1038/ngeo818

Tagliabue, A., Bowie, A. R., Boyd, P. W., Buck, K. N., Johnson, K. S., & Saito, M. A. (2017). The integral role of iron in ocean biogeochemistry. In *Nature* (Vol. 543, Issue 7643, pp. 51–59). Nature Publishing Group. https://doi.org/10.1038/nature21058

Thuróczy, C. E., Gerringa, L. J. A., Klunder, M., Laan, P., Le Guitton, M., & De Baar, H. J. W. (2011). Distinct trends in the speciation of iron between the shallow shelf seas and the deep basins of the Arctic Ocean. *Journal of Geophysical Research: Oceans*, *116*(C10), 10009. https://doi.org/10.1029/2010JC006835

Toner, B. M., Fakra, S. C., Manganini, S. J., Santelli, C. M., Marcus, M. A., Moffett, J. W., Rouxel, O., German, C. R., & Edwards, K. J. (2009). Preservation of iron(II) by carbon-rich matrices in a hydrothermal plume. *Nature Geoscience 2009 2:3*, *2*(3), 197–201. https://doi.org/10.1038/ngeo433

Topcuoğlu, S., Kirbaşoğlu, Ç., & Yilmaz, Y. Z. (2004). Heavy Metal Levels in Biota and Sediments in the Northern Coast of the Marmara Sea. *Environmental Monitoring and Assessment 2004 96:1*, *96*(1), 183–189. https://doi.org/10.1023/B:EMAS.0000031726.01364.47

Tugrul, S., Basturk, O., Saydam, C., & Yilmaz, A. (1992). Changes in the hydrochemistry of the Black Sea inferred from water density profiles. *Nature*, *359*(6391), 137–139. https://doi.org/10.1038/359137a0

Tuğrul, S., Beşiktepe, Ş. T., & Salihoğlu, I. (2002). Nutrient exchange fluxes between the Aegean and Black Seas through the Marmara Sea. *Mediterranean Marine Science*, *3*(1), 33–42. https://doi.org/10.12681/mms.256

Ünlülata, Ü., Oğuz, T., Latif, M. A., & Özsoy, E. (1990). On the Physical Oceanography of the Turkish Straits. In *The Physical Oceanography of Sea*

Straits (pp. 25–60). Springer, Dordrecht. https://doi.org/10.1007/978-94-009-0677-8_2

Völker, C., & Tagliabue, A. (2015). Modeling organic iron-binding ligands in a three-dimensional biogeochemical ocean model. *Marine Chemistry*, *173*, 67–77. https://doi.org/10.1016/J.MARCHEM.2014.11.008

von der Heyden, B. P., & Roychoudhury, A. N. (2015). A review of colloidal iron partitioning and distribution in the open ocean. *Marine Chemistry*, *177*, 9–19. https://doi.org/10.1016/j.marchem.2015.05.010

Wang, H., Yan, Q., Yang, Q., Ji, F., Wong, K. H., & Zhou, H. (2019). The Size Fractionation and Speciation of Iron in the Longqi Hydrothermal Plumes on the Southwest Indian Ridge. *Journal of Geophysical Research: Oceans*, *124*(6), 4029–4043. https://doi.org/10.1029/2018JC014713

Wang, Y., & Van Cappellen, P. (1996). A multicomponent reactive transport model of early diagenesis: Application to redox cycling in coastal marine sediments. *Geochimica et Cosmochimica Acta*, *60*(16), 2993–3014. https://doi.org/10.1016/0016-7037(96)00140-8

Waterbury, R. D., Yao, W., & Byrne, R. H. (1997). Long pathlength absorbance spectroscopy: Trace analysis of Fe(II) using a 4.5 m liquid core waveguide. *Analytica Chimica Acta*, *357*(1–2), 99–102. https://doi.org/10.1016/S0003-2670(97)00530-8

Wijsman, J. W.M., Middelburg, J. J., & Heip, C. H. R. (2001). Reactive iron in Black Sea Sediments: implications for iron cycling. *Marine Geology*, *172*(3–4), 167–180. https://doi.org/10.1016/S0025-3227(00)00122-5

Wijsman, Jeroen W.M., Middelburg, J. J., Herman, P. M. J., Böttcher, M. E., & Heip, C. H. R. (2001). Sulfur and iron speciation in surface sediments along the northwestern margin of the Black Sea. *Marine Chemistry*, *74*(4), 261–278. https://doi.org/10.1016/S0304-4203(01)00019-6

Wilkin, R. T., Arthur, M. A., & Dean, W. E. (1997). History of water-column anoxia in the Black Sea indicated by pyrite framboid size distributions. *Earth and Planetary Science Letters*, *148*(3–4), 517–525. https://doi.org/10.1016/s0012-821x(97)00053-8

Yakushev, E. V., & Newton, A. (2013). Introduction: Redox interfaces in marine waters. *Handbook of Environmental Chemistry*, *22*, 1–12. https://doi.org/10.1007/698_2012_167/FIGURES/1

Yang, H., Lu, H., & Ruffine, L. (2018a). Geochemical characteristics of iron in sediments from the Sea of Marmara. *Deep-Sea Research Part II: Topical Studies in Oceanography*, *153*(January), 121–130. https://doi.org/10.1016/j.dsr2.2018.01.010

Yang, H., Lu, H., & Ruffine, L. (2018b). Geochemical characteristics of iron in sediments from the Sea of Marmara. *Deep Sea Research Part II: Topical Studies in Oceanography*, *153*, 121–130. https://doi.org/10.1016/J.DSR2.2018.01.010

Yemenicioglu, S., Erdogan, S., & Tugrul, S. (2006a). Distribution of dissolved forms of iron and manganese in the Black Sea. *Deep Sea Research Part II: Topical Studies in Oceanography*, *53*(17–19), 1842–1855. https://doi.org/10.1016/J.DSR2.2006.03.014

Yemenicioglu, S., Erdogan, S., & Tugrul, S. (2006b). Distribution of dissolved forms of iron and manganese in the Black Sea. *Deep-Sea Research Part II: Topical Studies in Oceanography*, *53*(17–19), 1842–1855. https://doi.org/10.1016/j.dsr2.2006.03.014

Yilmaz, A. (2002). Türkiye denizlerinin biyojeokimyası: Dağılımlar ve dönüşümler. *Turkish Journal of Engineering and Environmental Sciences*, *26*(2), 219–235. https://app.trdizin.gov.tr/makale/TXpJMk1EazU/turkiye-denizlerinin-biyojeokimyasi-dagilimlar-ve-donusumler

Yücel, M. (2009). NEW PERSPECTIVES IN SULFUR-IRON CYCLING AT

THE OCEAN- SEAFLOOR INTERFACE: THE BLACK SEA SEDIMENTS AND DEEP-SEA HYDROTHERMAL VENTS. In *University of Delaware*.

Yücel, M., Gartman, A., Chan, C. S., & Luther, G. W. (2011). Hydrothermal vents as a kinetically stable source of iron-sulphide-bearing nanoparticles to the ocean. *Nature Geoscience*, *4*(6), 367–371. https://doi.org/10.1038/ngeo1148

Yücel, M., Konovalov, S. K., Moore, T. S., Janzen, C. P., & Luther, G. W. (2010). Sulfur speciation in the upper Black Sea sediments. *Chemical Geology*, *269*(3–4), 364–375. https://doi.org/10.1016/j.chemgeo.2009.10.010

Yücel, M., Luther, G. W., & Moore, W. S. (2010). Earthquake-induced turbidite deposition as a previously unrecognized sink for hydrogen sulfide in the Black Sea sediments. *Marine Chemistry*, *121*(1–4), 176–186. https://doi.org/10.1016/J.MARCHEM.2010.04.006

Yücel, M., Sevgen, S., & Le Bris, N. (2021). Soluble, Colloidal, and Particulate Iron Across the Hydrothermal Vent Mixing Zones in Broken Spur and Rainbow, Mid-Atlantic Ridge. *Frontiers in Microbiology*, *12*, 631885. https://doi.org/10.3389/FMICB.2021.631885/FULL